The Pennsylvania State University

The Graduate School

Department of Bioengineering

SHEAR STRESS ELICITS A TRANSIENT DOMAIN-DEPENDENT ALTERATION OF THE PLASMA MEMBRANE FLUIDITY IN ENDOTHELIAL CELLS

A Dissertation in

Bioengineering

by

Tristan Tabouillot

Submitted in Partial Fulfillment
of the Requirements
for the Degree of

Doctor of Philosophy

May 2009

The dissertation of Tristan Tabouillot was reviewed and approved* by the following:

Peter J. Butler
Associate Professor of Bioengineering
Dissertation Advisor
Chair of Committee

Ahmed A. Heikal
Associate Professor of Bioengineering

Erin D. Sheets
Assistant Professor of Chemistry

Herbert H. Lipowsky
Professor of Bioengineering
Head of the Department of Bioengineering

*Signatures are on file in the Graduate School

ABSTRACT

Blood flow-associated shear stress causes physiological and pathophysiological biochemical processes in endothelial cells that may be initiated by alterations in plasma membrane domains. Time scales of cells signaling cascades triggered by shear stress spans seconds to hours. Hence, a single-molecule fluorescence spectroscopy system was developed to investigate cellular molecular dynamics with high spatial and temporal resolution. We defined a procedure to locate lipoid dyes in cultured endothelial cells under physiological conditions. Thus, we assessed the photophysics and dynamics of the lipid analogues DiI-C_{12} and DiI-C_{18} in endothelial cells subjected to physiological fluid shear stress. These lipoid dyes have been proposed to segregate to domains of the membrane with thicknesses matching DiI alkyl chain length such that DiI-C_{12} partitions into the thinner liquid-disordered phase and DiI-C_{18} partitions into the thicker liquid-ordered phase. DiI fluorescence lifetime, molecular brightness, number of molecules, and lateral diffusion were obtained from time-correlated single photon counting data and analyzed as a function of shear stress and time. DiI-C_{12} fluorescence lifetime was 0.16 ns faster than DiI-C_{18} lifetime and the diffusion coefficient of DiI-C_{12} was 1.5 times greater than the DiI-C_{18} diffusion coefficient confirming that DiI-C_{12} probes more fluid membrane environments as compared to DiI-C_{18}. Domains probed by DiI-C_{12} dye exhibited a decrease of fluorescence lifetime from 5 to 20 seconds after the onset of shear while domains probed by DiI-C_{18} exhibited a decrease of fluorescence lifetime that was delayed 10 seconds but was sustained for the 2 minutes the cells were subjected to flow. Determination of the number of fluorophores in the observation volume from moment

analysis suggested that DiI-C_{12} -labeled domains increased in area while DiI-C_{18} -stained membrane did not. Taken together, the data suggest that shear stress induces an early rippling of DiI-C_{12} –stained domains and later change in lipid mobility of DiI-C_{18} – stained domains. These results help focus attention on the membrane microdomains interaction with glycocalyx and cytoskeleton as sites of shear sensitivity.

TABLE OF CONTENTS

LIST OF FIGURES

LIST OF TABLES

ACKNOWLEDGEMENTS

To those who left before I could end this work. I am grateful to my whole family for the patient support they gave me during this long journey.

I would like to thank my advisor, Dr. Peter Butler, for is support, and mechlab members – past and present – for sharing such an exciting and instructive segment of my life. To my encouraging friends, any part of the world they now live in, I would like to express my gratitude.

I would also like to thank my committee members, Dr. Erin Sheets, Dr. Ahmed Heikal and Dr. Herbert Lipowsky, for their helpful guidance; and particularly Dr. Heikal for his numerous advices on setting up our optical setup.

Chapter 1

INTRODUCTION

1.1 Endothelial plasma membrane

The cellular plasma membrane is made up of a lipid core onto and into which various proteins are anchored (Vance and Vance, 2002). The 5-nm thick core is composed of two phospholipids monolayers, stabilized by hydrophobic and van der Waals interactions. The multiple combinations of possibly more than a hundred (Lipowsky, 1995) of lipid hydrophilic headgroups and hydrophobic acyl chains permit the inclusion of various molecules like glycerophospholipids, sphingolipids, glycolipids and sterols. The membrane contains carbohydrates, transmembrane and peripheral (located outside) proteins, as well as glycosylphosphatidylinositol-anchored (GPI) proteins localized in cholesterol-enriched lipid domains on the exoplasmic leaflet (Figure 1-1). Hence, the plasma membrane is a heterogeneous and dynamic system that allows for the numerous properties and functions necessary for biological homeostasis in the face of a constantly changing mechanical and chemical environment.

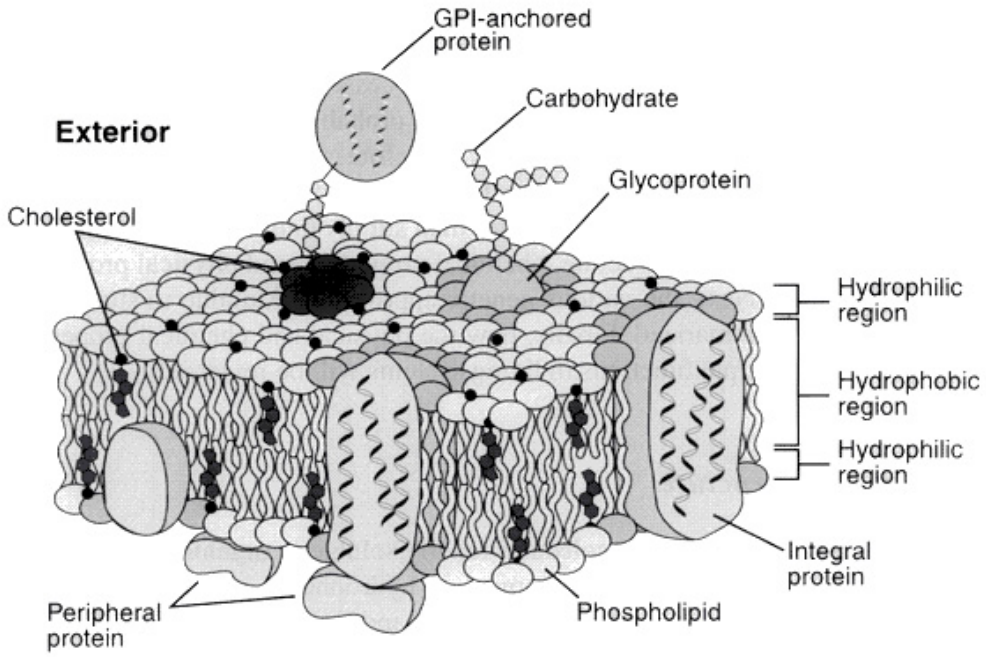

Figure 1-1: The plasma membrane is composed of a wide variety of phospholipids containing transmembrane proteins, peripheral membrane proteins and GPI-anchored proteins localized in lipid rafts (dark gray headgroups) (Vance and Vance, 2002).

1.1.1 Membrane domains

The very existence of lipid rafts is still controversial (Munro, 2003). Nevertheless, lipid domains exhibiting different physical properties have been demonstrated to exist in cell membranes (Brown and Rose, 1992;Rietveld and Simons, 1998;Simons and Ikonen, 1997). Lipid rafts are ordered environments in cell membrane where protein signaling occurs (Simons and Ikonen, 1997;Simons and Toomre, 2000;Smart et al., 1999). But beyond that functional description, membrane domains have been defined by the techniques used to detect and characterize them. Chemically,

they are detergent-resistant membrane fractions (DRMs) (Brown and Rose, 1992;Brown and London, 1997). Biophysically, they are clusters of lipids and proteins detectable using optical microscopy (Hwang et al., 1998;Vereb et al., 2000). Single-particle tracking (SPT) describe these clusters by the unique lateral movement restrictions they display (Jacobson and Dietrich, 1999;Saxton and Jacobson, 1997;Sheets et al., 1997). Although SPT can record viscosity measurements with high signal-to-noise ratio and appropriate time resolution – particularly with single dye tracing (Schutz and Hinterdorfer, 2002), there is a potential entanglement of large colloidal beads in the glycocalyx, which could lead to discrepancies between observed diffusion of the colloidal tracer and diffusion of actual lipids. (Lee et al., 1993). An alternative is fluorescent dye monitoring through an optical microscope. The associated techniques (i.e. Förster resonance energy transfer (FRET), fluorescence correlation spectroscopy (FCS), fluorescence lifetime and anisotropy) can be minimally invasive and has high selectivity for the molecule probed – at the expense of high signal-to-noise ratio. FRET studies, in particular, outlined the transient characteristic of rafts (Kenworthy et al., 2000). Depending on the technique used, the size of those domains spans a few to hundreds of nanometers. Domains have also been studied in model membranes (Dietrich et al., 2001) using the canonical "lipid raft" mixture conventionally defined by the mixing of glycerophospholipid:sphingolipid:cholesterol at a molar ratio of (1:1:1). The slow lateral diffusion of lipids in those domains is used to describe an arrangement of lipids called liquid-ordered (L_o), denoting that lipids are mobile but their acyl chain mobility is highly restricted. This is in contrast to a more fluidic liquid-disordered (L_d) phase. The constituents of a L_o phase are still above the transition temperature (i.e. not in gel phase)

but exhibit higher order and tighter packing. The accumulation of novel properties attributed to rafts has brought new theories on the dynamics of native membranes. The "thermo Lego model" (Subczynski and Kusumi, 2003) describes three levels of domains: a first domain of a few molecules, with milliseconds lifetime, build up into "core receptor rafts" centered on a GPI-anchored or transmembrane protein. Stability – in order of minutes – is provided by the addition of cholesterol. These domains coalesce to form "signaling rafts", which would start signal transduction in the plasma membrane. The "lipid shell model" emphasizes on encasing of membrane proteins in 7-nm cholesterol-sphingomyelin-enriched domains (Anderson and Jacobson, 2002). Multiple shells would then aggregate to bring the signaling functionality to the domains.

1.1.2 Functionality of the plasma membrane in endothelial cells

The endothelial cells plasma membrane interacts with many other cell components and is actively involved in the physiology of the cell. On the cytoplasmic side, it is connected to the cortical actin cytoskeleton. On the luminal side of the lipid bilayer is the glycocalyx, or endothelial surface layer (ESL) (Pries et al., 2000). The glycocalyx is composed of a complex ensemble of glycolipids, proteins, glycoproteins, proteoglycans (PGs) (Risau, 1995). PGs include syndecans and glypicans. Syndecans have a transmembrane domain and an intracellular domain that are linked to the cortical actin cytoskeleton (Tkachenko et al., 2005), whereas glypicans are attached to the plasma membrane by a glycosylphosphatidylinositol (GPI) anchor (Pries et al., 2000).

The cell surface is the site from which most of the signaling is initiated. After activation through binding of a specific receptor protein, a signaling cascade is initiated. Signaling cascades can be activated by force in a non-ligand-receptor-dependent manner provided that force induces a change the shape or conformational state of the molecule. A membrane protein would be mechanosensitive if it is affected by changes in the membrane properties due to mechanical strain (Hamill and Martinac, 2001). Interestingly, it has been shown that the physical state of biomembranes can be coupled to the function of enzymes or proteins (Burack et al., 1993;Giorgione et al., 1998). In this scenario, forces applied to the membrane are transmitted to the protein through changes in hydrophobic matching conditions (Mouritsen and Bloom, 1993) and lateral pressure profiles causing a change in protein conformation (Dan and Safran, 1998). Another interaction mechanism between lipids and membrane proteins is when lipid viscosity dictates ordering, sorting, and interaction between proteins. In this mechanism the membrane phase may be modified by force leading to changes in proteins aggregation and association. This mechanism, however, awaits experimental verification. Because many of these membrane biophysical properties are coupled, it becomes difficult to sort out the dependence of mechanotransduction on mechanosensitivity of the membrane. Effects of differences in hydrophobic thicknesses of proteins and lipid bilayers (hydrophobic mismatch), can result in changes in bilayer curvature and subsequent changes in interactions of phospholipid headgroups with proteins (reviewed in (Lee, 2004)).

1.2 Mechanotransduction

1.2.1 Endothelial mechanotransduction

Mechanotransduction is the process by which cells convert mechanical stimuli into biochemical signals, thus altering their structure and function. Osmotic and hydrostatic pressures, extracellular matrix deformations and shear stress from blood flow are among the physiological forces encountered. These forces may originate from whole organ or tissue deformations, but they will eventually reach a mechanosensor or cellular compartment, organelle, or single molecule that transmits the force in the cell interior. Thus, the mechanical stimulus will ultimately activate a mechanotransducer that will initiate a biochemical signaling cascade (Orr et al., 2006). Since variations in molecular concentration and activation state control general cell biology, mechanotransduction, most likely, works through the same processes. It has been shown to be relevant in bone remodeling, cell differentiation, vascular caliber control, atherosclerosis and other physiological phenomena (Orr et al., 2006).

Atherosclerotic plaques, for example, develop at the location of perturbed flow in blood vessels (Zarins et al., 1983) (Figure 1-2) suggesting a mechanics-based origin. Atherosclerotic plaques develop from the deposition and accumulation of lipid and fibrous tissue in the inner lining of an artery. The location of these plaques coincides with regions of low and oscillatory blood flow-induced shear stress. Consistent with this idea, endothelial cells (ECs) show both atherogenic and atheroprotective properties (Chien, 2006;Davies, 1995;Honda et al., 2001;Kim et al., 1989;Ku et al., 1985;Nerem et al.,

1981;Weinbaum and Chien, 1993;Zarins et al., 1983) depending on the spatial (Davies et al., 1997;dePaola et al., 1992) and temporal (Bao et al., 2000;Butler et al., 2002;Frangos et al., 1996) gradients in shear stress. Mechanotransduction has been show to be dependent on changes at focal adhesions (Girard and Nerem, 1995;Li et al., 1997), on the actin cytoskeleton (Galbraith et al., 1998;Girard and Nerem, 1993), on cell-cell junctions (Fujiwara et al., 2001) and on the glycocalyx (Florian et al., 2003;Mochizuki et al., 2003;Pahakis et al., 2007). But because of the lack of molecular scale readouts of mechanosensation and the disparate time course of these mechanically induced changes, experimental evidence supporting the hypothesis that any of these structures are, themselves, mechanosensors, has remained elusive.

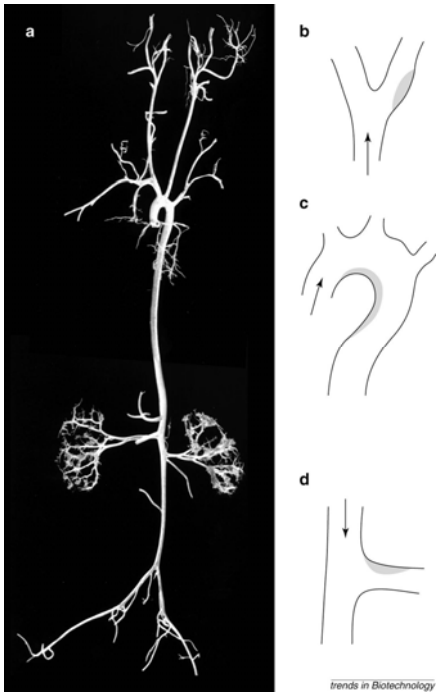

Figure 1-2: Cast of a mammalian arterial system (a). Bifurcations (b), curvatures (c) and branches (d) are regions of disturbed flow where atherosclerotic lesion (shaded areas) tend to build up (Davies et al., 1999).

The time-dependent activation – spanning seconds to days – of endothelial cell components upon onset of shear has been thoroughly reviewed (Davies, 1995;Davies, 1997;Takahashi et al., 1997). Within seconds stretch-activated calcium channels are already involved (Goligorsky, 1988), potassium ion channels activation induces depolarization (Cooke et al., 1991;Olesen et al., 1988), G proteins are activated (Gudi et al., 1996), IP_3 concentration shows a transient increase (Prasad et al., 1993;Rosales and Sumpio, 1992), neurotransmitters are released (Milner et al., 1990;Ralevic et al., 1990), and alteration of the ionic balance decreases the intracellular pH (Ziegelstein et al., 1992). Subsequent to these initial response, during the first minute after a step increase in shear, there is a release of PGI_2 prostaglandin (Frangos et al., 1985;Grabowski et al., 1985) and calcium-dependent nitric oxide (NO) (Cooke et al., 1991;Noris et al., 1995). As stress is sustained, a chronic response sets off signaling cascades that will lead to cell adaptation. Among others, the mitogen-activated protein (MAP) kinase signaling is initiated (Shyy et al., 1995;Tseng et al., 1995) through PKC and Ras pathways and the cytoskeleton reorganizes. Although many players have been identified, many signaling pathways are intertwined and orders and timescales of activation remain obscure. A complementary effect of flow could be the modulation of the local concentrations in extracellular molecules, thus modulating binding kinetics at membrane receptor sites (Tschumperlin et al., 2004). Interestingly, acute responses mimic receptor-binding responses, thus potentially sharing ensuing signaling cascades.

1.2.2 Plasma membrane mechanotransduction

The endothelial plasma membrane has been shown to be sensitive to shear stress through activation of potassium (Jacobs et al., 1995;Ohno et al., 1993;Olesen et al., 1988) and stretch-activated calcium (Naruse and Sokabe, 1993;Sigurdson et al., 1993) channels, phosphorylation of G proteins (Frangos and Gudi, 1997;Kuchan et al., 1994) and caveolae (Rizzo et al., 1998). Physical perturbations of the plasma membrane have elicited altered gene expression (Butler et al., 2002;Gudi et al., 1998). Although increases in lateral mobility of the lipid bilayer were also shown (Butler et al., 2001), the consequent mechanisms for signal transduction affecting membrane-bound proteins are not yet identified (Hamill and Martinac, 2001;Lee, 2004). Membrane fluidity affects G protein activation (Frangos and Gudi, 1997) and transmembrane proteins like calcium channels can be activated by increasing the plasma membrane tension (Naruse and Sokabe, 1993) – although the phenomenon could arguably be linked to increased lipid fluidity. Since fluid flow does not seem to reach the plasma membrane (Damiano et al., 2004;Secomb et al., 2001), it has been suspected that stress from the flow is carried directly from the glycocalyx to the actin cytoskeleton (Thi et al., 2004;Weinbaum et al., 2003). However, there are interactions between glycocalyx, actin cytoskeleton and membrane lipid domains. Possible candidates are domains associated with the glycocalyx: decreased lipid fluidity would come from an active or passive alteration of the packing and organization of lipid domains surrounding glypicans (Simons and Ikonen, 1997) and syndecans (Chu et al., 2004;Fuki et al., 2000;Tkachenko and Simons, 2002). Despite evidence that membrane domains may be mechanosensitive, no study to

date has aimed at looking at the effect of shear stress on lipid domains in endothelial plasma membranes.

1.3 Monitoring the effect of shear stress on cellular lipid membrane

1.3.1 Lipoid dyes to probe membrane dynamics

Biophysical studies are more apt to capture the dynamic nature of domains in cells and fluorescence labeling, in particular, seems to be the best way to accurately report lipid dynamic changes in response to shear stress. GM1-bound cholera toxin B has been used to track lipid raft diffusion in cells, but potential link of the ganglioside to the cortical cytoskeleton (Caroni, 2001;Seveau et al., 2001;Yoon et al., 2003) elicited a very low mobility and photobleaching of the dye (Bacia et al., 2004). Lipoid dyes, like dialkylindocarbocyanines (DiI), localize within the lipid bilayer (Gullapalli et al., 2008) and are good representatives of the lipid mobility. They confer very low cytotoxicity (De Clerck et al., 1994), particularly at low concentration. In model membranes, such as giant unilamellar vesicles (GUV), DiI-C_{12} preferably probes liquid phases and DiI-C_{18} gel phases (Klausner and Wolf, 1980;Spink et al., 1990). In cells, DiI-C_{12} remains in the fluid phase while DiI-C_{18} segregates in separate more ordered domains (Hao et al., 2001). Thus, DiI-C_{12} and DiI-C_{18} dyes are useful experimental tools to investigate domain dynamics because these dialkylindocarbocyanine dyes differ only by the length of their hydrocarbon chains. The interpretation of the change in bi-exponential fluorescence lifetime of the fluorophores with respect to the surrounding lipid phase is, therefore, more

straightforward and can be more definitively ascribed to changes in the domains they probe.

1.3.2 Confocal molecular dynamics microscope and time-correlated single photon counting for single-molecule studies in cells

The setup of a specific optical system was needed to record molecular dynamics in living cells under specific and controlled application of force. To successfully study the membrane response to shear, certain design criteria were specified: (i) probes need to be selective for certain organelles or molecules, (ii) the system spatial resolution should be able to capture subcellular events, and (iii) the system must be able to acquire data in live cells on cellular and molecular timescales.

Because cellular activity is mainly controlled by fluctuations in molecular concentration or activation state, it is likely that mechanotransduction may rise from similar cellular processes. Thus, we built an optical system to record molecular dynamics in living cells under specific and controlled application of force. The setup was designed as a confocal molecular dynamics microscope (CMDM) comprised of multimodal microscopy (differential interference contrast (DIC), epifluorescence and total internal reflection fluorescence (TIRF)) as well as integrated time-correlated single photon counting (TCSPC) for time-resolved fluorescence spectroscopy (Figure 1-3). Whole-field imaging is primarily used to check the integrity of the sample and for alignment with respect to the laser focus.

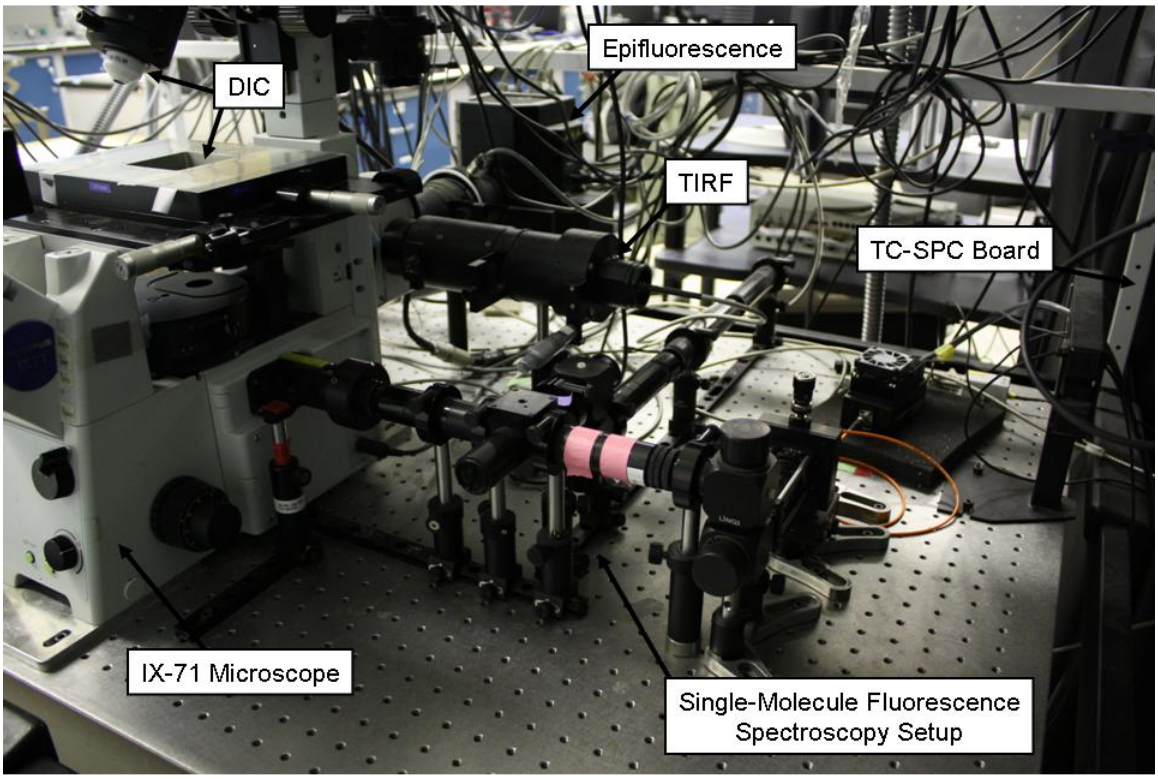

Figure 1-3: The confocal molecular dynamics microscope (CMDM) combines multimodal microscopy (DIC, epifluorescence and TIRF) with integrated time-correlated single photon counting (TCSPC), for time-resolved fluorescence spectroscopy (FCS, moment analysis from fluorescence fluctuations and fluorescence lifetime).

Fluorescence recovery after photobleaching (FRAP) has been used for lateral mobility measurements; however the dye concentrations used are very high (10-100 μM), increasing the propensity for cytotoxicity and the chance of dye molecules to aggregate. The technique also increases the local temperature in the membrane a hundred-fold and could cause dye endocytosis (Bacia et al., 2004). The TCSPC system can simultaneously collect data on relevant time scales spanning nanoseconds to seconds depending on the mode of analysis (e.g. lifetime or fluorescence correlation spectroscopy (FCS)). We use

TCSPC technology to obtain data on the expected transient nature of endothelial cell membrane response to shear stress (Butler et al., 2001;Davies, 1995;Gudi et al., 1996). With potential single-molecule detection level, arrival times of each fluorescence photon are collected with respect to the laser pulse time and with the beginning of the experiment. Processing of such data gives diffusion coefficients from FCS (Elson and Magde, 1974;Magde et al., 1974), an accurate number of fluorescent molecules and molecular brightness from moment analysis (Qian and Elson, 1990) and fluorescence lifetimes. TCSPC has been used in cell membrane studies involving FCS, Förster resonance energy transfer (FRET) and fluorescence lifetime imaging (FLIM) (Caiolfa et al., 2007;Davey et al., 2007;Duncan et al., 2004;Sharma et al., 2003), but only a few studies take advantage of the possibility of combining fluorescence lifetime and FCS from the same data in cells (Becker et al., 2006). Furthermore, to our knowledge, no cell study using time-dependent use of fluorescence correlation spectroscopy has been reported to date.

1.4 Main results of this study

In this study, we use a novel combination of time-correlated single photon counting techniques and multimodal microscopy to monitor the effect of fluid shear stress on different membrane domains in cultured endothelial cells. The main results are as follows. First, we built an optical setup for cellular fluorescence spectroscopy studies of mechanosensation. In order to track alterations in the physical properties of plasma membrane of cultured endothelial cells occurring at the molecular scale, adequate spatial

resolution was necessary to capture the local inhomogeneities of the cellular behavior. The timeframe of the measurement must also match that of the mechanotransduction event. FCS, moment analysis from fluorescence fluctuations and fluorescence lifetime are techniques combining both molecular and cellular spatial and time resolutions required for this particular study. Thus, the construction of an optical system allowing FCS and fluorescence lifetime measurements in cultured cells was completed.

Second we studied the effect of step shear on endothelial plasma membrane lipid dynamics and topography using domain-specific lipoid molecules and measurements of their fluorescence lifetimes, diffusion, and molecular brightness. Endothelial membrane lipid dynamics and their dependence on shear stress was monitored. No previous study has combined high spatial and temporal resolution, minimal invasiveness by the use of low dye concentration, and live cells to study the role of endothelial cell plasma membrane in mechanotransduction. FCS, molecular brightness analysis and fluorescence lifetime was used to monitor lateral diffusion, number of molecules and local packing fluctuations respectively of dye molecules embedded in the membrane. The study emphasized lipid domains heterogeneities with the use of domain-specific dyes DiI-C_{12} and DiI-C_{18}. We found that domains defined by DiI-C_{12} and DiI-C_{18} react to shear stress with differences in diffusion coefficients, fluorescence lifetimes, and number of molecules in the probe volume; results that can be explained by transient, domain-specific shear-induced changes in lipid viscosity, domain organization, and surface topography. These results are the first to demonstrate molecular scale mechanosensation in subcompartments of living intact cells under physiological mechanical stimulation.

1.5 References

1. Anderson, R. G. and K. Jacobson. 2002. A role for lipid shells in targeting proteins to caveolae, rafts, and other lipid domains. *Science* 296:1821-1825.

2. Bacia, K., D. Scherfeld, N. Kahya, and P. Schwille. 2004. Fluorescence correlation spectroscopy relates rafts in model and native membranes. *Biophys. J.* 87:1034-1043.

3. Bao, X., C. B. Clark, and J. A. Frangos. 2000. Temporal gradient in shear-induced signaling pathway: involvement of MAP kinase, c-fos, and connexin43. *Am. J. Physiol Heart Circ. Physiol* 278:H1598-H1605.

4. Becker, W., A. Bergmann, E. Haustein, Z. Petrasek, P. Schwille, C. Biskup, L. Kelbauskas, K. Benndorf, N. Klocker, T. Anhut, I. Riemann, and K. Konig. 2006. Fluorescence lifetime images and correlation spectra obtained by multidimensional time-correlated single photon counting. *Microscopy Research and Technique* 69:186-195.

5. Brown, D. A. and E. London. 1997. Structure of detergent-resistant membrane domains: does phase separation occur in biological membranes? *Biochem. Biophys. Res. Commun.* 240:1-7.

6. Brown, D. A. and J. K. Rose. 1992. Sorting of GPI-anchored proteins to glycolipid-enriched membrane subdomains during transport to the apical cell surface. *Cell* 68:533-544.

7. Burack, W. R., Q. Yuan, and R. L. Biltonen. 1993. Role of lateral phase separation in the modulation of phospholipase A2 activity. *Biochemistry* 32:583-589.

8. Butler, P. J., G. Norwich, S. Weinbaum, and S. Chien. 2001. Shear stress induces a time- and position-dependent increase in endothelial cell membrane fluidity. *Am. J. Physiol Cell Physiol* 280:C962-C969.

9. Butler, P. J., T. C. Tsou, J. Y. Li, S. Usami, and S. Chien. 2002. Rate sensitivity of shear-induced changes in the lateral diffusion of endothelial cell membrane lipids: a role for membrane perturbation in shear-induced MAPK activation. *FASEB J.* 16:216-218.

10. Caiolfa, V. R., M. Zamai, G. Malengo, A. Andolfo, C. D. Madsen, J. Sutin, M. A. Digman, E. Gratton, F. Blasi, and N. Sidenius. 2007. Monomer-dimer dynamics and distribution of GPI-anchored uPAR are determined by cell surface protein assemblies. *Journal of Cell Biology* 179:1067-1082.

11. Caroni, P. 2001. New EMBO members' review: actin cytoskeleton regulation through modulation of PI(4,5)P(2) rafts. *EMBO J.* 20:4332-4336.

12. Chien, S. 2006. Molecular basis of rheological modulation of endothelial functions: importance of stress direction. *Biorheology* 43:95-116.

13. Chu, C. L., J. A. Buczek-Thomas, and M. A. Nugent. 2004. Heparan sulphate proteoglycans modulate fibroblast growth factor-2 binding through a lipid raft-mediated mechanism. *Biochem. J.* 379:331-341.

14. Cooke, J. P., Rossitch E Jr, N. A. Andon, J. Loscalzo, and V. J. Dzau. 1991. Flow activates an endothelial potassium channel to release an endogenous nitrovasodilator. *J. Clin. Invest* 88:1663-1671.

15. Damiano, E. R., D. S. Long, and M. L. Smith. 2004. Estimation of viscosity profiles using velocimetry data from parallel flows of linearly viscous fluids: application to microvascular haemodynamics. *Journal of Fluid Mechanics* 512:1-19.

16. Dan, N. and S. A. Safran. 1998. Effect of lipid characteristics on the structure of transmembrane proteins. *Biophys. J.* 75:1410-1414.

17. Davey, A. M., R. P. Walvick, Y. X. Liu, A. A. Heikal, and E. D. Sheets. 2007. Membrane order and molecular dynamics associated with IgE receptor cross-linking in mast cells. *Biophysical Journal* 92:343-355.

18. Davies, P. F. 1997. Overview: temporal and spatial relationships in shear stress-mediated endothelial signalling. *J. Vasc. Res.* 34:208-211.

19. Davies, P. F. 1995. Flow-mediated endothelial mechanotransduction. *Physiol Rev.* 75:519-560.

20. Davies, P. F., K. A. Barbee, M. V. Volin, A. Robotewskyj, J. Chen, L. Joseph, M. L. Griem, M. N. Wernick, E. Jacobs, D. C. Polacek, N. dePaola, and A. I. Barakat. 1997. Spatial relationships in early signaling events of flow-mediated endothelial mechanotransduction. *Annu. Rev. Physiol* 59:527-549.

21. Davies, P. F., D. C. Polacek, J. S. Handen, B. P. Helmke, and N. dePaola. 1999. A spatial approach to transcriptional profiling: mechanotransduction and the focal origin of atherosclerosis. *Trends Biotechnol.* 17:347-351.

22. De Clerck, L. S., C. H. Bridts, A. M. Mertens, M. M. Moens, and W. J. Stevens. 1994. Use of fluorescent dyes in the determination of adherence of human leucocytes to endothelial cells and the effect of fluorochromes on cellular function. *J. Immunol. Methods* 172:115-124.

23. dePaola, N., M. A. Gimbrone, Jr., P. F. Davies, and C. F. Dewey, Jr. 1992. Vascular endothelium responds to fluid shear stress gradients. *Arterioscler. Thromb.* 12:1254-1257.

24. Dietrich, C., L. A. Bagatolli, Z. N. Volovyk, N. L. Thompson, M. Levi, K. Jacobson, and E. Gratton. 2001. Lipid rafts reconstituted in model membranes. *Biophys. J.* 80:1417-1428.

25. Duncan, R. R., A. Bergmann, M. A. Cousin, D. K. Apps, and M. J. Shipston. 2004. Multi-dimensional time-correlated single photon counting (TCSPC) fluorescence lifetime imaging microscopy (FLIM) to detect FRET in cells. *Journal of Microscopy-Oxford* 215:1-12.

26. Elson, E. L. and D. Magde. 1974. Fluorescence Correlation Spectroscopy .1. Conceptual Basis and Theory. *Biopolymers* 13:1-27.

27. Florian, J. A., J. R. Kosky, K. Ainslie, Z. Pang, R. O. Dull, and J. M. Tarbell. 2003. Heparan sulfate proteoglycan is a mechanosensor on endothelial cells. *Circ. Res.* 93:e136-e142.

28. Frangos, J. A., S. G. Eskin, L. V. McIntire, and C. L. Ives. 1985. Flow effects on prostacyclin production by cultured human endothelial cells. *Science* 227:1477-1479.

29. Frangos, J. A. and S. R. Gudi. 1997. Shear Stress Activates Reconstituted G-Proteins in the Absence of Protein Receptors By Modulating Lipid Bilayer Fluidity. A521.

30. Frangos, J. A., T. Y. Huang, and C. B. Clark. 1996. Steady shear and step changes in shear stimulate endothelium via independent mechanisms--superposition of transient and sustained nitric oxide production. *Biochem. Biophys. Res. Commun.* 224:660-665.

31. Fujiwara, K., M. Masuda, M. Osawa, Y. Kano, and K. Katoh. 2001. Is PECAM-1 a mechanoresponsive molecule? *Cell Struct. Funct.* 26:11-17.

32. Fuki, I. V., M. E. Meyer, and K. J. Williams. 2000. Transmembrane and cytoplasmic domains of syndecan mediate a multi-step endocytic pathway involving detergent-insoluble membrane rafts. *Biochem. J.* 351 Pt 3:607-612.

33. Galbraith, C. G., R. Skalak, and S. Chien. 1998. Shear stress induces spatial reorganization of the endothelial cell cytoskeleton. *Cell Motil. Cytoskeleton* 40:317-330.

34. Giorgione, J. R., R. Kraayenhof, and R. M. Epand. 1998. Interfacial membrane properties modulate protein kinase C activation: role of the position of acyl chain unsaturation. *Biochemistry* 37:10956-10960.

35. Girard, P. R. and R. M. Nerem. 1993. Endothelial cell signaling and cytoskeletal changes in response to shear stress. *Front Med. Biol. Eng* 5:31-36.

36. Girard, P. R. and R. M. Nerem. 1995. Shear stress modulates endothelial cell morphology and F-actin organization through the regulation of focal adhesion-associated proteins. *J. Cell Physiol* 163:179-193.

37. Goligorsky, M. S. 1988. Mechanical stimulation induces Ca2+i transients and membrane depolarization in cultured endothelial cells. Effects on Ca2+i in co-perfused smooth muscle cells. *FEBS Lett.* 240:59-64.

38. Grabowski, E. F., E. A. Jaffe, and B. B. Weksler. 1985. Prostacyclin production by cultured endothelial cell monolayers exposed to step increases in shear stress. *J. Lab Clin. Med.* 105:36-43.

39. Gudi, S., J. P. Nolan, and J. A. Frangos. 1998. Modulation of GTPase activity of G proteins by fluid shear stress and phospholipid composition. *Proc. Natl. Acad. Sci. U. S. A* 95:2515-2519.

40. Gudi, S. R., C. B. Clark, and J. A. Frangos. 1996. Fluid flow rapidly activates G proteins in human endothelial cells. Involvement of G proteins in mechanochemical signal transduction. *Circ. Res.* 79:834-839.

41. Gullapalli, R. R., M. C. Demirel, and P. J. Butler. 2008. Molecular dynamics simulations of DiI-C18(3) in a DPPC lipid bilayer. *Phys. Chem. Chem. Phys.* 10:3548-3560.

42. Hamill, O. P. and B. Martinac. 2001. Molecular basis of mechanotransduction in living cells. *Physiol Rev.* 81:685-740.

43. Hao, M., S. Mukherjee, and F. R. Maxfield. 2001. Cholesterol depletion induces large scale domain segregation in living cell membranes. *Proc. Natl. Acad. Sci. U. S. A* 98:13072-13077.

44. Honda, H. M., T. Hsiai, C. M. Wortham, M. Chen, H. Lin, M. Navab, and L. L. Demer. 2001. A complex flow pattern of low shear stress and flow reversal promotes monocyte binding to endothelial cells. *Atherosclerosis* 158:385-390.

45. Hwang, J., L. A. Gheber, L. Margolis, and M. Edidin. 1998. Domains in cell plasma membranes investigated by near-field scanning optical microscopy. *Biophys. J.* 74:2184-2190.

46. Jacobs, E. R., C. Cheliakine, D. Gebremedhin, E. K. Birks, P. F. Davies, and D. R. Harder. 1995. Shear activated channels in cell-attached patches of cultured bovine aortic endothelial cells. *Pflugers Arch.* 431:129-131.

47. Jacobson, K. and C. Dietrich. 1999. Looking at lipid rafts? *Trends Cell Biol.* 9:87-91.

48. Kenworthy, A. K., N. Petranova, and M. Edidin. 2000. High-resolution FRET microscopy of cholera toxin B-subunit and GPI-anchored proteins in cell plasma membranes. *Mol. Biol. Cell* 11:1645-1655.

49. Kim, D. W., B. L. Langille, M. K. Wong, and A. I. Gotlieb. 1989. Patterns of endothelial microfilament distribution in the rabbit aorta in situ. *Circ. Res.* 64:21-31.

50. Klausner, R. D. and D. E. Wolf. 1980. Selectivity of fluorescent lipid analogues for lipid domains. *Biochemistry* 19:6199-6203.

51. Ku, D. N., D. P. Giddens, C. K. Zarins, and S. Glagov. 1985. Pulsatile flow and atherosclerosis in the human carotid bifurcation. Positive correlation between plaque location and low oscillating shear stress. *Arteriosclerosis* 5:293-302.

52. Kuchan, M. J., H. Jo, and J. A. Frangos. 1994. Role of G proteins in shear stress-mediated nitric oxide production by endothelial cells. *Am. J. Physiol* 267:C753-C758.

53. Lee, A. G. 2004. How lipids affect the activities of integral membrane proteins. *Biochim. Biophys. Acta* 1666:62-87.

54. Lee, G. M., F. Zhang, A. Ishihara, C. L. McNeil, and K. A. Jacobson. 1993. Unconfined lateral diffusion and an estimate of pericellular matrix viscosity revealed by measuring the mobility of gold-tagged lipids. *J. Cell Biol.* 120:25-35.

55. Li, S., M. Kim, Y. L. Hu, S. Jalali, D. D. Schlaepfer, T. Hunter, S. Chien, and J. Y. Shyy. 1997. Fluid shear stress activation of focal adhesion kinase. Linking to mitogen-activated protein kinases. *J. Biol. Chem.* 272:30455-30462.

56. Lipowsky, R. 1995. Structure and dynamics of Membranes.

57. Magde, D., E. L. Elson, and W. W. Webb. 1974. Fluorescence Correlation Spectroscopy .2. Experimental Realization. *Biopolymers* 13:29-61.

58. Milner, P., K. A. Kirkpatrick, V. Ralevic, V. Toothill, J. Pearson, and G. Burnstock. 1990. Endothelial cells cultured from human umbilical vein release ATP, substance P and acetylcholine in response to increased flow. *Proc. Biol. Sci.* 241:245-248.

59. Mochizuki, S., H. Vink, O. Hiramatsu, T. Kajita, F. Shigeto, J. A. Spaan, and F. Kajiya. 2003. Role of hyaluronic acid glycosaminoglycans in shear-induced endothelium-derived nitric oxide release. *Am. J. Physiol Heart Circ. Physiol* 285:H722-H726.

60. Mouritsen, O. G. and M. Bloom. 1993. Models of lipid-protein interactions in membranes. *Annu. Rev. Biophys. Biomol. Struct.* 22:145-171.

61. Munro, S. 2003. Lipid rafts: elusive or illusive? *Cell* 115:377-388.

62. Naruse, K. and M. Sokabe. 1993. Involvement of stretch-activated ion channels in Ca2+ mobilization to mechanical stretch in endothelial cells. *Am. J. Physiol* 264:C1037-C1044.

63. Nerem, R. M., M. J. Levesque, and J. F. Cornhill. 1981. Vascular endothelial morphology as an indicator of the pattern of blood flow. *J. Biomech. Eng* 103:172-176.

64. Noris, M., M. Morigi, R. Donadelli, S. Aiello, M. Foppolo, M. Todeschini, S. Orisio, G. Remuzzi, and A. Remuzzi. 1995. Nitric oxide synthesis by cultured endothelial cells is modulated by flow conditions. *Circ. Res.* 76:536-543.

65. Ohno, M., G. H. Gibbons, V. J. Dzau, and J. P. Cooke. 1993. Shear stress elevates endothelial cGMP. Role of a potassium channel and G protein coupling. *Circulation* 88:193-197.

66. Olesen, S. P., D. E. Clapham, and P. F. Davies. 1988. Haemodynamic shear stress activates a K+ current in vascular endothelial cells. *Nature* 331:168-170.

67. Orr, A. W., B. P. Helmke, B. R. Blackman, and M. A. Schwartz. 2006. Mechanisms of mechanotransduction. *Dev. Cell* 10:11-20.

68. Pahakis, M. Y., J. R. Kosky, R. O. Dull, and J. M. Tarbell. 2007. The role of endothelial glycocalyx components in mechanotransduction of fluid shear stress. *Biochem. Biophys. Res. Commun.* 355:228-233.

69. Prasad, A. R., S. A. Logan, R. M. Nerem, C. J. Schwartz, and E. A. Sprague. 1993. Flow-related responses of intracellular inositol phosphate levels in cultured aortic endothelial cells. *Circ. Res.* 72:827-836.

70. Pries, A. R., T. W. Secomb, and P. Gaehtgens. 2000. The endothelial surface layer. *Pflugers Arch.* 440:653-666.

71. Qian, H. and E. L. Elson. 1990. On the analysis of high order moments of fluorescence fluctuations. *Biophys. J.* 57:375-380.

72. Ralevic, V., P. Milner, O. Hudlicka, F. Kristek, and G. Burnstock. 1990. Substance P is released from the endothelium of normal and capsaicin-treated rat hind-limb vasculature, in vivo, by increased flow. *Circ. Res.* 66:1178-1183.

73. Rietveld, A. and K. Simons. 1998. The differential miscibility of lipids as the basis for the formation of functional membrane rafts. *Biochim. Biophys. Acta* 1376:467-479.

74. Risau, W. 1995. Differentiation of endothelium. *FASEB J.* 9:926-933.

75. Rizzo, V., A. Sung, P. Oh, and J. E. Schnitzer. 1998. Rapid mechanotransduction in situ at the luminal cell surface of vascular endothelium and its caveolae. *J. Biol. Chem.* 273:26323-26329.

76. Rosales, O. R. and B. E. Sumpio. 1992. Changes in cyclic strain increase inositol trisphosphate and diacylglycerol in endothelial cells. *Am. J. Physiol* 262:C956-C962.

77. Saxton, M. J. and K. Jacobson. 1997. Single-particle tracking: applications to membrane dynamics. *Annu. Rev. Biophys. Biomol. Struct.* 26:373-399.

78. Schutz, G. J. and P. Hinterdorfer. 2002. Single molecule fluorescence and force microscopy. *Exp. Gerontol.* 37:1495-1511.

79. Secomb, T. W., R. Hsu, and A. R. Pries. 2001. Effect of the endothelial surface layer on transmission of fluid shear stress to endothelial cells. *Biorheology* 38:143-150.

80. Seveau, S., R. J. Eddy, F. R. Maxfield, and L. M. Pierini. 2001. Cytoskeleton-dependent membrane domain segregation during neutrophil polarization. *Mol. Biol. Cell* 12:3550-3562.

81. Sharma, M. R., E. C. Koc, P. P. Datta, T. M. Booth, L. L. Spremulli, and R. K. Agrawal. 2003. Structure of the mammalian mitochondrial ribosome reveals an expanded functional role for its component proteins. *Cell* 115:97-108.

82. Sheets, E. D., G. M. Lee, R. Simson, and K. Jacobson. 1997. Transient confinement of a glycosylphosphatidylinositol-anchored protein in the plasma membrane. *Biochemistry* 36:12449-12458.

83. Shyy, J. Y., M. C. Lin, J. Han, Y. Lu, M. Petrime, and S. Chien. 1995. The cis-acting phorbol ester "12-O-tetradecanoylphorbol 13-acetate"-responsive element is involved in shear stress-induced monocyte chemotactic protein 1 gene expression. *Proc. Natl. Acad. Sci. U. S. A* 92:8069-8073.

84. Sigurdson, W. J., F. Sachs, and S. L. Diamond. 1993. Mechanical perturbation of cultured human endothelial cells causes rapid increases of intracellular calcium. *Am. J. Physiol* 264:H1745-H1752.

85. Simons, K. and E. Ikonen. 1997. Functional rafts in cell membranes. *Nature* 387:569-572.

86. Simons, K. and D. Toomre. 2000. Lipid rafts and signal transduction. *Nat. Rev. Mol. Cell Biol.* 1:31-39.

87. Smart, E. J., G. A. Graf, M. A. McNiven, W. C. Sessa, J. A. Engelman, P. E. Scherer, T. Okamoto, and M. P. Lisanti. 1999. Caveolins, liquid-ordered domains, and signal transduction. *Mol. Cell Biol.* 19:7289-7304.

88. Spink, C. H., M. D. Yeager, and G. W. Feigenson. 1990. Partitioning Behavior of Indocarbocyanine Probes Between Coexisting Gel and Fluid Phases in Model Membranes. *Biochimica et Biophysica Acta* 1023:25-33.

89. Subczynski, W. K. and A. Kusumi. 2003. Dynamics of raft molecules in the cell and artificial membranes: approaches by pulse EPR spin labeling and single molecule optical microscopy. *Biochim. Biophys. Acta* 1610:231-243.

90. Takahashi, M., T. Ishida, O. Traub, M. A. Corson, and B. C. Berk. 1997. Mechanotransduction in endothelial cells: temporal signaling events in response to shear stress. *J. Vasc. Res.* 34:212-219.

91. Thi, M. M., J. M. Tarbell, S. Weinbaum, and D. C. Spray. 2004. The role of the glycocalyx in reorganization of the actin cytoskeleton under fluid shear stress: a "bumper-car" model. *Proc. Natl. Acad. Sci. U. S. A* 101:16483-16488.

92. Tkachenko, E., J. M. Rhodes, and M. Simons. 2005. Syndecans: new kids on the signaling block. *Circ. Res.* 96:488-500.

93. Tkachenko, E. and M. Simons. 2002. Clustering induces redistribution of syndecan-4 core protein into raft membrane domains. *J. Biol. Chem.* 277:19946-19951.

94. Tschumperlin, D. J., G. Dai, I. V. Maly, T. Kikuchi, L. H. Laiho, A. K. McVittie, K. J. Haley, C. M. Lilly, P. T. So, D. A. Lauffenburger, R. D. Kamm, and J. M. Drazen. 2004. Mechanotransduction through growth-factor shedding into the extracellular space. *Nature* 429:83-86.

95. Tseng, H., T. E. Peterson, and B. C. Berk. 1995. Fluid shear stress stimulates mitogen-activated protein kinase in endothelial cells. *Circ. Res.* 77:869-878.

96. Vance, D. E. and J. E. Vance. 2002. Biochemistry of Lipids, Lipoproteins and Membranes. Elsevier.

97. Vereb, G., J. Matko, G. Vamosi, S. M. Ibrahim, E. Magyar, S. Varga, J. Szollosi, A. Jenei, R. Gaspar, Jr., T. A. Waldmann, and S. Damjanovich. 2000. Cholesterol-dependent clustering of IL-2Ralpha and its colocalization with HLA and CD48 on T lymphoma cells suggest their functional association with lipid rafts. *Proc. Natl. Acad. Sci. U. S. A* 97:6013-6018.

98. Weinbaum, S. and S. Chien. 1993. Lipid transport aspects of atherogenesis. *J. Biomech. Eng* 115:602-610.

99. Weinbaum, S., X. Zhang, Y. Han, H. Vink, and S. C. Cowin. 2003. Mechanotransduction and flow across the endothelial glycocalyx. *Proc. Natl. Acad. Sci. U. S. A* 100:7988-7995.

100. Yoon, S. S., K. I. Jung, Y. L. Choi, E. Y. Choi, I. S. Lee, S. H. Park, and T. J. Kim. 2003. Engagement of CD99 triggers the exocytic transport of ganglioside GM1 and the reorganization of actin cytoskeleton. *FEBS Lett.* 540:217-222.

101. Zarins, C. K., D. P. Giddens, B. K. Bharadvaj, V. S. Sottiurai, R. F. Mabon, and S. Glagov. 1983. Carotid bifurcation atherosclerosis. Quantitative correlation of plaque localization with flow velocity profiles and wall shear stress. *Circ. Res.* 53:502-514.

102. Ziegelstein, R. C., L. Cheng, and M. C. Capogrossi. 1992. Flow-dependent cytosolic acidification of vascular endothelial cells. *Science* 258:656-659.

Chapter 2

MULTIMODAL IMAGING AND TIME-CORRELATED FLUORESCENCE SPECTROSCOPY SETUP FOR MECHANOTRANSDUCTION STUDIES

Foreword

The following chapter is taken from the manuscript: "Integrated multimodal microscopy, time-resolved fluorescence, and optical-trap rheometry: toward single molecule mechanobiology", Gullapalli RR, Tabouillot T, Mathura R, Dangaria JH, and Butler PJ, Journal of Biomedical Optics, 12: 014012, 2007.

2.1 Introduction

Biological cells convert forces to intracellular biochemical signaling cascades by mechanotransduction, a process that is responsible for diverse physiological phenomena including bone and vascular wall remodeling, vascular caliber control, and embryonic development (Orr et al., 2006). In contrast, atherosclerosis, sensory dysfunction in diabetes mellitus, and hair cell damage in the inner ear leading to vertigo are examples of cellular mechanical regulatory processes gone awry (Ingber, 2003). Physiological forces arise from blood flow-induced shear stresses, hydrostatic pressure, extracellular matrix deformations, intracellular contractions, and osmotic swelling. The length-scale of these forces spans single molecules, cellular organelles, cells, tissues, organs, and physiological systems; the time-scales span nanoseconds to days (Davies, 1997) .

The essential ingredients to a comprehensive understanding of mechanotransduction are a well-defined force, cellular mechanical properties, and a physiological readout directly related to the force. Well-defined forces arise from fluid flow (Barbee et al., 1995), atomic force microscopes (Mathur et al., 2000;Trache and Meininger, 2005), optical traps (Wang et al., 2005), and magnetic vedas (Huang et al., 2002). Cellular deformations to these forces can be modeled using continuum mechanics (Charras and Horton, 2002;Ferko et al., 2006b;Huang et al., 2002), or ultrastructural characterization of load-bearing structures (Osborn et al., 2006;Sultan et al., 2004;Wang and Suo, 2005). Examples of readouts of force-induced physiological responses include calcium signaling (Geiger et al., 1992), ion channel activity (Levitan et al., 2000), phosphorylation of proteins (Li et al., 1997), and transcription of new RNA(McCormick et al., 2001). A major challenge in mechanotransduction is to differentiate mechanosensors (cellular structures which are perturbed by physical forces), mechanotransducers (molecules which undergo biochemical changes in response to force and initiate signaling cascades), and mechanobiology (the resultant changes in cellular structure and function).

Analysis of single-molecules in cells subjected to force can provide the link between force and mechanotransduction. Major technical and computational advances in analysis of fluorescence fluctuations provide new methods to assess single-molecule dynamics in model and cellular systems (Hess et al., 2002;Vukojevic et al., 2005). For example, time-correlated single photon counting (TCSPC) instrumentation is available on a single compact PCI-card which, when integrated with pulsed and continuous wave-lasers, can be used to assess nanosecond- to second- scale dynamics of single fluorescent

molecules. Analysis methods including fluorescence correlation spectroscopy (FCS) and fluorescence lifetime can then be used to gain information on diffusion, conformational changes, aggregation, chemical kinetics and other important biomolecular phenomena (Vukojevic et al., 2005;Hess et al., 2002).

In this chapter, we describe the construction and calibration of a confocal molecular dynamics microscope (CMDM) capable of (i) applying cell-scale forces using micropipette aspiration, optical traps, and fluid flow, (ii) assessing cellular mechanical properties using optical trap and particle-tracking microrheology, and (iii) correlating molecular-scale physiological readouts from TCSPC with cellular structures imaged with multimodal microscopy. The intended application of this system is to assess force-induced changes in dynamics of molecules occurring on a time scale of nanoseconds, while addressing long-term adaptive responses of cells on the order of hours. It is anticipated that these new tools will enable a comprehensive analysis of cellular mechanobiology and lead to major clinical advances in treating or preventing diseases such as atherosclerosis which have their origins in mechanotransduction (Ingber, 2003).

We begin with a background on the theory of fluorescence correlation spectroscopy (FCS), optical traps, and multimodal microscopy. We then describe the detailed construction and implementation of the CMDM. Finally, we present results of calibration experiments in which molecular diffusion is analyzed in solutions and in model and cellular membranes.

2.2 Background

2.2.1 Fluorescence Correlation Spectroscopy

The detection of single molecules in femtoliter volumes was made possible by the development of confocal optics, high-sensitivity detectors, and robust fluorophores (Haustein and Schwille, 2003). Probe molecules move into and out of a confocal volume yielding fluorescence fluctuations (Figure 2-1). Autocorrelation analysis of these fluctuations can provide diffusion coefficients and other single-molecule information (Elson and Magde, 1974;Magde et al., 1974).

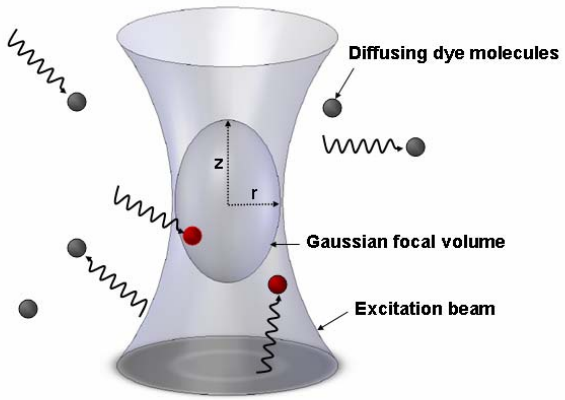

Figure 2-1: Confocal volume for fluorescence correlation spectroscopy. The radial dimension, *r*, of the confocal volume is close to the diffraction limit of the objective and is determined by keeping the (*r*/*z*) parameter constant (<10) in Eq. **2.6** when fitting the autocorrelation curve from R6G molecules in water. The radius thus obtained from experiment is 277 ± 10 nm. Fluorescent molecules are excited by the entire laser beam and fluorescence emission is only collected in the confocal volume. When particles move in and out of the confocal volume in x,y and z directions, 3-D diffusion is considered. When particles only move in x-y plane, 2-D diffusion is considered.

In the following analysis, we consider the relationship between autocorrelation of fluorescence fluctuations and molecular diffusion. We start with the Stokes-Einstein relationship for the diffusion coefficient, D, of a sphere with a hydrodynamics radius, R, in a solvent of viscosity, η (Eq. 2.1):

$$D = \frac{k_B T}{6\pi\eta R} \tag{2.1}$$

where k_B is the Boltzmann constant, and T is absolute temperature. We define a characteristic molecular diffusion transit time, τ_D, across a small area of radius, r, such that (Eq. 2.2):

$$r^2 = 4D\tau_D \tag{2.2}$$

Under conditions of equilibrium, the fluorescence fluctuates around an average value $\langle F \rangle$, due to diffusion. The intensity of these fluctuations, $\delta F(t)$, can be autocorrelated to obtain the autocorrelation function, $G(\tau)$, given by (Eq. 2.3),

$$G(\tau) = \frac{\langle \delta F(t+\tau)\delta F(t) \rangle}{\langle F(t) \rangle} \tag{2.3}$$

where t (time) and τ (lag time) vary over all times of the data collection period. The fluorescence fluctuations are related to the instantaneous change in concentration in the observation volume, $\delta C(r,t)$. To relate the autocorrelation function to diffusion, we use the diffusion equation (Eq. 2.4):

$$D\nabla^2 \delta C(r,t) = \frac{\partial \delta C(r,t)}{\partial t} \tag{2.4}$$

and the relationship between fluorescence fluctuations and concentration of the fluorescent molecules in the confocally-defined optical probe volume (Eq. 2.5):

$$\delta F(t) = K \int_{Volume} \delta C(r,t) I(r) \theta(r) \qquad 2.5$$

where $I(r)$ is the excitation intensity profile, $\theta(r)$ is the collection efficiency profile, and K is a proportionality constant. The confocal probe volume is created by placing a small aperture (pinhole or fiber optic) in an image plane that is conjugate to the focus of a high numerical-aperture, infinity-corrected objective. The laser beam has a Gaussian intensity profile that fills the back aperture of the objective, leading to a Gaussian illumination profile, $I(r)$, such that $I(r) = I_0 e^{-r^2/z^2}$ where r and z are the probe volume radius and height, respectively, and are defined as the point where the intensity falls of to $1/e^2$ of the maximum (center) intensity (Figure 2-1). A single constant factor known as the structure factor, ω, is defined as the ratio of z / r. The autocorrelation obtained from the experiment and its relation to the theoretical Gaussian confocal volume and the characteristic diffusion time is (Eq. 2.6) (Elson and Magde, 1974;Magde et al., 1974;Zander et al., 2002):

$$G(\tau) = \frac{1}{N}\left(\frac{1}{1+\left(\tau/\tau_D\right)}\right)\left(\frac{1}{1+\left(1/\omega\right)^2\left(\tau/\tau_D\right)}\right)^{1/2} \qquad 2.6$$

where N is the average number of diffusing fluorophores in the confocal volume. The number of fluorescent molecules present in the sample volume is the inverse of the term $G(0)$.

The relationship between the autocorrelation function and diffusion on 2-dimensional structures (e.g. plasma membrane) is given by Eq. 2.7:

$$G(\tau) = \frac{1}{N} \cdot \left(\frac{1}{1 + \left(\tau / \tau_D \right)} \right) \qquad 2.7$$

This measurement in two dimensions can be extended to include multicomponent diffusion of multiple non-interacting species of fluorescent molecules, according to Eq. 2.8:

$$G(\tau) = \sum_{i=1}^{n} b_i \left(\frac{1}{1 + \left(\tau / \tau_{Di} \right)} \right) \qquad 2.8$$

where b_i is the relative proportion of the non-interacting diffusing molecules.

In the case of two-dimensional anomalous diffusion (e.g. in a cellular membrane), the time-dependence of the mean square displacements is not linear but of the form $\langle \Delta r^2 \rangle = \Gamma \tau^{\alpha}$, and the autocorrelation is given by Eq. 2.9 (Schwille et al., 1999c):

$$G(\tau) = \frac{1}{N} \cdot \frac{1}{1 + \Gamma \tau^{\alpha} / r^2} \qquad 2.9$$

where Γ is the transport coefficient and α is the temporal exponent with values between zero and one. For a more comprehensive description of FCS including analysis of other sources of fluorescence fluctuations and detailed derivations of the equations presented here, the reader is referred to the excellent book by Zander *et al* (Zander et al., 2002).

2.2.2 Fluorescence Lifetime

Time-resolved fluorescence lifetime spectroscopy enables analysis of subtle changes in photophysics of fluorescent molecules (Lakowicz, 1999). When a fluorescent molecule is excited to a higher energy state using a picosecond pulse of laser light, it remains in the excited state for a finite time before it decays to the ground level energy state. Using a high-frequency pulsed laser, histograms of photon emission times relative to excitation times can be generated and fit with a negative exponential (or multiple exponentials) with a characteristic decay time (or lifetime), τ, (different from the characteristic diffusion time, τ_D, of FCS). Fluorescence lifetime depends on local molecular microenvironmental factors including ionic strength, hydration, oxygen concentration, binding to macromolecules and the proximity to other molecules that can deplete the excited state by resonance energy transfer (Lakowicz, 1999). The fluorescence lifetime and quantum yield are related to intrinsic photophysical characteristics of a fluorescent molecule such as radiative and non-radiative decay mechanisms. The fluorescence quantum yield, Q, is the ratio of the number of photons emitted to the number of photons absorbed, according to Eq. 2.10:

$$Q = \frac{k_r}{k_r + k_{nr}} \qquad 2.10$$

where k_r and k_{nr} are the radiative and non-radiative decay rates of the molecule, respectively. Fluorescence lifetime is given by Eq. 2.11:

$$\tau = \frac{1}{k_r + k_{nr}} \qquad 2.11$$

The value for k_{nr} is dependent on the mode of the non-radiative decay, such as collisional quenching, hydration, and vibrational relaxation. Thus, any alteration of the k_{nr} parameter also leads to a detectable change in the value of lifetime.

The value for lifetime is obtained by an iterative reconvolution of an instrument response function (IRF) with the fluorescence intensity using an assumed decay law, which can be approximated by a sum of exponentials Eq. 2.12 (Lakowicz, 1999):

$$I(t) = \sum_i \alpha_i \exp(-t/\tau_i) \qquad 2.12$$

where α_i is the fraction of molecules with lifetime τ_i, normalized to unity. Fluorescence lifetimes are independent of fluorescence probe concentrations and can provide information not obtainable from intensity variations alone. When polarized light is used to excite a molecule whose excitation dipole is oriented parallel to the polarization of the pulse, it is possible to separate the parallel and perpendicular components of the emitted fluorescence signal and to extract rotational diffusion constants (Lakowicz, 1999).

2.2.3 Optical Trap

Optical traps apply pN-level forces to small beads or organelles using momentum transfer from focused laser light. Although the ability of light to apply forces to matter was discovered by 1873 by James C. Maxwell, it is only in the last two decades that laser and optics developments permitted application of optical trapping forces to cells and molecules (Neuman and Block, 2004;Yanai et al., 2004). Briefly, the energy carried as momentum by a traveling photon is translated into a net force on an object hit by that

photon. The integrated photonic force on a particle in a Gaussian laser beam is given by Eq. 2.13 (Simmons et al., 1996;Hough and Ou-Yang, 1999):

$$\begin{aligned}\vec{F} &= -\alpha \frac{n_1 V}{cR^2}\left(\frac{{n_2}^2 - {n_1}^2}{{n_2}^2 + 2{n_1}^2}\right) I_0 e^{-r^2/R^2} r\hat{r} \\ &\equiv -k_{ot} r e^{-r^2/R^2}\hat{r}\end{aligned} \qquad 2.13$$

where α is a geometrical factor of order one, n_1 and n_2 are the refractive indices of the surrounding medium and the particle, respectively, V is the volume of the bead, c is the speed of light in a vacuum, I_0 is the intensity of the incident light, r is the distance between the centers of the bead and laser beam, $\hat{r}$ is a unit vector, and R is the laser beam $1/e^2$ radius. In practice, when $r << R$, the trap acts as a linear spring for small displacements with a spring constant, k_{ot}, determined by equating the variance of 1-D displacements, $\left\langle (x - x_o)^2 \right\rangle$, with the thermal fluctuations according to the equipartition theorem (Eq. 2.14):

$$\tfrac{1}{2} k_{ot} \left\langle (x - x_o)^2 \right\rangle = \tfrac{1}{2} k_b T \qquad 2.14$$

where x_0 is the mean value of x, k_B is the Boltzmann constant (1.38×10^{-23} J/K), T is absolute temperature, and $\langle\ \rangle$ refers to the time average. Alternatively, the trap strength can be measured by quantifying the displacement of the bead due to applied force, F, (e.g. from fluid flow) (i.e. $F = k_{ot} x$) (Guilford et al., 1997).

2.2.4 Multimodal Microscopy

In order to correlate molecular-scale events with cellular structures and their locations, we have integrated TCSPC and an optical trap into a multimodal microscope consisting of differential interference contrast (DIC), total internal reflection fluorescence (TIRF), and epifluorescence microscopy followed by deconvolution using Autodeblur software (Autoquant, Albany, NY, USA). A 3-D piezoelectric stage provides high-resolution positioning, such that molecular-scale analysis can be associated with subcellular regions of live adherent cells. Much of this hardware is commercially available, making these techniques accessible to researchers in biology and mechanobiology. The engineering challenge is to integrate these modalities on a single platform. In response to this challenge, microscope manufactures have developed microscopes with multiple input and output ports and increased infinity space for the introduction of custom optics. To make this setup accessible to other researchers, we list all the component parts in Table 2-1. For detailed description of our multimodal microscopy setup the reader is referred to Ferko *et al* (Ferko et al., 2006b;Ferko et al., 2006a).

2.3 Instrumentation and Setup

In this section we describe the details of the microscope and associated optics. All parts, part numbers, and manufacturers are listed in Table 2-1 .

Table 2-1: Components used in construction of confocal molecular dynamics microscope (CMDM). The CMDM is comprised of modules for single molecule spectroscopy, multimodal microscopy, and an optical trap.

Components	Part Number and Supplier	Description
Microscope	IX-71 (Olympus, Tokyo, Japan)	Inverted microscope with left (camera), right (single-molecule fluorescence system) and back (epifluorescence & TIRFM) ports
Lasers	35-KAP-431-220 (Melles Griot, Carlsbad, CA, USA)	CW Argon/Krypton-ion laser with 476-676nm excitation; output power 4-20mW
	PicoTRAIN (High-Q Laser, Hohenems, Austria)	water-cooled 532nm, 80 MHz, 5.4 ps pulsed YAG laser; output power ~ 75mW
	BHL-150 (Becker & Hickl, Berlin, Germany)	650nm diode laser pulsed at 50MHz; output power 0.1mW to 2mW
Optical fibers	Kineflex-P-3-S-488/568/647-0.65-FCP (Point-Source, Southampton, UK)	Polarization-maintaining single-mode optical fiber for 488/514/647nm light
	M14L01 (Thorlabs, Newton, NJ, USA)	50µm-diameter 0.22NA optical fiber used as confocal pinhole
Microscope objectives	LUMPlanFl (Olympus, Tokyo, Japan)	60X water-immersion objective 0.9 NA, used as condenser for DIC
	UPLAPO60XW (Olympus, Tokyo, Japan)	60X universal plan apochromat water-immersion objective, NA 1.2, WD 0.25mm, correction collar for 0.13-0.21mm coverslips
	PLAPO60XO/TIRFM-2 (Olympus, Tokyo, Japan)	60X plan apochromat oil-immersion objective, NA 1.45, WD 0.15mm. High NA is needed for Total Internal Reflection Fluorescence Microscopy
Dichroic mirrors and interference filters	Z520/10X, Z650/20X (Chroma technology, Rockingham, VT, USA)	Excitation/clean-up filters for 520 & 650nm respectively
	Z520RDC-SP-POL, Z650RDC-SP-POL (Chroma technology, Rockingham, VT, USA)	Dichroic mirrors for S & P polarization at 520 & 650nm, respectively
	3RD560-640 (Omega Optical) XF3083/25 595AF60 (Omega Optical, Brattleboro, VT, USA)	Emission filters for 520nm (Omega) & 650nm (Chroma) 3RD560-640 (O.D.>8), 595AF60 & HQ700/75 (O.D.>6)
	HQ700/75 (Chroma technology, Rockingham, VT, USA)	
Neutral density filters	NT46-495 (Edmund Optics, Barrington, NJ, USA)	Linear ND filter fused silica, 11 steps, 0.04 to 2.0 optical density
Lenses and mirrors	F-LA15 (Newport, Irvine, CA, USA)	Diode laser collimating aspherical lens
	COL-UV/VIS-FCPC (Avantes, Broomfield, CO, USA)	UV/VIS/NIR collimating lens for optical fiber output with adjustable focus
	KPX021AR.14 KPX058.AR14 (Newport, Irvine, CA, USA)	Keplerian beam expander (31.8FL and 88.3FL respectively)
	KPX112AR.14 (Newport, Irvine, CA, USA)	300FL tube lens, focusing emission beam onto the fiber core (acting as confocal pinhole)
	34 0523 (Linos Photonics, Milford, MA, USA)	oval mirrors to align excitation and emission beams
Optical mounts	065235 065096 (Linos Photonics, Milford, MA, USA)	Beam deflector cubes c-mount with beam steerer mount
	MT1 ST1XY-D (Thorlabs, Newton, NJ, USA)	1/2" translation stage, XY translator with differential drives and various posts, post holders
	Edmund-Optics, Newport (Irvine, CA, USA)	Various c-mount tubing, rings, posts and post holders
Detectors	H7422-40P (Hamamatsu, Tokyo, Japan)	Photomultiplier tube 320-700nm wavelength range with quantum efficiency = 40% at 580nm
	SensiCamQE (Cooke, Romulus, MI, USA)	Peltier-cooled 12-bit digital CCD camera 500ns-3600s exposure time, read-out noise 4e-rms
TC-SPC system	SPC-630 (Becker & Hickl, Berlin, Germany)	TC-SPC card. 7ps time resolution, 125ns dead time, allows single-molecule measurements (lifetime/FCS/FCCS) with mulit-detector operations
	HFAC-26 (Becker & Hickl, Berlin, Germany)	1µA 26dB TC-SPC preamplifier
	HRT-81 (Becker & Hickl, Berlin, Germany)	8-channel TC-SPC router for PMTs
Microscope stage	NanoView & NanoDrive (Mad City Labs, Madison, WI, USA)	Manual micrometer 2-axis coarse positioning with a piezo-actuated 100x100x100µm 0.2nm resolution 3-axis nanopositioner; NanoDrive interfaces with National Instruments PCI-6071E board
Optical trap	iFLEX 1000 (Point Source, Southampton, UK)	830nm CW laser with output power 50mW
	COL-UV/VIS/NIR-FCPC (Avantes, Broomfield, CO, USA)	UV/VIS/NIR collimating lens for optical fiber output with adjustable focus
	LA1422-B LA1608-B (Thorlabs, Newton, NJ, USA)	Keplerian beam expander (40FL and 75FL respectively) with IR coating
	675DCSPXR (Omega Optical, Brattleboro, VT, USA)	Dichroic mirror 21X33mm at 675nm
	PDQDT-10S-SI (Noah, Melbourne, FL, USA)	Quadrant photodetector module, 1 × 1 mm total active area, 350 – 1100 nm spectral range
Computers	Precision 530 (Dell, Round Rock, TX, USA)	Dual Intel Xeon 2.0GHz CPU 1Gb RAM, hosts National Instruments PCI-6071E & PCI-6711 boards and Cooke board
	Optiplex GX 240 (Dell, Round Rock, TX, USA)	Intel P4 1.5GHz CPU 512Mb RAM, hosts Becker & Hickl SPC-630 TC-SPC board
Chambers and temperature control	FCS2 & controller (Bioptechs, Butler, PA, USA)	Focht live-cell chamber system with temperature controller
	Objective heater & controller (Bioptechs, Butler, PA, USA)	Objective heater with temperature controller
Optical table	VH36660W-OPT (Newport, Irvine, CA, USA)	Research-grade vibration-free optical table

2.3.1 Microscope, Optics, and Camera

The CMDM is based on an Olympus IX71 and associated optics firmly secured to a vibration table. In the diascopic light path, a 100 W halogen light provides brightfield illumination for phase contrast and DIC microscopy. Our DIC setup employs a high-NA objective (LUMPlanFl 60X/0.9 N.A, WD 0.9 mm) as a condenser to increase contrast over traditional condenser designs. We use a water-immersion objective (UPLAPO 60×/1.2 NA, WD 0.25 mm) or an oil-immersion objective (PLAPO 60×/1.45 NA, TIRFM-2, WD 0.15 mm) for DIC, FCS, fluorescence lifetime measurements, and TIRF (oil only).

For TIRF, laser light is fiber-coupled to the TIRF illuminator on one end of the epiport and is focused off-center on the back aperture of the objective. Due to the high NA (1.45) of the objective, the incoming light is transmitted to the glass coverslip at an angle greater than the critical angle and is internally reflected there, resulting in an evanescent wave of light that decays exponentially with distance away from the coverslip. The fluorescent molecules at this interface within a distance of 200 nm from the top of the coverslip are selectively excited. The angle of incidence of the laser beam at the interface is controlled by a micrometer on the TIRF illuminator attachment.

A CCD camera is attached to the left side-port of the microscope. The camera exhibits high resolution and sensitivity due to the small CCD sensor element size (1376 × 1040 pixels; 6.45 × 6.45 μm^2 pixel size), high quantum efficiency (65%) in the visible range, and a two-stage Peltier cooling system (capable of attaining a temperature of -11^{o}C). The cooling fan is placed remotely and connected to the camera by flexible plastic

tubing in order to minimize transmission of vibrations from the fan to the microscope. The camera has been modified with a fast shutter to enable the collection of two successive images with an interval of 500 ns.

2.3.2 Laser Sources

A continuous wave (CW) Krypton-Argon-ion laser with stable TEM_{00} mode laser light is used for both fluorescence correlation spectroscopy and TIRF illumination. The laser is air-cooled and is placed away from the main table to reduce the propagation of the vibrations from the cooling fan to the microscope. The laser contains a prism-based micrometer adjustment to deliver wavelengths of 476, 483, 488, 496, 514, 520, 530, 568, 647 and 676 nm. A fiber coupling system has four adjustable screws to align the fiber with the laser. Once the four screws are aligned properly, the fiber head can be removed interchangeably for use with multiple fibers. An additional red, pulsed-diode laser (λ = 650 nm) is used for time-resolved fluorescence lifetime and FCS experiments in the far red excitation wavelength range. The average power of the diode laser is 100 μW to 2 mW, with a repetition rate of 50 MHz and a pulse width of ~90 ps. For lifetime measurements on dyes in the green excitation wavelength range, we use a water-cooled 80 MHz, 5.4 ps, 75 mW, pulsed solid state laser (λ = 532 nm, High-Q Laser, Hohenems, Austria).

2.3.3 3-D Piezo-Stage and nm-scale Positioning

For high precision and high resolution 3-D positioning, we employ a piezoelectric microscope stage. The stage consists of a manual microstage and a 3-axis piezo nanostage with 100 μm of travel in each of three orthogonal directions. The nanostage can carry a load of up to 0.5 kg. Customized LabView code controls the movement of the nanostage and coordinates 3-D positioning of the focused laser beam with images from the camera.

2.3.4 Time-Correlated Single Photon Counting and Single-Molecule Fluorescence Spectroscopy

Fluorescence spectroscopy optics are connected to the right side-port of the microscope (Figure 2-2). The laser light exits the fiber, is expanded and collimated, reflects off the dichroic mirrors, and travels through the side-port to the objective, which defines the probe volume and collects emitted fluorescence. The beam diameter was matched to the objective back aperture (7.2 mm) to ensure a Gaussian excitation profile and full use of objective numerical aperture. Alternative beam parameters are discussed in Hess *et al* (Hess and Webb, 2002). A laser power of 90 μW measured at the objective back aperture ensures a good signal to noise ratio (SNR) without significant photobleaching or triplet state formation. Elimination of stray non-fluorescent light is assured using emission filters with attenuation optical densities (OD) of 6 or more. High-quality emission filters are necessary to ensure good signal-to-noise ratios in single-molecule experiments.

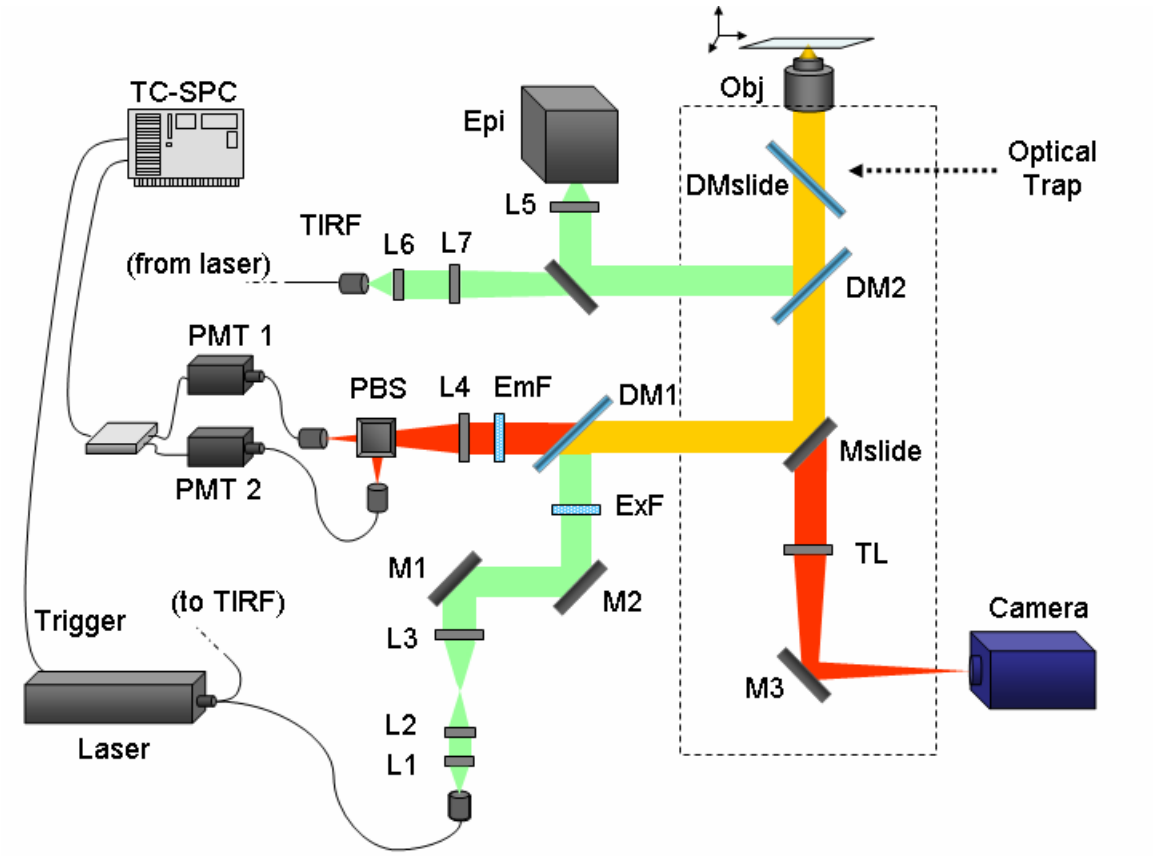

Figure 2-2: Optical setup. The Kr/Ar-ion or Pulsed Nd:YAG laser beam is transmitted via fiber coupling to the TIRF or confocal port. For confocal illumination, upon exiting the fiber, the beam is collimated with lens L1, expanded by L2 and L3, steered by the mirrors M1 and M2, reflected off the dichroic mirror (DM1), and enters the right side port of the microscope (note that the tube lens for the side port has been removed). After excitation of the sample, the fluorescence emission signal is collimated by the objective and exits the side port, passes through the dichroic mirror and is focused – using lens L4 – onto the optical fiber which is connected to the photomultiplier tube (PMT). A polarizing beam splitter (PBS) can be introduced before the fiber to separate light with polarization that is parallel or perpendicular to that of the excitation light. The PMTs convert single photons to electrical pulses which are routed to the TCSPC board. Laser light from the TIRF system shares the back port of the microscope with the epifluorescence tube (Epi). Lens L5 and L6 collimate the epifluorescence and TIRF light respectively. The TIRF illumination is focused at the objective back aperture by the lens L7. When the sliding mirror, Mslide1, is removed from the light path, the right side port is closed and the emission signal can be collected by the camera via the tube lens (TL). In addition, the optical trap can be inserted above the fluorescence cube turret with an infrared dichroic mirror (DMslide) mounted on a custom-built slider (not shown).

Collimated fluorescence light is focused with a 250 mm focal length lens onto a 50 μm, 0.22 NA optical fiber, which serves as the confocal pinhole. The optical fiber entrance is mounted on a 3-axis manual micrometer stage in order to optimize the confocal probe volume such that autocorrelation curves are consistent with diffusion models. The fluorescence light emerging from the optical fiber is focused onto a GaAsP photomultiplier tube (PMT) which has high gain and is optimized for single-photon counting for wavelengths 320-700 nm with a peak wavelength of 580 nm. The quantum efficiency of the PMT is 40% at peak wavelength (manufacturer's data) and its response time is ~8 ps.

The photon detection event is converted into an electronic pulse, which is routed through an 8-channel router to the TCSPC module for collection and analysis. The TCSPC electronics digitally tag incoming pulses such that the photon arrival time relative to the beginning of the experiment (macrotime) and relative to the laser pulse time (microtime) are measured. A preamplifier prevents overloading of the PMT by shutting it down in response to high photon counts. The data is continuously written into a FIFO (first in first out) buffer in the SPC-630 board. For a detailed description of the principles behind time-correlated single photon counting, the reader is referred to the excellent monograph by Becker (Becker, 2006).

2.3.5 Optical Trap

The optical trap was first modeled using ray-tracing software (Optics-Lab, Carlsbad, CA, USA) to assist in lens placement. The trap was constructed using C-mount

components and is introduced into the expanded infinity space under the microscope objective (Figure 2-2). Coherent 830 nm laser light can be continuous or TTL-modulated using a 5 V square wave with 50% duty cycle from an A/D board (National Instruments, Austin, TX, USA). A water-immersion 63X/1.2 NA objective is used to focus the collimated and expanded laser beam down to a diffraction-limited spot. The coordinates of the laser focal point corresponding to the image is determined by imaging the focused beam reflecting off the back of a glass coverslip. Dielectric polystyrene beads in a solution of 1% albumin and DPBS were then successfully trapped and tracked with a spatial sensitivity of ~10 nm using time-lapse digital imaging and particle tracking algorithms based on the methods of Gelles *et al* (Gelles et al., 1988). TTL-modulation of the laser power permitted precise modulation of trap strength for rapid mechanical testing of 3% gelatin/water solution, which has elastic properties similar to EC cytoplasm (Yamada et al., 2000). We have recently integrated a quadrant photodiode above the condenser which will enable three-dimensional tracking of trapped microbeads and photonic force microscopy (Pralle et al., 1999).

2.3.6 Chambers for Micromanipulation and Flow

We designed a temperature-controlled micromanipulation chamber (Figure 2-3) for TCSPC measurements and imaging of cells and membranes undergoing application of forces with a micropipette or an optical trap. The position of the micropipette inside the chamber is controlled by a motorized, 3-axis micromanipulator with a computer interface (MP-285, Sutter instruments, Novato, CA, USA). The micropipette tip is shaped on a

microscope-based microforge using a low-melting-temperature glass bead and a micromanipulator.

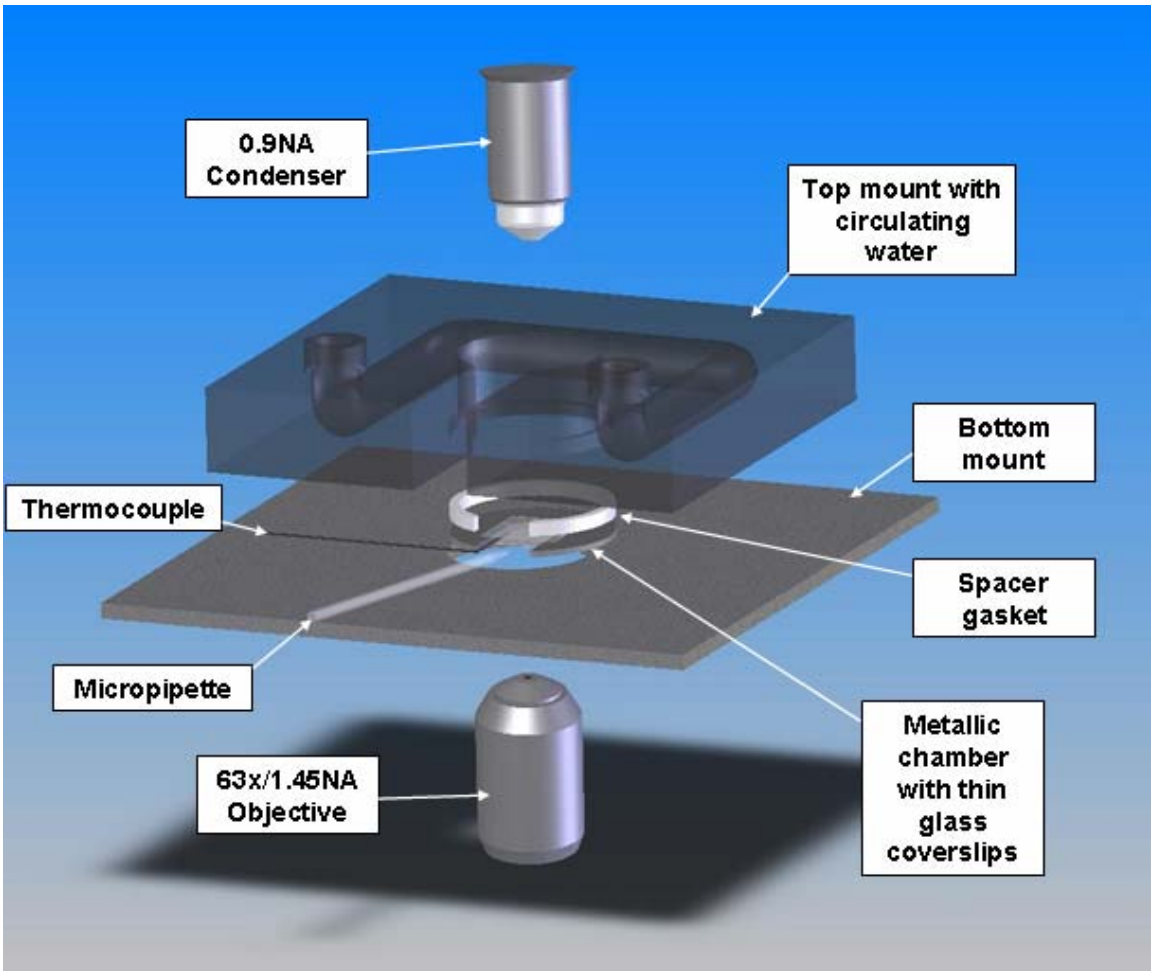

Figure 2-3: Custom micromanipulation chamber comprised of mounting plate, silicone spacers, metallic chamber with a side aperture, thermocouple for temperature monitoring, micropipette for micromanipulation, and the water circulation chamber.

For microaspiration, raising or lowering an adjustable reservoir relative to a reference reservoir produces an intake or outflow of water at the tip of the micropipette. A variable-pressure transducer (Validyne, Northridge, CA, USA) attached to both reservoirs generates a voltage proportional to the relative height difference, which is then converted to a digital signal using an A/D board (National Instruments, Austin, TX,

USA). The transducer system is sensitive to pressure changes of 10 dyn/cm^2 (~0.001 cm of water).

Chamber temperature is monitored using a thermocouple and maintained by using circulating water from a temperature-controlled water bath (TC500, Brookfield, Middleboro, MA, USA). The accuracy and stability of the temperature control in the chamber is ± 0.1 °C. For microscopy of live cells under continuous shear flow we use a commercial flow chamber system (FCS2 system, Bioptechs, Butler, PA, USA). The chamber has a thermistor-based temperature controller and an objective heater to maintain constant temperature. Physiological pH is maintained by perfusing humidified CO_2 gas and culture media through an oxygenator (Living Systems Inc., Brattleboro, VT, USA).

2.4 Materials and Methods

2.4.1 Preparation of Dye Solutions for FCS and Fluorescence Lifetime Measurements

9-(2-(ethoxycarbonyl)phenyl)-3,6-bis(ethylamino)-2,7-dimethyl,chloride (Rhodamine 6G (R6G)) powder was obtained from Invitrogen (Eugene, OR, USA) and used without further purification. The dye solutions were dissolved and diluted in distilled water to a final R6G-concentration ranging from 1 to 8 nM. Fresh dye solutions were prepared before the start of each experiment. In experiments designed to demonstrate the relationship between diffusion and solvent viscosity, water-based solutions containing 5 nM of R6G and 10-80 % (v/v) of reagent-grade glycerol (Fisher

Scientific, Hampton, NH, USA) were prepared. The bulk viscosities of the prepared solutions were measured using a cone-and-plate viscometer (Haake Rotovisco 1, Thermo Electron, Waltham, MA, USA). For the simultaneous FCS and lifetime measurements, a pulsed 650 nm red laser was used to excite 1,1'-dioctadecyl-3,3,3',3'-tetramethylindodicarbocyanine, 4-chlorobenzenesulfonate (DiD, Probes, Eugene, OR, USA) in dimethylsulfoxide (DMSO, EMD chemicals, Gibbstown, NJ, USA), ethanol, methanol, or dimethyl formamide (DMF) (Sigma-Aldrich, St.Louis, MO, USA). Experiments were performed at room temperature unless otherwise specified.

2.4.2 Preparation of Giant Unilamellar Vesicles

Giant unilamellar vesicles were prepared based on the method by Angelova *et al*. with minor modifications (Dimitrov and Angelova, 1986). Briefly, 1,2-Dimyristoyl-*sn*-Glycero-3-Phosphocholine (DMPC) (Avanti polar lipids, Alabaster, AL, USA) and 0.001 mol% 1,1'-dioctadecyl-3,3,3',3'-tetramethylindocarbocyanine perchlorate (DiI-C_{18}) (Invitrogen, Eugene, OR, USA) were dissolved in chloroform. After vacuum drying this mixture onto nitinol wires, the assembly was placed in a 55°C chamber containing 0.1 M sucrose and an alternating current was applied across the wire electrodes. A LabView-controlled A/D board (National Instruments, Austin, TX, USA) was used to apply to the wires 0 to 1 V in increments of 50 mV at 5 minute intervals, followed by a constant voltage of 1.2 V for 3 hours. The sizes of the resulting giant unilamellar vesicles varied from 10 to 70 μm.

2.4.3 Cell Culture and Staining Protocols

Bovine aortic endothelial cells (BAECs) (VEC Technologies, Rensselaer, NY, USA) were sub-cultured between passages 3-10 in T-25 flasks. MCDB-131 complete medium (450 ml) with 50 ml FBS, 10 ng/ml EGF and 1 μg/ml hydrocortisone with addition of 50 μl/ml 100X antibiotic/antimycotic solution, 90 μg/ml heparin and 0.2 mg/ml ENDO GRO (VEC Technologies, Rensselaer, NY, USA) was used as the culture medium. Cells were incubated at 37°C with 5% CO_2 and grown to confluence on No.1 glass coverslips. Cell membranes were stained using DiI-C_{18}. The DiI-C_{18} stock solution was prepared in DMSO and diluted with phosphate-buffered saline (PBS) (no calcium, magnesium, or albumin) to a final concentration of 1 μM (for imaging) and 1 nM (for FCS measurements). After rinsing the cells three times in PBS without calcium or magnesium, the cells were incubated with the staining solution for 3-5 minutes at 37°C. The cells were rinsed five times and returned to PBS with calcium, magnesium, and 1% albumin. The cells were maintained at physiological pH and temperature in the incubators and while conducting the FCS measurements.

2.4.4 Curve Fitting of Autocorrelation and Lifetime Data

Autocorrelation curves were fit with Eq. 2.6, 2.7, 2.8, or 2.9 as appropriate, using the Levenberg-Marquardt non-linear least squares regression algorithm with the aid of Origin software (Originlab, Northampton, MA, USA). Quality of fits was assessed by minimizing residuals and χ^2 values. The structure factor obtained from the fit was between 2 and 6 in all the experiments performed. Fluorescence decay curves were

extracted from photon-counting histograms by a process of iterative reconvolution using Eq. 2.12 in Fluofit software (PicoQuant, Berlin, Germany). Data were fit using a biexponential decay curve with the χ^2 values of the fit between 1 and 1.5. Using an additional exponential did not result in an improved fit. In some cases, diffusion coefficients and lifetimes are expressed as averages ± standard deviation.

2.5 Results

2.5.1 Effects of Dye Concentration on FCS-Determined Diffusion Coefficients

Rhodamine 6G (R6G) was used to calibrate FCS because of its known diffusion coefficient (2.8×10^{-6} cm^2/s in water), high quantum yield (~0.95), and the relatively large absorption cross section (1.7×10^{-16} cm^2 at 514.4 nm) (Widengren et al., 1995;Kubin and Fletcher, 1982). Using these known values for rhodamine dye diffusion, we computed the radius of the focal volume to be 0.277 ± 0.010 μm. This value compares favorably with the theoretically-computed values of the radius of the focal volume of 0.264 μm. This experimental radius of the confocal volume was used in all subsequent experiments on cells and vesicles to compute the respective diffusion coefficients. In order to test whether dye concentration would affect the resulting diffusion coefficients (for example, due to aggregation), we measured the dye diffusion coefficient at progressively increasing concentrations of R6G of 1, 2, 5, and 8 nM in distilled water at room temperature. For each concentration level, ten autocorrelation curves were obtained and the resulting diffusion coefficients were averaged (Figure 2-4). The value of the

autocorrelation curve at $\tau = 0$ s, $G(0)$, is inversely proportional to the average number of molecules present in the confocal volume (Eq. 2.6). $G(0)$ increased from 0.03 to 1.49 corresponding to a decreasing average particle concentrations of 7.58 to 0.67 which are consistent with the number of molecules calculated from the known concentration of diffusing dye (data not shown). The values of τ_D for the four concentrations of R6G measured (1-8 nM) was approximately ~70 μs (inset of Figure 2-4) indicating that diffusion of the R6G dye for very dilute concentrations is independent of the number of molecules in the confocal volume.

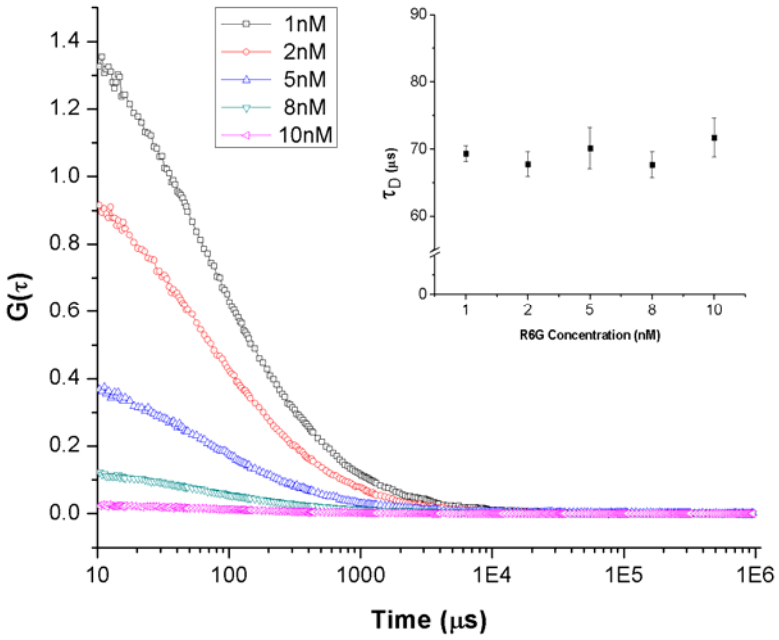

Figure 2-4: Dependence of the autocorrelation curve on R6G concentration. R6G concentration ranged from 1-8 nM. $G(0)$ (inversely proportional to the average number of particles in the observation volume) was determined by fitting autocorrelation functions with Eq. 2.6. Figure inset: The average diffusion times, τ_D, of R6G molecules obtained from fitting autocorrelation curves with Eq. 2.6. (error bars indicate the standard deviation of 10 measurements).

2.5.2 Effects of Solvent Viscosity on FCS-Determined Diffusion Coefficients

In order to assess whether FCS-determined diffusion coefficients are sensitive to solvent viscosity, fluorescence fluctuation analysis was performed on R6G dye dissolved in aqueous solutions of varying glycerol concentrations ranging from 10 to 80% glycerol in 10% increments. The solution bulk viscosities were measured in a cone-and-plate viscometer. Ten FCS measurements were collected for each solution, autocorrelation curves were computed, and diffusion coefficients were averaged (Figure 2-5). All the experiments were performed at room temperature. The average τ_D shifted from a value of 0.1 ms for 10% glycerol to 6.5 ms for 80% glycerol. Data in Figure 2-6 show that FCS-determined diffusion coefficients decrease with increasing viscosity in a manner consistent with Eq. 2.1. In addition, values of viscosity obtained from FCS-determined diffusion coefficients using Eq. 2.1 differed from bulk viscosity measurements obtained by cone-and–plate viscometry by 4-20% indicating a good correspondence between the two methods (data not shown).

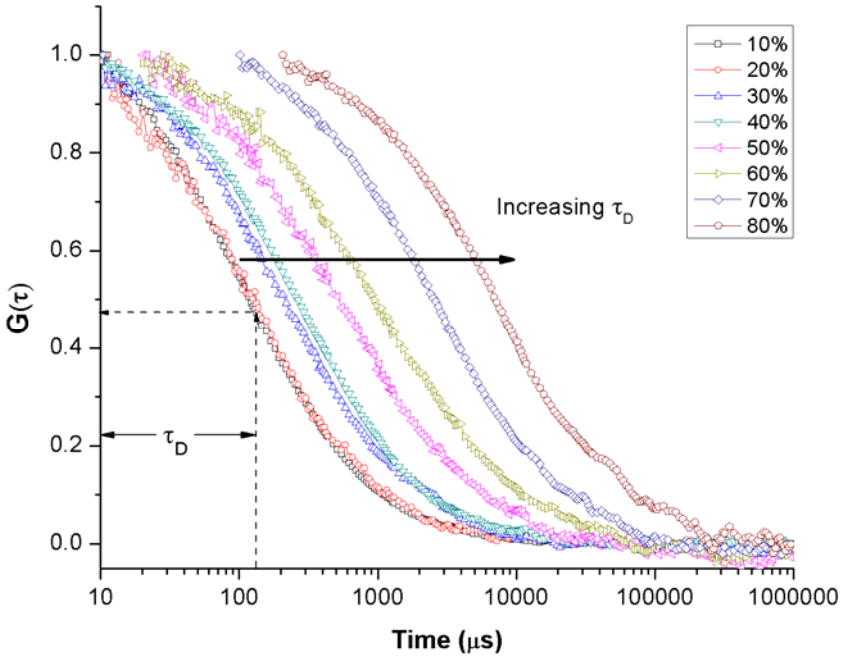

Figure 2-5: Dependence of the autocorrelation curve of R6G on viscosity of glycerol/water solution. Increase of viscosity (corresponding to increasing percentage of glycerol, v/v) leads to longer characteristic diffusion times, τ_D.

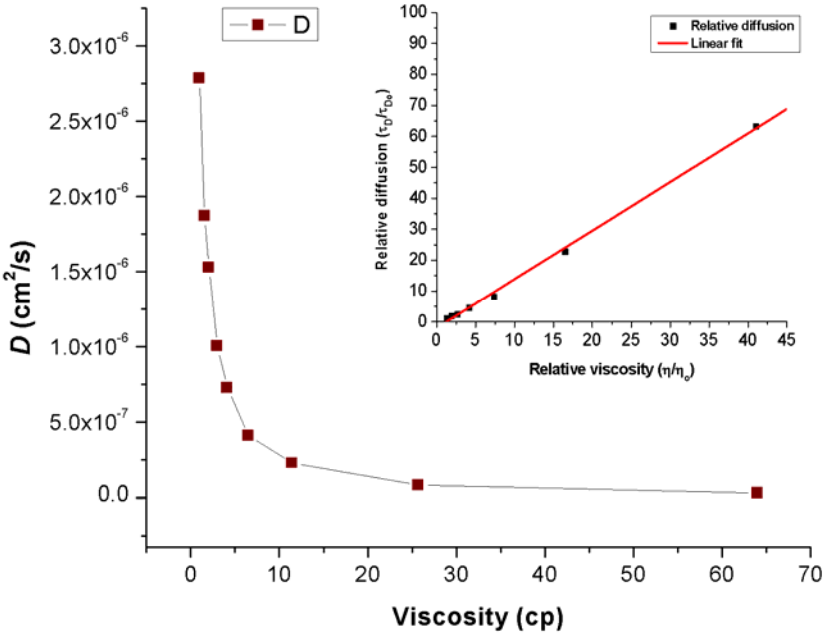

Figure 2-6: Diffusion coefficients (*D*) of 5 nM R6G obtained by fitting autocorrelation curves in A with Eq. 2.6. The x-axis indicates the values of viscosity of the dye solution measured with a cone-and-plate viscometer. Inset figure: The relationship between normalized viscosity (η/η_0) and normalized characteristic diffusion time (τ_D/τ_{D0}) was fit with a line. η_0 and τ_{D0} are viscosity and characteristic diffusion time, respectively, of dye in pure water.

2.5.3 FCS Measurements of DMPC Giant Unilamellar Vesicles and BAEC Membranes

FCS measurements were performed on DMPC vesicles and endothelial cell membranes stained with DiI-C_{18} dye excited with 520 nm light from the CW laser and 532 nm light from the pulsed solid-state laser. Fluorescence light with wavelength of 545 nm and longer was collected for analysis. For cells and vesicles, 5 nM DiI was found to best ensure sufficient fluorescence signal and ease-of-fit of autocorrelation curves. About

40,000 photons per second were collected and the number of fluorescent molecules in the probe volume at any time was between 1 and 8. The laser beam position in the x and y plane, relative to the imaging system, was assessed by preparing a single monolayer of DiI on a glass coverslip and bleaching it with the laser. The coordinates of the laser spot were then recorded using the camera. During FCS measurements, the position of the focus in the z-axis was adjusted to correspond to the membrane by moving the microscope objective such that fluorescence intensity was maximized.

For DMPC vesicles, 20 FCS measurements were taken at the GUV apical region, and no more than 5 measurements were obtained on a single vesicle. The temperature in the chamber was maintained at 26°C, which is above the phase-transition temperature (24 °C) for DMPC. The results were fit using the equation for 2-dimensional diffusion (Eq. **2.7**) to obtain a diffusion coefficient for $DiIC_{18}$ in DMPC vesicles of $(5.7 \pm 1.4) \times 10^{-8}$ cm^2/s.

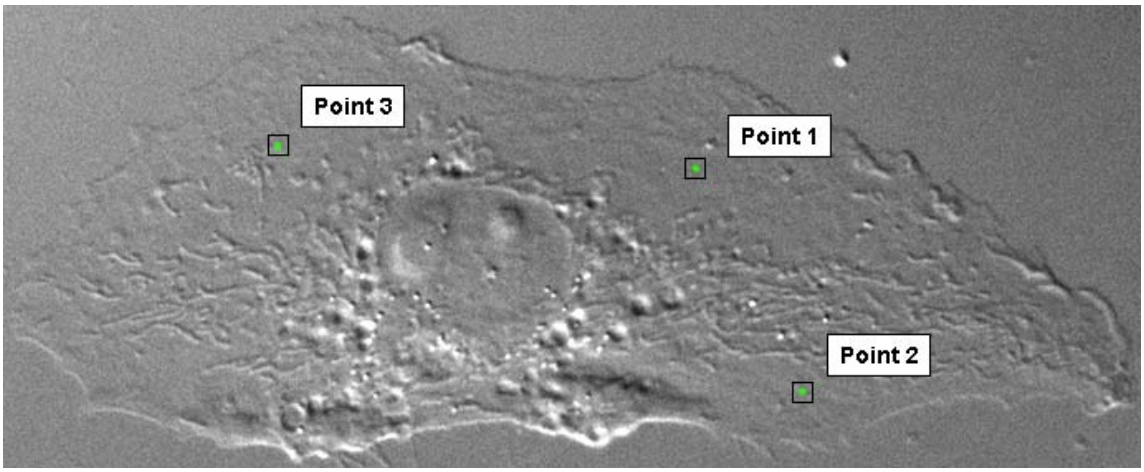

Figure 2-7: Bovine aortic endothelial cell imaged with DIC microcopy. Superimposed points in the image indicate location of confocal volume on the membrane surface of a representative cell from which fluorescence fluctuation data were collected. The cell in this figure corresponds to cell 1 in Table 2-2.

In BAECs, moving the stage to the desired location on the membrane apical surface enabled FCS measurements on spatially distinct points on a cell (Figure 2-7). FCS measurements were performed on 5 cells at 3 points in each cell, and 5 measurements were recorded at each point for a total of 75 measurements. Schwille *et al.* showed that the diffusion of DiI in rat basophilic leukemia cell membrane can be assessed using models for 2-D, 2-species fit or anomalous diffusion (Schwille et al., 1999b). In another recent study, Gielen *et al.* report that the diffusion on a nerve cell was well described using a 2-D, 2-species fit (Gielen et al., 2005). Consistent with this finding, we observed that a model for 2-D, 2-species diffusion fit the autocorrelation curves better than models for either anomalous subdiffusion or 2-D single species. Thus Eq. 2.8 was used to determine diffusion coefficients in BAEC membranes. Values given in Table 2-2 represent averages of 5 FCS measurements taken on the cell and point indicated. Analysis of a 2-D, 2-species fit gives a fast fraction (considered to be unbound dye) and a slow fraction (which is considered to be the membrane mobile fraction). The proportion of dye in the membrane, therefore, ranged from 78-93%, with an average value of 83% and exhibited diffusion coefficients ranging from $(1.75 \pm 0.3) \times 10^{-8}$ to $(7.03 \pm 1.5) \times 10^{-8}$ cm^2/s. The value of the fast fraction (or unbound dye) ranged from 7-22% with an average value of 17% with a diffusion coefficient ranging from $(2.11 \pm 1.1) \times 10^{-6}$ to $(6.27 \pm 3.5) \times 10^{-6}$ cm^2/s. Two sample t-Test statistics were used to analyze the differences between diffusion coefficients at different points on a given cell with $p < 0.05$. The difference in the measurements obtained from different spatial points were found to be significant in the case of 3 cells (cell 1, 2 and 3) measured. Remaining two cells (cell 4 and 5) showed minor differences which were found not to be statistically

significant (See Table 2-2). Representative plots of the autocorrelation function, curve fits, and residuals from model and cell membranes are shown in Figure 2-9 and Figure 2-8 .

Table 2-2: Diffusion coefficients of FCS measurements obtained from BAECs. 2-D, 2-species fit was performed on 75 measurements, obtained from 5 different cells. Three different spatial points were chosen for each individual cell. D_1 and D_2 are diffusion coefficients of the fast and slow moving DiI molecules, respectively. b_2 and 1-b_2 are their respective relative fractions. An * indicates significant difference (Two sample t-test) between point 1 and points 2 or 3 while significant difference between point 2 and point 3 is indicated by the superscript † ($p<0.05$).

Cell	**Bovine aortic endothelial cells – diffusion coefficient using 2-dimensional, 2-species fit** (D_1 ×10^{-6}cm^2/s, D_2 ×10^{-8}cm^2/s)								
	Point 1			Point 2			Point 3		
	D_1	b_2	D_2	D_1	b_2	D_2	D_1	b_2	D_2
1	2.58 ± 0.4	0.84 ± 0.01	2.54 ± 0.1	3.01 ± 0.6	0.79 ± 0.79	3.95 ± 0.3 *	3.15 ± 1.6	0.82 ± 0.02	2.74 ± 0.7 †
2	2.32 ± 1.1	0.82 ± 0.02	1.75 ± 0.3	4.29 ± 0.9	0.79 ± 0.01	1.75 ± 0.3 *	4.29 ± 0.9	0.82 ± 0.02	4.48 ± 1.3 *†
3	2.85 ± 1.4	0.82 ± 0.02	3.62 ± 0.3	5.29 ± 2	0.85 ± 0.01	5.20 ± 0.4 *	6.27 ± 3.5	0.93 ± 0.01	5.94 ± 0.4 *
4	2.86 ± 2.7	0.78 ± 0.06	5.17 ± 3.0	4.08 ± 3.3	0.88 ± 0.01	3.99 ± 1.1	4.91 ± 1.1	0.85 ± 0.02	7.03 ± 1.5
5	3.58 ± 2.4	0.86 ± 0.01	5.21 ± 1.7	5.47 ± 0.8	0.85 ± 0.01	6.91 ± 0.7	2.11 ± 1.1	0.85 ± 0.03	2.19 ± 0.1

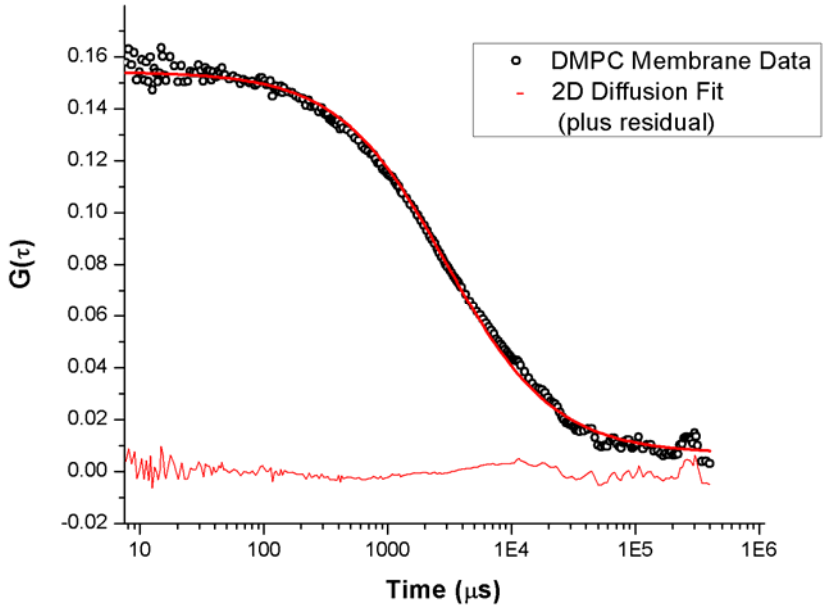

Figure 2-8: Representative autocorrelation curve and 2-D diffusion fit of DiI-C_{18} in a DMPC membrane. The residual of the fit is shown at the bottom of the graph.

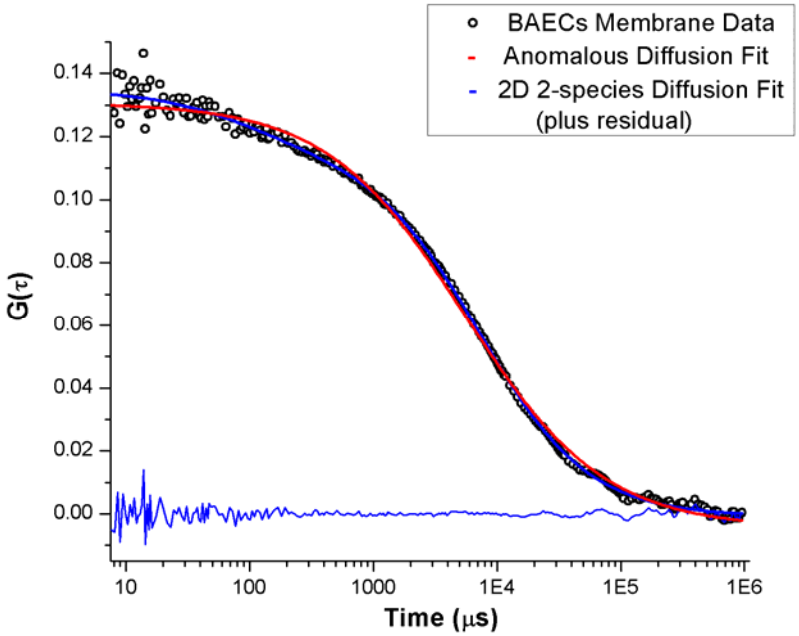

Figure 2-9: Representative plots of the autocorrelation of fluorescence intensity fluctuations arising from BAEC membranes stained with 5 nM DiI-C_{18}. Autocorrelation functions were fit with Eq. 2.7, 2.8 and 2.9 which describe 2-D diffusion (1-species), 2-D diffusion (2-species), and anomalous diffusion, respectively. The residual of the 2-D, 2-species fit is shown at the bottom of the graph (blue line).

2.5.4 Fluorescence Lifetime Measurements

We measured the fluorescence lifetime of DiD dissolved in the polar protic solvents, ethanol and methanol, and polar aprotic solvents, dimethyl sulfoxide (DMSO) and dimethyl formamide (DMF). In contrast to polar aprotic solvents, polar protic solvents have dissociable H^+ and can form hydrogen bonds. They also have lower dielectric constants and lower dipole moments than polar aprotic solvents. Since fluorescence lifetime is dependent on the electronic cloud configuration of the dye

molecule, these solvents are expected to affect fluorescence lifetime by altering electron distribution and intramolecular charge transfer. In each solvent, fluorescence lifetimes were best fit using biexponential decays (Eq. 2.12) consistent with earlier results for DiI (Packard and Wolf, 1985). Each value reported in Table 3 represents the average of ten measurements. Lifetime values for ethanol and methanol were (τ_1, τ_2) 0.48, 1.22 and 0.40, 1.02 ns, respectively, suggesting that fluorescence lifetime can be different even in closely-related solvents. The characteristic diffusion time, τ_D, of DiD in DMSO and DMF were 51.2 and 47.8 μs respectively. However, the fluorescence lifetimes of the dye (using a biexponential decay) were 0.74, 1.57 and 1.10, 1.93 ns, in DMSO and DMF, respectively (Table 2-3). Thus molecules with similar diffusion characteristics can be readily distinguished based on lifetime. Fluorescence emission of DiD in ethanol and methanol is intrinsically weak and therefore autocorrelation curves were noisy and could not be fit with models for FCS.

Table 2-3: Fluorescence lifetimes of DiD in polar and non-polar solvents. Pulsed laser excitation (650 nm) and TCSPC were used to determine fluorescence lifetime. Photon counting histograms were fit with a biexponential decay (Eq. 2.12). Diffusion of DiD in the non-polar solvents, DMF and DMSO, was determined using FCS and Eq. 2.6. Fluorescence emission of DiD in polar solvents, ethanol and methanol, was sufficient for lifetime analysis but too weak to generate an autocorrelation curve which could be fit. (a) From the Handbook of chemistry and physics tables

SOLVENT	Diffusion Time (μs)	Lifetime (ns) – Experiment ($\tau1$,$\tau2$)	$\chi2$	Dielectric Constant (a)	Dipole Moment (a)
Ethanol	NA	0.48, 1.22	1.18	24.3	1.69
Methanol	NA	0.40, 1.02	1.14	33	1.70
Dimethyl Sulfoxide (DMSO)	51.8	1.10, 1.93	1.30	47.2	3.96
Dimethyl Formamide (DMF)	47.2	0.74, 1.57	1.50	38.3	3.82

2.5.5 Optical Trap Microrheometry

The value of the optical trap's spring constant (~11 pN/μm) was determined from particle trajectories in water and the equipartition theorem using Hooke's Law. The spring constant of an optical trap was modulated by a TTL pulse delivered to the laser controller. The result was a trap stiffness exerted on polystyrene beads that varied as a square wave. Bead displacement as a function of time depended on this time-varying trap stiffness and the mechanical properties of the matrix surrounding the bead. To demonstrate the interaction of beads and a viscoelastic environment, a mixture of 3% gelatin and filtered water – intended to mimic the cytoplasm – was combined with beads in a solution of 1% albumin and DPBS. Trapped-bead locations were imaged and tracked with custom tracking software. When the trap was turned on, a large time-dependent displacement of the bead toward the center of the trap was observed (Figure 2-10). The time-lag of displacement relative to the laser power indicated that the bead was in a viscoelastic environment. Thus modulating optical trap forces and measuring the time-dependent displacements of beads provides a convenient means to measure the viscoelastic properties of endothelial cells without moving the cells or the trap location.

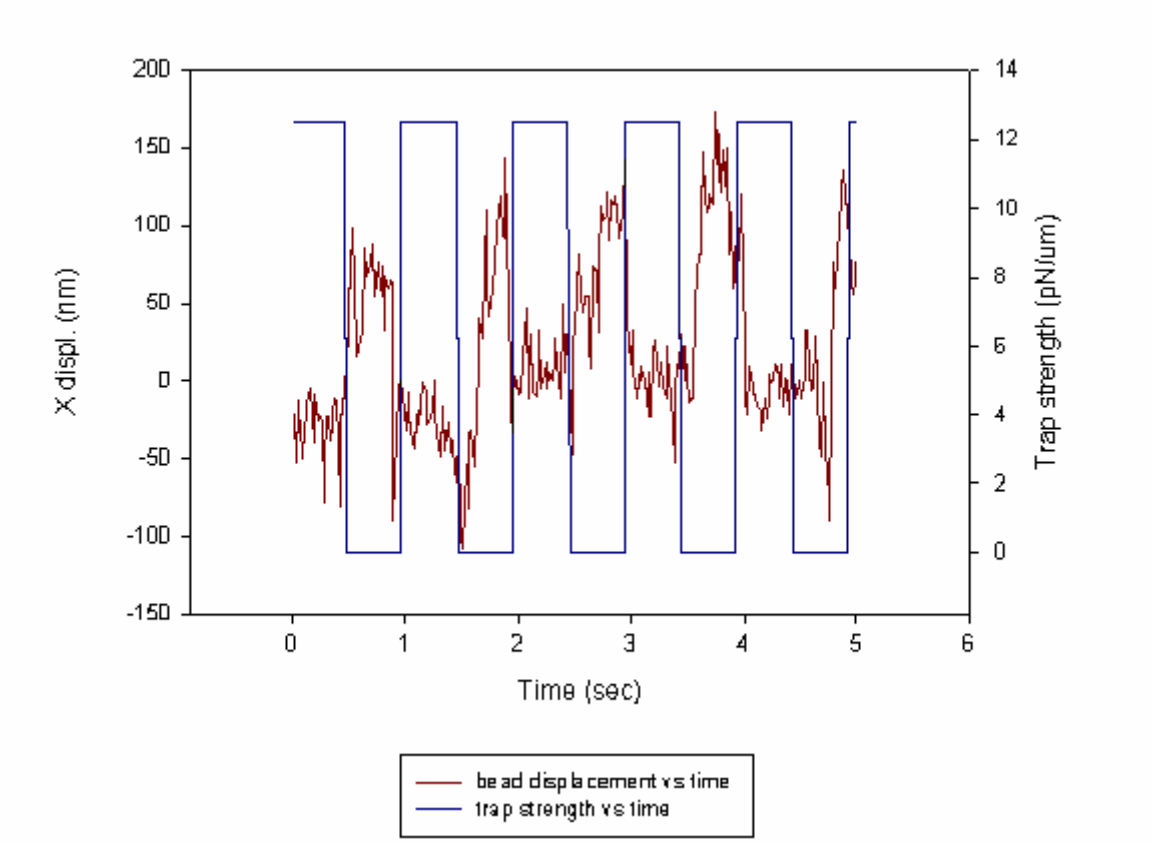

Figure 2-10: TTL-trap induced displacement of a 0.5 µm bead embedded in a 3% gelatin solution. The TTL trap can also operate in continuous mode. Trap stiffness was determined to be 11 pN/µm by tracking thermally-induced displacements of trapped 0.5 µm polystyrene beads in DPBS and 1% albumin. The statistical variance of x-coordinates for trapped beads was computed and compared to the potential energy and trap spring constant using Hooke's law and the equipartition theorem. TTL modulation enables analysis of time-dependent responses of the surrounding environment of the bead in response to step changes in trap strength.

2.5.6 Multimodal Microscopy

The optical system permits sequential imaging from DIC, epifluorescence, and TIRF imaging modalities with minimal instrument manipulation. As an example, DIC, epifluorescence, and TIRF images of DiI-C_{18}-stained BAECs are shown in Figure 2-11.

The great majority of the cells were stained on the membrane. The TIRF imaging is sensitive to membrane basal topography in which bright areas correspond to membrane that is adherent to the cover glass.

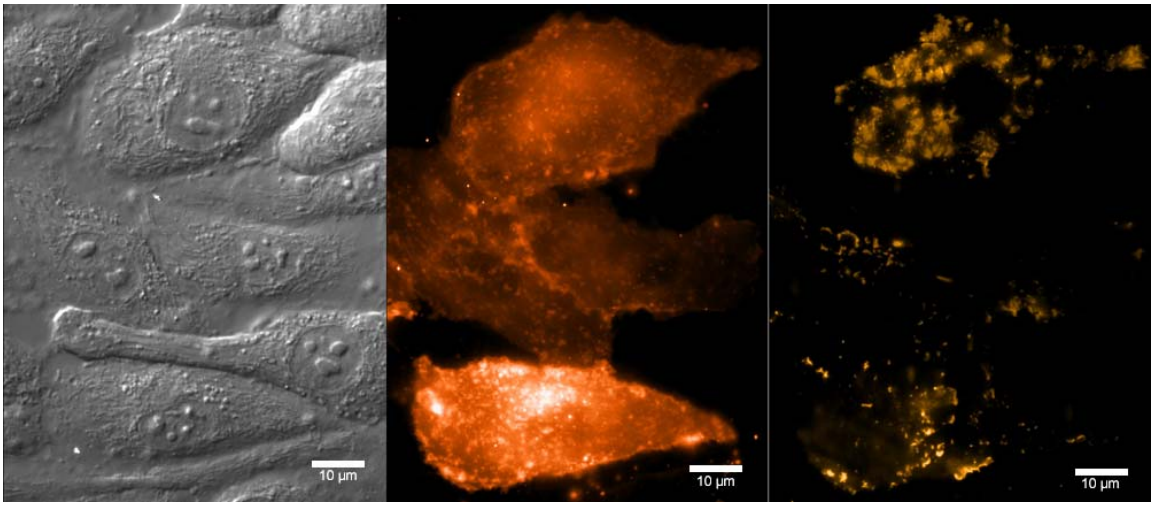

Figure 2-11: DiI-C_{18}-stained bovine aortic endothelial cells imaged sequentially with DIC, epifluorescence and TIRF.

2.6 Discussion

The CMDM described in this study was designed to address the following fundamental issues in mechanotransduction research: (i) forces are spatially distributed, (ii) relationships between force application and cell perturbation requires the integration of continuum and molecular-scale predictive models, and (iii) determination of molecular activation requires temporal and spatial registration of single-molecule events in live, intact cells under controlled conditions. To meet these design criteria, we have constructed and calibrated a multimodal microscope for cellular imaging and single-molecule fluorescence detection and analysis. First, collection volume of the fluorescence

emission was reduced to ~1 femtoliter using a fiber-aperture placed in a plane confocal to the laser focus. Second, fluorescence was collected with high-detection efficiency photomultiplier tubes (PMTs). Third, noise arising from stray laser light, autofluorescence, and fluorescence from glass coverslips and impurities in the solution was systematically reduced or eliminated by using high-quality optical filters. Fourth, all systems (confocal and trap) were spatially correlated to positions on the cell through careful 3-D calibration of the focus point and imaging plane of the multimodal microscope.

2.6.1 Improvements in FCS Instrumentation

In contrast to majority of the more traditional FCS instruments, which use avalanche photodiodes (APDs) for photon detection, we employ single photon counting photomultiplier tubes (PMTs). These newer PMTs (e.g. Hamamatsu H7422-40P) have a higher quantum efficiency than older generation PMTs making them suitable for photon correlation studies.(Becker, 2006) In addition, PMTs are easier to align (because their active area is larger (~mm^2 vs ~μm^2), less susceptible to photon-induced degradation, and have a superior response time (10's of picoseconds) compared to APDs (100's of picoseconds). These properties also make them optimal for fluorescence lifetime measurements. Thus use of PMTs enables fluorescence lifetime and FCS data to be obtained from a single set of measurements (Becker et al., 2006).

We use software to generate autocorrelation curves from FIFO data obtained from time-correlated single photon counting instrumentation (i.e. TCSPC-FCS). Hardware

autocorrelator cards can also generate autocorrelation curves in near real-time using current fluctuations from APDs or PMTs. However, when combined with pulsed-laser excitation, TCSPC instrumentation records all photon arrival times and saves them into memory directly. This feature makes all the raw photon data available for additional computational analysis necessary for generation of photon counting histograms (PCH), multispectral fluorescence lifetime imaging (FLIM), burst-induced fluorescence lifetimes (BIFL), and higher-order correlations without the need for an additional, expensive, hardware correlator (Becker, 2006;Becker et al., 2006). Advances in TCSPC instrumentation and modern autocorrelation software algorithms (e.g. multi-tau time correlation method) ensure near real-time autocorrelation curves that were previously only possible with dedicated hardware correlators (Wahl et al., 2003). Recent studies support the increasing use of TCSPC for FCS and lifetime measurements (Becker et al., 2006).

2.6.2 FCS-Determined Diffusion Coefficients are Sensitive to Subtle Changes in Dye Concentrations

In order to test whether the system could detect subtle changes in concentration of diffusing species, we performed FCS analysis of autocorrelation curves arising from diffusion of rhodamine dye which varied in concentration from 1 to 8 nM. These calibration experiments support the use of FCS to determine the absolute number of molecules in the observation volume. Absolute molecular concentrations are essential in the study of the binding kinetics of molecules present on the surfaces of cell membranes and in solution (Pramanik and Rigler, 2001). In the context of mechanotransduction, it is

thus possible to follow a surface signal transduction pathway by following the association and disassociation of a receptor complex in response to an externally-imposed force from fluid flow. One of the main limitations of the technique of FCS is the requirement of extremely low concentrations of probe molecules. We observed rapid degradation of correlation signal with dye concentrations greater than 10^{-8} M. While requirement for low concentrations of molecules in FCS makes imaging impractical, it is an advantage in studies of binding kinetics in cells, where the concentrations of aggregating molecules are typically low. The low concentration also means the molecular events in cells can be studied with relatively less perturbation of the biological system compared to methods which require high concentrations of fluorescent molecules such as fluorescence recovery after photobleaching (FRAP) and any imaging-based methods such as fluorescence resonance energy transfer (FRET).

2.6.3 FCS-determined diffusion coefficients are sensitive to small changes in viscosity

In our calibration experiment, we show that increases in glycerol concentration resulted in right-shifted autocorrelation curves indicating longer diffusion times for increasingly viscous environments (Figure 2-5). Thus FCS is likely to be sufficiently sensitive to monitor subtle changes in the local microviscosity which may be biologically significant. In our recent study we showed that the diffusion of DiI in cellular membranes is not uniform and varies substantially in response to applied shear over the cells (Butler et al., 2001a). Combined with 3-D piezo-scanning, FCS can monitor such changes

occurring in cells due to imposed fluid flow or other mechanical perturbations to determine spatially-resolved mechanical effects on membranes.

2.6.4 Differences in DiI diffusion in cell and model membranes determined by FCS

In order to test whether the CMDM could detect spatially-varying diffusion of lipids in cell and model membranes we measured the fluorescence fluctuations arising from DiI in model DMPC membranes and bovine aortic endothelial cells. Model membranes are useful in studying diffusion in lipid bilayers, phase segregation in lipids, and model protein diffusion in vesicles (Korlach et al., 1999;Bacia et al., 2004). They are compositionally simple and homogenous in nature enabling one to fit the simple 2-D equation (Eq. 2.7) of diffusion to the autocorrelation curves. In DMPC vesicles above the phase transition temperature, we obtained diffusion coefficient values of $5.7 \pm 1.4 \times 10^{-8}$ cm^2/s. More importantly, the variation of diffusion values obtained within measurements performed on one vesicle and between different individual vesicles is quite small, supporting the assumption that they are homogenous in nature. The values obtained are also consistent with values reported in literature of the diffusion coefficient on DMPC vesicles using FRAP (Almeida et al., 1992). FRAP experiments in model membranes of POPC (l-palmitoyl-2-oleoyl-sn-glycero-3-phosphocholine) show unrestricted translational diffusion $D = 4.4 \times 10^{-8}$ cm^2/s in fluid membrane and restricted diffusion $D = 0.7 \times 10^{-9}$ cm^2/s in polymer-stabilized membranes (Schutz et al., 1997). Previous FCS experiments on DLPC (dilauroyl phosphatidylcholine) revealed a translational diffusion coefficient of 3×10^{-8} cm^2/s (Korlach et al., 1999).

FCS analysis of DiI fluorescence from stained endothelial cells revealed two important observations. First, the choice of diffusion models used to fit autocorrelation curves of DiI fluorescence in cell membranes is not straightforward, consistent with observations by others (Schwille et al., 1999a;Gielen et al., 2005). To fit our cell lipid diffusion data, we used models for both 2-D, 2-species (Eq. 2.8) and anomalous subdiffusion (Eq. 2.9). In general we found that fitting of autocorrelation curves with a model for 2-D, 2-species fit resulted in uncorrelated residuals and smaller χ^2 values. The spatially heterogeneous nature of the cell membrane necessitates the requirement for a complex fit such as that for 2-D, 2-species. In our study, the 2-D, 2-species fit reveals the existence of a fast moving component, whose origin is unclear but may reflect unbound dye, as has been suggested in other studies (Gielen et al., 2005). It has been speculated that the fast component of the diffusion might arise from the unwashed dye present in the focal volume (Gielen et al., 2005). Measurements of dye in solution away from the membrane support this hypothesis. However, the relatively high fraction of the mobile membrane component is greater than 83% confirming that FCS is effective in measuring cell membrane lipid diffusion. The results obtained by the 2-D, 2-species method of fit compare favorably with membrane diffusion values in the literature using either FCS or FRAP (Gielen et al., 2005;Schwille et al., 1999d;Butler et al., 2001b).

The second important observation in this study is that translational diffusion coefficients for different measurement points on endothelial cells vary significantly (cells 1-5, Table 2-2). The values for the membrane diffusion on different points on the cells used in this study ranged from $(1.75 \pm 0.3) \times 10^{-8}$ cm^2/s to $(7.03 \pm 1.5) \times 10^{-8}$ cm^2/s. While all the values for membrane diffusion exist within the same range of magnitude,

the inter-point variation within a single cell or between individual cells used in this study is not trivial, but represents an example of the heterogeneous nature of the membrane surface. The variability in the values of the diffusion coefficient might arise from the complexity of the cellular membrane including differences in lipid phase and density, local protein concentration and aggregation (Kusumi and Suzuki, 2005), and membrane interaction with the cytoskeleton and glycocalyx (Tarbell and Pahakis, 2006). Thus the ability to obtain FCS data from specific locations is an important step toward assessing the nature of spatial heterogeneity of molecular dynamics in live cells.

2.6.5 Time-Resolved Fluorescence Of DiD in Polar Protic and Aprotic Solvents

We used our pulsed, red laser to generate data for fluorescence lifetime and FCS to test the ability of the system to deflect subtle differences in how DiD interacts with its immediate surroundings. The measurement of lifetime is independent of dye concentration and is solely determined by changes in the dye's photophysics induced by inter- and intra-molecular interactions. Data reported in Table 2-3 suggest that the same fluorescent molecule, DiD, has longer fluorescence lifetimes in aprotic solvents compared to protic solvents (Table 2-3). Fluorescence lifetime depends on non-radiative decay mechanisms. Thus, the shorter fluorescence lifetimes in protic solvents may be due to such non-radiative decay mechanisms as hydrogen bonding and intermolecular proton transfer. Newer modalities of FLIM (fluorescence lifetime imaging) exploit this ultrasensitivity of a fluorophore for changes in its immediate surrounding to generate spatial maps of lifetime (Becker et al., 2006). It is expected that lifetime analysis will

enable rapid mapping of molecular-scale perturbation of the dye-lipid-water microenvironments in intact cell membranes.

2.6.6 Optical Trap Microrheometry of Viscoelastic Gelatin Solutions

An additional goal of this project was to integrate a means for mechanical testing and force application on single adherent cells. Thus, we constructed an optical trap which used a simple, well-controlled TTL waveform to modulate the trap stiffness in order to assess the time-dependent mechanical properties of living cells. A TTL-modulated optical trap proved successful in identifying viscous and elastic properties of a gel matrix, but further analysis is needed to ensure that polystyrene beads are attached to the gel matrix. Future research will also include the development of a mathematical model of viscoelasticity for a time-dependent spring constant.

2.7 Conclusions

Integrated instrumentation and interdisciplinary approaches will help solve biological and medical problems originating from the interface of cellular signaling and cell mechanics, an emerging area of biology. Finite element modeling, Monte Carlo simulations, and molecular dynamics can provide predictive multi-scale models of cell behavior. However, due to the level of complexity involved in the cellular signal transduction and inherent compartmentalization of cellular signaling in microenvironments, verification of models needs to be done at the single-molecule level

on intact cells with high-precision spatial registration. Alterations in dynamics of molecules are assumed to accompany changes in their signaling (e.g. phosphorylation and dimerization). Such changes are detectable by FCS and fluorescence lifetime analysis, making single-molecule spectroscopy an ideal tool to address the precise molecular mechanism by which forces induce changes in cellular biology.

In response to these challenges, we have successfully built a multimodal microscope that combines microscale monitoring of molecular dynamics at multiple timescales with prescribed macroscale force conditions. This system addresses an unmet need for integration of force application, analysis of cell mechanics, and molecular-scale mechanotransduction detection. It is now possible to forge new research directions in which cell-specific, multicomponent models of mechanotransduction are developed from 3-D live cell imaging and validated with molecular-scale biological readouts.

2.8 References

1. Almeida, P. F., W. L. Vaz, and T. E. Thompson. 1992. Lateral diffusion in the liquid phases of dimyristoylphosphatidylcholine/cholesterol lipid bilayers: a free volume analysis. *Biochemistry* 31:6739-6747.

2. Bacia, K., D. Scherfeld, N. Kahya, and P. Schwille. 2004. Fluorescence correlation spectroscopy relates rafts in model and native membranes. *Biophys. J.* 87:1034-1043.

3. Barbee, K. A., T. Mundel, R. Lal, and P. F. Davies. 1995. Subcellular distribution of shear stress at the surface of flow-aligned and nonaligned endothelial monolayers. *Am. J. Physiol* 268:H1765-H1772.

4. Becker, W. 2006. Advanced Time-Correlated Single Photon Counting Techniques. Springer.

5. Becker, W., A. Bergmann, E. Haustein, Z. Petrasek, P. Schwille, C. Biskup, L. Kelbauskas, K. Benndorf, N. Klocker, T. Anhut, I. Riemann, and K. Konig. 2006. Fluorescence lifetime images and correlation spectra obtained by multidimensional time-correlated single photon counting. *Microsc. Res. Tech.* 69:186-195.

6. Butler, P. J., G. Norwich, S. Weinbaum, and S. Chien. 2001b. Shear stress induces a time- and position-dependent increase in endothelial cell membrane fluidity. *Am. J. Physiol Cell Physiol* 280:C962-C969.

7. Butler, P. J., G. Norwich, S. Weinbaum, and S. Chien. 2001a. Shear stress induces a time- and position-dependent increase in endothelial cell membrane fluidity. *Am. J. Physiol Cell Physiol* 280:C962-C969.

8. Charras, G. T. and M. A. Horton. 2002. Determination of cellular strains by combined atomic force microscopy and finite element modeling. *Biophys. J.* 83:858-879.

9. Davies, P. F. 1997. Overview: temporal and spatial relationships in shear stress-mediated endothelial signalling. *J. Vasc. Res.* 34:208-211.

10. Dimitrov, D. S. and M. I. Angelova. 1986. Swelling and Electroswelling of Lipids - Theory and Experiment. *Studia Biophysica* 113:15-20.

11. Elson, E. and D. Magde. 1974. Fluorescence Correlation Spectroscopy. I. Conceptual Basis and Theory. *Biopolymers* 13:1-27.

12. Ferko, M. C., M. B. Garcia, and P. J. Butler. 2006a. Finite element stress analysis of a muticomponent model of sheared and focally-adhered endothelial cells.

13. Ferko, M. C., Patterson B.P., and P. J. Butler. 2006b. High-resolution solid modeling of biological samples imaged with 3-D fluorescence microscopy.

14. Geiger, R. V., B. C. Berk, R. W. Alexander, and R. M. Nerem. 1992. Flow-induced calcium transients in single endothelial cells: spatial and temporal analysis. *Am. J. Physiol* 262:C1411-C1417.

15. Gelles, J., B. J. Schnapp, and M. P. Sheetz. 1988. Tracking kinesin-driven movements with nanometre-scale precision. *Nature* 331:450-453.

16. Gielen, E., J. Vercammen, J. Sykora, J. Humpolickova, M. Vandeven, A. Benda, N. Hellings, M. Hof, Y. Engelborghs, P. Steels, and M. Ameloot. 2005. Diffusion of sphingomyelin and myelin oligodendrocyte glycoprotein in the membrane of OLN-93 oligodendroglial cells studied by fluorescence correlation spectroscopy. *C. R. Biol.* 328:1057-1064.

17. Guilford, W. H., D. E. Dupuis, G. Kennedy, J. Wu, J. B. Patlak, and D. M. Warshaw. 1997. Smooth muscle and skeletal muscle myosins produce similar unitary forces and displacements in the laser trap. *Biophys. J.* 72:1006-1021.

18. Haustein, E. and P. Schwille. 2003. Ultrasensitive investigations of biological systems by fluorescence correlation spectroscopy. *Methods* 29:153-166.

19. Hess, S. T., S. Huang, A. A. Heikal, and W. W. Webb. 2002. Biological and chemical applications of fluorescence correlation spectroscopy: a review. *Biochemistry* 41:697-705.

20. Hess, S. T. and W. W. Webb. 2002. Focal volume optics and experimental artifacts in confocal fluorescence correlation spectroscopy. *Biophys. J.* 83:2300-2317.

21. Hough, L. A. and H. D. Ou-Yang. 1999. A new probe for mechanical testing of nanostructures in soft materials. *Journal of Nanoparticle Research* 1:495-499.

22. Huang, H., C. Y. Dong, H. S. Kwon, J. D. Sutin, R. D. Kamm, and P. T. So. 2002. Three-dimensional cellular deformation analysis with a two-photon magnetic manipulator workstation. *Biophys. J.* 82:2211-2223.

23. Ingber, D. E. 2003. Mechanobiology and diseases of mechanotransduction. *Ann. Med.* 35:564-577.

24. Korlach, J., P. Schwille, W. W. Webb, and G. W. Feigenson. 1999. Characterization of lipid bilayer phases by confocal microscopy and fluorescence correlation spectroscopy. *Proc. Natl. Acad. Sci. U. S. A* 96:8461-8466.

25. Kubin, R. F. and A. N. Fletcher. 1982. Fluorescence Quantum Yields of Some Rhodamine Dyes. *Journal of Luminescence* 27:455-462.

26. Kusumi, A. and K. Suzuki. 2005. Toward understanding the dynamics of membrane-raft-based molecular interactions. *Biochim. Biophys. Acta* 1746:234-251.

27. Lakowicz, J. R. 1999. Principles of Fluorescence Spectroscopy. Springer.

28. Levitan, I., A. E. Christian, T. N. Tulenko, and G. H. Rothblat. 2000. Membrane cholesterol content modulates activation of volume-regulated anion current in bovine endothelial cells. *J. Gen. Physiol* 115:405-416.

29. Li, S., M. Kim, Y. L. Hu, S. Jalali, D. D. Schlaepfer, T. Hunter, S. Chien, and J. Y. Shyy. 1997. Fluid shear stress activation of focal adhesion kinase. Linking to mitogen-activated protein kinases. *J. Biol. Chem.* 272:30455-30462.

30. Magde, D., E. Elson, and W. W. Webb. 1974. Fluorescence Correlation Spectroscopy. II. An Experimental Realization. *Biopolymers* 13:29-61.

31. Mathur, A. B., G. A. Truskey, and W. M. Reichert. 2000. Atomic force and total internal reflection fluorescence microscopy for the study of force transmission in endothelial cells. *Biophys. J.* 78:1725-1735.

32. McCormick, S. M., S. G. Eskin, L. V. McIntire, C. L. Teng, C. M. Lu, C. G. Russell, and K. K. Chittur. 2001. DNA microarray reveals changes in gene expression of shear stressed human umbilical vein endothelial cells. *Proc. Natl. Acad. Sci. U. S. A* 98:8955-8960.

33. Neuman, K. C. and S. M. Block. 2004. Optical trapping. *Review of Scientific Instruments* 75:2787-2809.

34. Orr, A. W., B. P. Helmke, B. R. Blackman, and M. A. Schwartz. 2006. Mechanisms of mechanotransduction. *Dev. Cell* 10:11-20.

35. Osborn, E. A., A. Rabodzey, C. F. Dewey, Jr., and J. H. Hartwig. 2006. Endothelial actin cytoskeleton remodeling during mechanostimulation with fluid shear stress. *Am. J. Physiol Cell Physiol* 290:C444-C452.

36. Packard, B. S. and D. E. Wolf. 1985. Fluorescence lifetimes of carbocyanine lipid analogues in phospholipid bilayers. *Biochemistry* 24:5176-5181.

37. Pralle, A., M. Prummer, E. L. Florin, E. H. K. Stelzer, and J. K. H. Horber. 1999. Three-dimensional high-resolution particle tracking for optical tweezers by forward scattered light. *Microscopy Research and Technique* 44:378-386.

38. Pramanik, A. and R. Rigler. 2001. Ligand-receptor interactions in the membrane of cultured cells monitored by fluorescence correlation spectroscopy. *Biol. Chem.* 382:371-378.

39. Schutz, G. J., H. Schindler, and T. Schmidt. 1997. Single-molecule microscopy on model membranes reveals anomalous diffusion. *Biophys. J.* 73:1073-1080.

40. Schwille, P., J. Korlach, and W. W. Webb. 1999c. Fluorescence correlation spectroscopy with single-molecule sensitivity on cell and model membranes. *Cytometry* 36:176-182.

41. Schwille, P., J. Korlach, and W. W. Webb. 1999b. Fluorescence correlation spectroscopy with single-molecule sensitivity on cell and model membranes. *Cytometry* 36:176-182.

42. Schwille, P., J. Korlach, and W. W. Webb. 1999a. Fluorescence correlation spectroscopy with single-molecule sensitivity on cell and model membranes. *Cytometry* 36:176-182.

43. Schwille, P., J. Korlach, and W. W. Webb. 1999d. Fluorescence correlation spectroscopy with single-molecule sensitivity on cell and model membranes. *Cytometry* 36:176-182.

44. Simmons, R. M., J. T. Finer, S. Chu, and J. A. Spudich. 1996. Quantitative measurements of force and displacement using an optical trap. *Biophys. J.* 70:1813-1822.

45. Sultan, C., D. Stamenovic, and D. E. Ingber. 2004. A computational tensegrity model predicts dynamic rheological behaviors in living cells. *Ann. Biomed. Eng* 32:520-530.

46. Tarbell, J. M. and M. Y. Pahakis. 2006. Mechanotransduction and the glycocalyx. *J. Intern. Med.* 259:339-350.

47. Trache, A. and G. A. Meininger. 2005. Atomic force-multi-optical imaging integrated microscope for monitoring molecular dynamics in live cells. *J. Biomed. Opt.* 10:064023.

48. Vukojevic, V., A. Pramanik, T. Yakovleva, R. Rigler, L. Terenius, and G. Bakalkin. 2005. Study of molecular events in cells by fluorescence correlation spectroscopy. *Cell Mol. Life Sci.* 62:535-550.

49. Wahl, M., I. Gregor, M. Patting, and J. Enderlein. 2003. Fast calculation of fluorescence correlation data with asynchronous time-correlated single-photon counting. *Optics Express* 11:3583-3591.

50. Wang, N. and Z. Suo. 2005. Long-distance propagation of forces in a cell. *Biochem. Biophys. Res. Commun.* 328:1133-1138.

51. Wang, Y., E. L. Botvinick, Y. Zhao, M. W. Berns, S. Usami, R. Y. Tsien, and S. Chien. 2005. Visualizing the mechanical activation of Src. *Nature* 434:1040-1045.

52. Widengren, J., U. Mets, and R. Rigler. 1995. Fluorescence Correlation Spectroscopy of Triplet States in Solution: A Theoretical and Experimental Study. *J. Phys. Chem.* 99:13368-13379.

53. Yamada, S., D. Wirtz, and S. C. Kuo. 2000. Mechanics of living cells measured by laser tracking microrheology. *Biophys. J.* 78:1736-1747.

54. Yanai, M., J. P. Butler, T. Suzuki, H. Sasaki, and H. Higuchi. 2004. Regional rheological differences in locomoting neutrophils. *Am. J. Physiol Cell Physiol* 287:C603-C611.

55. Zander, C., J. Enderlein, and R. A. Keller. 2002. Single-Molecule Detection in Solution Methods and Applications. Wiley-VCH.

Chapter 3

MEMBRANE DYE LOCALIZATION IN CELLS

Foreword

The following chapter is taken from the manuscript: "Multimodal microscopy and single molecule spectroscopy for mechanotransduction research" Tabouillot T, Gullapalli RR, Butler PJ. Transactions of Optics East (SPIE), 2006.

3.1 Introduction

The objective of this study was to carefully analyze the placement of the confocal observation volume in the vicinity of the membrane using fluorescence correlation spectroscopy (FCS). Results suggested that there exists an offset between maximal count and location of the membrane. These results will assist in the analysis of time-correlated single photon counting (TCSPC) in cellular physiology and molecular mechanobiology experiments.

3.2 Methods

Bovine aortic endothelial cells (BAECs, VEC Technologies, Rensselaer, NY) were sub-cultured between passages 3-10 in T-25 flasks. MCDB-131 complete medium (450 ml) with 50 ml FBS, 10 ng/ml EGF and 1 μg/ml hydrocortisone with addition of 50 μl/ml 100X antibiotic/antimycotic solution, 90 μg/ml heparin and 0.2 mg/ml ENDO GRO

(VEC Technologies, Rensselaer, NY, USA) was used as the culture medium. The cells were incubated at 37°C with 5% CO2 and grown to confluence on No.1 glass coverslips. The cell staining protocol is as follows: the cells are rinsed 3 times using DPBS (without calcium or magnesium), then incubated for 3 minutes in DPBS with 5×10^{-9} M DiI-C_{18} (Invitrogen, Carlsbad, CA, USA), and then rinsed 5 times with DPBS (with calcium and magnesium).

Depending on the nature of the specimen under investigation, the fluorescence autocorrelation data were fit for either three-dimensional (3-D) diffusion (Eq. 3.1):

$$G(\tau) = \frac{1}{N}\left(\frac{1}{1+\left(\tau/\tau_D\right)}\right)\left(\frac{1}{1+\left(1/\omega\right)^2\left(\tau/\tau_D\right)}\right)^{1/2} \qquad 3.1$$

where N is the average number of particles, ω, the structure factor, is defined as the ratio of z / r, axial and radial dimensions of the observation volume respectively; or 2-D, 2-species diffusion (Eq. 3.2):

$$G(\tau) = \sum_{i=1}^{n} b_i \left(\frac{1}{1+\left(\tau/\tau_{Di}\right)}\right) \qquad 3.2$$

where b_i, the weight factor, is the relative proportion of the non-interacting diffusing molecules, i is the species or component index, and n is the number of species.

Curvefits were performed by levenberg-marquardt algorithms with the aid of Origin software (OriginLab, Northampton, MA, USA) and fit quality was assessed by minimizing χ2 values and correlation of residuals. The structure factor was minimized and determined before every experiment by fitting Eq. 3.1 to autocorrelation data of

rhodamine 6G (R6G) using the theoretical diffusion coefficient of R6G in water. The radial dimension of our system is ~277 nm and the structure factor is ~4. The position of the laser beam in relation to the imaging system was determined by photobleaching a DiI-coated coverslip with the TCSPC laser and recording the spot center using the digital camera.

3.3 Results

The main goal of these studies was to optimize the spatial and temporal precision of TCSPC for use on cells during mechanical stimulation. Because the axial dimension of the probe volume is ~4 times that of the lateral dimension, and the Gaussian nature of the probe volume leads to errors when the membrane is out of focus (Figure 3-1) there is a need for detailed analysis of axial scans of FCS to determine the precise relationship between diffusion coefficient, molecule number, and membrane position. Thus, fluorescence correlation spectroscopy measurements were performed on bovine aortic endothelial cells (BAECs) stained with the amphiphilic dye DiI-C_{18} to record the exact location of the membrane in relation to the observation volume location. The results account for 5 cells sampled during 3 separate sets of experiments. For each cell, 2 points were axially scanned with 200 nm increments, one over the cytoplasm and one over the nucleus. The distances are recorded with respect to the coverslip on which the cells are grown. Because in all instances our structure factor (z/r) was ~4, the observation volume spanned ~2 μm in the axial direction. The autocorrelation data were fit for 2-D, 2-species

using Eq. 3.2. A representative DIC image of a cell is shown in Figure 3-2 with TCSPC points labeled.

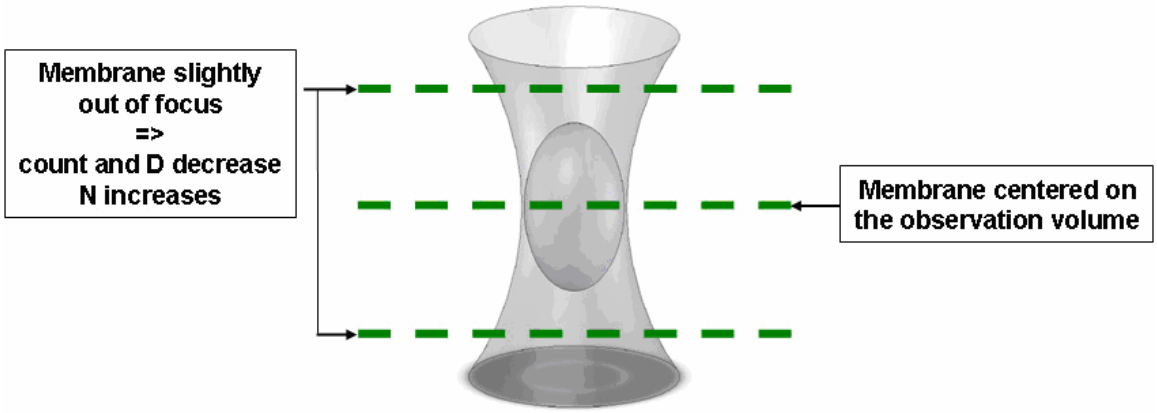

Figure 3-1: Optical probe volume for confocal TCSPC. Equations for FCS assume that membrane crosses center of probe volume. When out of focus, this assumptions leads to errors in *N* and *D* with *N* increasing and *D* decreasing with distance from center

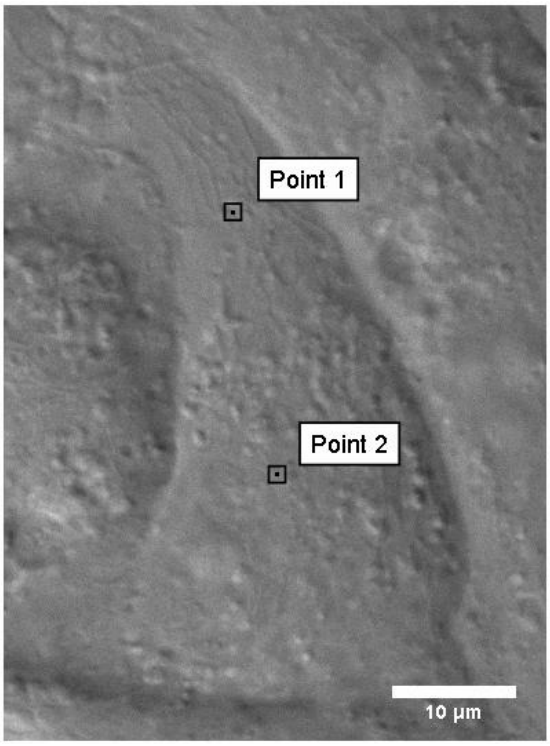

Figure 3-2: Representative differential interference contrast (DIC) generated image of endothelial cells in a confluent monolayer. Points refer to membrane locations where TCSPC data was collected.

For two cells out of the five studied, it was possible to compute the exact difference in height determined by the brightest point, given by the shortest collection time (the TCSPC board records a fixed number of total photons), and the actual position of the lipid bilayer, given by the lowest number *N* of particles (Figure 3-3 and Figure 3-4(a)) and fastest apparent diffusion, *D*. These values for offset for each cell were ~0.6 and ~0.8 µm, respectively.

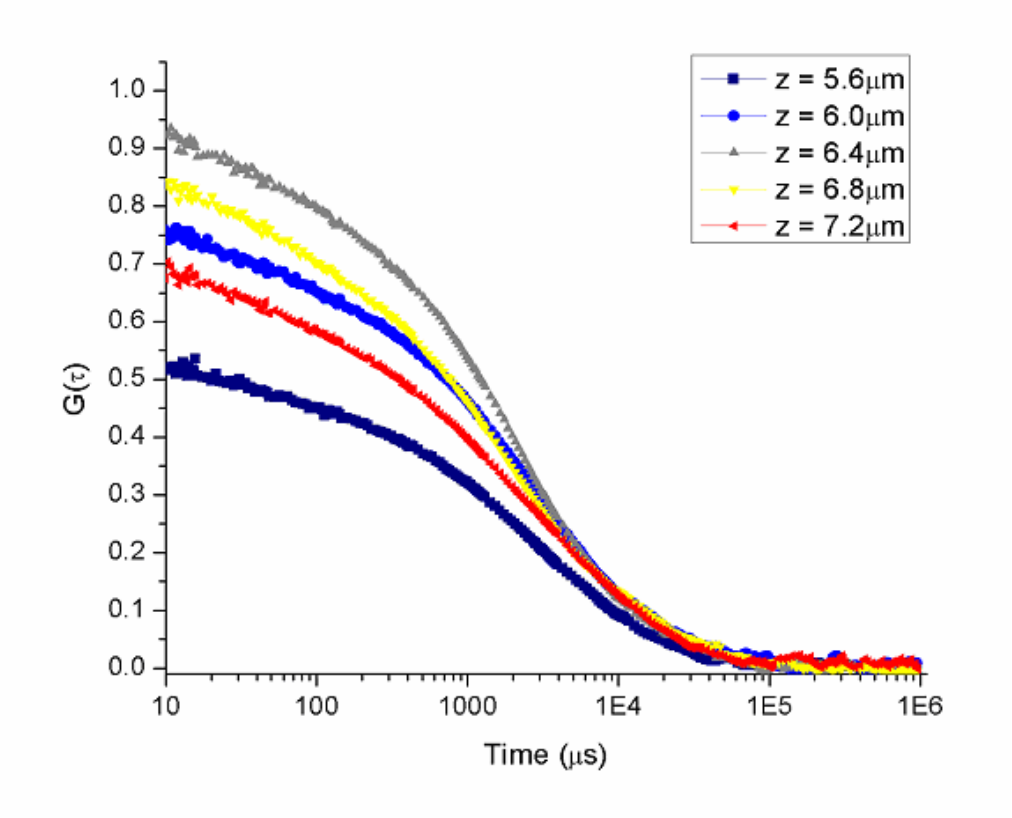

Figure 3-3: Autocorrelation curves from DiI-C_{18} on a sample BAEC plasma membrane along an axial scanning which moved in the positive z-direction away from the coverslip. The curves show a maximum G(0) and largest τ_D at ~6.4 μm from the coverslip.

From Figure 3-4, it is clear that *N* and *D* are much more sensitive measures of membrane location than is the count rate. In this figure, minima of *N* and maxima of *D* correspond to membrane location. Thus one can readily differentiate the basal (closer) and apical (further from the coverslip) plasma membrane from local minima in the number of molecules *N*. Also, the weight factor b_2 and diffusion coefficient D_2, for the slow component, peak at approximately the same axial location (Figure 3-4(b)). An inverse tendency is seen for the fast component (b_1), where the minima in b_1 are at the

slow component (b_2) maxima (data not shown). Those results confirm that the location of the dye in the membrane is represented by the slower of the species.

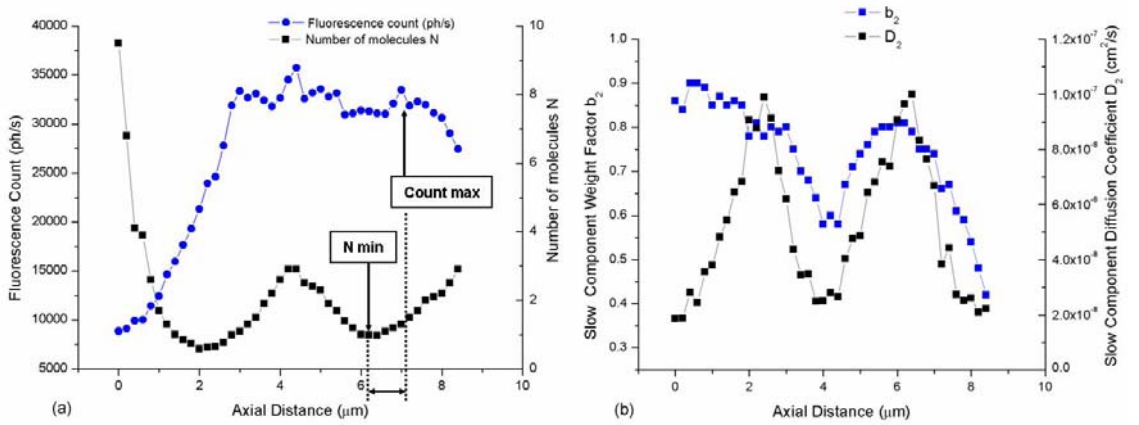

Figure 3-4: (a) The maximum fluorescence count and minimum number of molecules *N* in the observation volume are located at different axial location with respect to the coverslip. (b) The weight factor b_2 and diffusion coefficient D_2 for the slow component have a local maximum at a similar height as the minimum number of molecules *N*.

3.4 Discussion

Our TCSPC-based spectroscopy system was able to determine precise membrane location of the cell beyond the optical diffraction limit by determination of trends in *N* and *D* determined from FCS analysis and position stepping. Diffusion coefficients, in addition to other significant parameters, were derived from the recorded data permitting new insights into cellular membrane dynamics.

DiI-C_{18} localizes to the membrane lipid bilayer in cells (Packard and Wolf, 1985). Imaging of endothelial cells under epifluorescence illumination shows the same distribution when the cells are incubated with saline containing micromolar concentration of dye (data not shown). No such imaging is possible for nanomolar-range staining. Thus,

we used FCS to locate the dye in the specimen. We found that the number of molecules N increases and the slow-component diffusion coefficient D_2 decreases away from the membrane. Those results match a similar trend, previously shown on model membranes using the same spectroscopic technique (Milon et al., 2003;Schwille et al., 1999). Indeed, the waist of the observation volume increases away from the focal point, leading to an increased number of molecules being monitored and a slower apparent diffusion.

In previous cellular membrane studies involving this particular dye, the axial positioning was performed by recording the brightest point and positioning the observation volume at that particular location (Schwille et al., 1999). However, we have seen that the position of the highest fluorescent count does not match that of the least number of molecules and maximal diffusion coefficient. In addition, the count is not nearly as sensitive as are N and D in determining membrane location. A difference of ~0.6 μm to ~0.8 μm was recorded over the nucleus of two cells.

Endothelial cells have a developed surface layer, called glycocalyx, which performs various physiological functions, one of which is to limit the diffusion of charged and relatively large molecules (Vink and Duling, 2000). This layer has been shown to be approximately 0.5 μm in thickness (Vink and Duling, 1996). From our results, we could infer that the dye giving the highest photon count has not penetrated the layer, due to its charge and possible aggregation. This hypothesis could be confirmed by disrupting the glycocalyx (e.g. by heparinase or hyaluronidase) and performing axial FCS. If this is the case, the difference between the location of the highest count and the membrane should still appear constant for every cell and could be used as a ruler for quick axial positioning of the optical system. In addition, TCSPC may be a useful tool to

study the glycocalyx, an area of increasing interest among cell biologists (Tarbell and Pahakis, 2006).

3.5 Conclusion

We built an optical setup combining multimodal microscopy and diffraction-limited TCSPC-based spectroscopy system. The setup permits high-spatial spectroscopic measurements in locations and timescales matching the needs in cellular mechanotransduction studies. We show the applicability of TCSPC instrumentation for cellular studies, in terms of sensitivity as well as in time response of the system. The system could differentiate cellular components in their location (membrane and glycocalyx) and physical properties (diffusion coefficient). The results obtained in endothelial cells show an uneven partitioning of the membrane stain DiI-C_{18} in the axial direction and a novel method to locate the plasma membrane more precisely.

3.6 References

1. Milon, S., R. Hovius, H. Vogel, and T. Wohland. 2003. Factors influencing fluorescence correlation spectroscopy measurements on membranes: simulations and experiments. *Chemical Physics* 288:171-186.

2. Packard, B. S. and D. E. Wolf. 1985. Fluorescence lifetimes of carbocyanine lipid analogues in phospholipid bilayers. *Biochemistry* 24:5176-5181.

3. Schwille, P., J. Korlach, and W. W. Webb. 1999. Fluorescence correlation spectroscopy with single-molecule sensitivity on cell and model membranes. *Cytometry* 36:176-182.

4. Tarbell, J. M. and M. Y. Pahakis. 2006. Mechanotransduction and the glycocalyx. *J. Intern. Med.* 259:339-350.

5. Vink, H. and B. R. Duling. 1996. Identification of distinct luminal domains for macromolecules, erythrocytes, and leukocytes within mammalian capillaries. *Circ. Res.* 79:581-589.

6. Vink, H. and B. R. Duling. 2000. Capillary endothelial surface layer selectively reduces plasma solute distribution volume. *Am. J. Physiol Heart Circ. Physiol* 278:H285-H289.

Chapter 4

SINGLE-MOLECULE FLUORESCENCE STUDY OF ENDOTHELIAL CELL MEMBRANE DOMAIN PERTURBATION BY SHEAR STRESS

4.1 Introduction

Mechanotransduction is a cellular process by which the sensation of mechanical stimuli is converted to biochemical signaling pathways. Although it is a phenomenon recurrent in animal biology (Orr et al., 2006), vascular endothelial cell (EC) mechanotransduction of fluid shear stress has received special attention because of the strong correlation between hemodynamics and the physiology and pathophysiology of blood vessels (reviewed in (Davies, 1995)). Multiple lines of investigation have established that ECs are sensitive to spatial (Davies et al., 1997;dePaola et al., 1992;LaMack and Friedman, 2007) and temporal gradients (Bao et al., 2000;Butler et al., 2002;Frangos et al., 1996) in shear stress and that these changes are mediated by proteins in focal adhesions (Girard and Nerem, 1995;Li et al., 1997), the actin cytoskeleton (Galbraith et al., 1998;Girard and Nerem, 1993), cell-cell junctions (Bao et al., 2000;Fujiwara et al., 2001;Tzima, 2006) and the glycocalyx (Florian et al., 2003;Mochizuki et al., 2003;Pahakis et al., 2007). In addition, the endothelial plasma membrane is sensitive to shear stress as indicated in studies measuring lipid mobility (Butler et al., 2001;Haidekker et al., 2001), activation of potassium (Jacobs et al., 1995;Ohno et al., 1993;Olesen et al., 1988) and stretch-activated calcium (Naruse and Sokabe, 1993;Sigurdson et al., 1993) channels, phosphorylation of G proteins

(Chachisvilis et al., 2006;Frangos and Gudi, 1997;Kuchan et al., 1994), conformational changes of GPCRs, caveolae (Park et al., 2000;Rizzo et al., 1998) and diffusion of raft-associated proteins Lyn (Seong et al., 2009).

Many recent studies have now established that the plasma membrane is highly heterogeneous and dynamic. For example, membrane compartments originally designated as detergent-resistant membrane (DRM) (Brown and Rose, 1992;Brown and London, 1997), are now known to exist in highly transient states (Anderson and Jacobson, 2002;Subczynski and Kusumi, 2003), and are likely to assist in sorting membrane proteins into domains in order to regulate membrane-based signaling (Sheets et al., 1997;Baird et al., 1999;Drevot et al., 2002;Roy et al., 1999). In addition, interaction of the membrane with the cytoskeleton (Kusumi and Suzuki, 2005) and glycocalyx (Tarbell and Pahakis, 2006) are likely to play a role in membrane organization by virtue of chemical and steric interaction with lipids and membrane bound proteins. Since fluid flow does not seem to reach the plasma membrane (Damiano et al., 2004;Secomb et al., 2001), it has been assumed that stress from the flow was carried directly from the glycocalyx to the actin cytoskeleton (Thi et al., 2004;Weinbaum et al., 2003). Because of this complex membrane structure, its complicated interaction with extracellular and intracellular components, and the unique force distributions in ECs arising from shear imposition (Barbee, 2002;Ferko et al., 2006), it is important to establish the effects of shear stress on intact cell membranes in their natural in situ state. Potential fluorescence methods available to probe intact membranes are fluorescence labeling of GM1-bound cholera toxin B to track lipid raft diffusion in cells, but potential link of the ganglioside to the cortical cytoskeleton (Caroni, 2001;Seveau et al., 2001;Yoon et al., 2003) elicited a

very low mobility that contributed to photobleaching of the dye (Bacia et al., 2004). Lipoid dyes such as dialkylindocarbocyanines (DiI), on the other hand are more representative of the lipid mobility (Gullapalli et al., 2008) and induce negligible cytotoxicity (De Clerck et al., 1994). In model membranes, DiI-C_{12} preferentially partitions into liquid phases and DiI-C_{18} into gel phases (Klausner and Wolf, 1980;Spink et al., 1990). In cells, DiI-C_{12} predominantly probes fluid phases while DiI-C_{18} segregates in more ordered domains (Hao et al., 2001). The photophysics (e.g. fluorescence lifetime, quantum yield) has been well characterized (Packard and Wolf, 1985;Sims et al., 1974), and because these dyes share identical chromophores and differ only by their chain lengths, they are useful in definitively assigning their unique photophysical properties to different domains. For most other "raft" associated dyes there is no structurally equivalent counter stain.

It is hypothesized in this study that shear stress leads to differential perturbation of membrane microdomains. To obtain data on the transient character of the endothelial plasma membrane domain responses to a step shear (Davies, 1997;Takahashi et al., 1997), we used time-correlated single photon counting (TCSPC) technology applied to single molecule fluorescence of membrane domain-specific fluorescent dyes. TCSPC can record the arrival times of each fluorescence photon with respect to the laser pulse time with resolution down to tens of picoseconds and at repetition rates in the MHz range. Post-processing of accumulated fluorescence photon arrival times provides determination of fluorescence lifetimes, diffusion coefficients, using fluorescence correlation spectroscopy (FCS) (Elson and Magde, 1974;Magde et al., 1974), and number of fluorescent molecules and molecular brightness from moment analysis (Qian and Elson,

1990). TCSPC has been used in cell membrane studies involving FCS, Forster resonance energy transfer (FRET) and fluorescence lifetime imaging (FLIM) (Caiolfa et al., 2007;Davey et al., 2007;Duncan et al., 2004;Sharma et al., 2003), but only a few studies combining fluorescence lifetime and FCS from the same data have been reported in cells (Becker et al., 2006), and no studies, to date, have used the technique to elucidate mechanotransduction mechanisms. Here we show that domains defined by DiI-C_{12} and DiI-C_{18} react to shear stress with differences the time-dependence of diffusion coefficients, fluorescence lifetimes, and number of molecules in the probe volume, results that can be explained by transient, domain-specific shear-induced changes in lipid viscosity, domain organization, and surface topography.

4.2 Materials and methods

4.2.1 Flow setup

The flow loop setup was thoroughly described previously (Dangaria and Butler, 2007). Briefly, a step shear stress of 0 to 10 dyn/cm^2 (with 0.36 sec halftime rise) was induced from a pressure gradient delivered through a computer-controlled, six-port modular valve positioner (Hamilton, Reno, NV) connected to four media reservoirs. Inducing flow using equal and opposite pressure changes ensures that there is not pressure change in the chamber itself, and thus prevents coverslip deflection, which could create artifacts in analysis of FCS and other parameters from TCSPC (Tabouillot et al., 2006). Physiological conditions were preserved by the use of temperature control in the

parallel-plate flow chamber Focht Chamber System (FCS2) (Bioptechs, Butler, PA) and the superfusion of 5% CO_2 over the media reservoirs. A differential pressure transducer DP-15 (Validyne Engineering, Northridge, CA) continuously monitored and recorded pressure changes across the flow chamber.

4.2.2 Cell culture and staining

Bovine aortic endothelial cells (BAECs) (VEC Technologies, Rensselaer, NY) were cultured in MCDB-131 complete medium (450 mL) supplemented with 50 mL FBS (fetal bovine serum), 10 ng/mL EGF (epidermal growth factor), and 1 μg/mL hydrocortisone with addition of 50 μL/mL 100× antibiotic/antimycotic solution, 90 μg/mL heparin, and 0.2 mg/mL ENDO GRO (VEC Technologies, Rensselaer, NY). Cells, passages 5 to 10, were incubated in this medium at 37°C with 5% CO_2 and grown to confluence on No. 1 glass coverslips. The medium was changed to phenol-red free Dulbecco's modified Eagle's medium (DMEM) (GIBCO, Carlsbad, CA) with 10% FBS 24h before experiment.

Cell membranes were stained using either 1,1′-dioctadecyl-3,3,3′,3′-tetramethylindocarbocyanine perchlorate (DiI-C_{18}) or 1,1′-didodecyl-3,3,3′,3′-tetramethylindocarbocyanine perchlorate (DiI-C_{12}) (Invitrogen, Eugene, OR). Stock solutions were prepared in ethanol: 1mM for DiI-C_{18} and 100mM for DiI-C_{12}. Subsequent dilutions were performed in ethanol and Dulbecco's phosphate-buffered saline (DPBS) with calcium and magnesium to a final concentration of 1 μM. The cells were washed three times in DPBS, then, incubated with the staining solution for 3-4 min

at 37°C. The cells were washed again five times in DPBS and mounted on the flow chamber in phenol-red free DMEM with 10% FBS.

4.2.3 GUV Preparation

Giant unilamellar vesicles were formed using a modified electroformation technique (Dimitrov and Angelova, 1987): an oscillating electric field created between two transparent ITO-coated coverslips, used as electrodes, caused the electroformation of vesicles. Briefly, a lipid mixture comprising of lipid and chloroform solvent was dissolved and 2 microliters of the solution was then placed on the surface of one coverslip and blown-dried with argon. After a 30-min vacuum drying period, the mixture was covered with 0.1 M sucrose solution at 55°C, a small chamber was assembled and the whole was then placed in a baking oven constantly maintained at a temperature of 55°C. An alternating current was applied across the wire electrodes for 4-5 hours. A LabView-controlled A/D board (National Instruments, Austin, TX, USA) was used to apply to the wires 0 to 1 V in increments of 50 mV at 5 minute intervals, followed by a constant voltage of 1.2 V for 3 hours. Subsequently, the whole chamber is disconnected from the function generator and the vesicles are gradually cooled to room temperature.

4.2.4 Optical setup

A detailed description of our confocal molecular dynamics microscope (CMDM) was described previously (Gullapalli et al., 2007). In summary, the excitation beam from

a PicoTRAIN water-cooled 532-nm, 80-MHz, 5.4-ps pulsed laser (High-Q Laser, Hohenems, Austria) entered the side of an IX-71 microscope (Olympus, Tokyo, Japan) and underfilled the back aperture of an Olympus 60× / 1.2-NA water-immersion objective (Hess and Webb, 2002). Emitted light passed a polarizer positioned at the magic angle, and was focused onto a 50-μm, 0.22-NA optical fiber – acting as pinhole. The signal from the photomultiplier tube went to a preamplifier and the time-correlated single photon counting (TCSPC) board (HFAC-26 and SPC-630, Becker & Hickl, Berlin, Germany). The sample was positioned using a high resolution 3-D piezo-electric stage (NanoView, Mad City Labs, Madison, WI) and imaged using a high-sensitivity CCD camera (Sensicam EM, Cooke Corporation, Romulus, MI).

4.2.5 Single-Molecule Fluorescence Spectroscopy

Time-correlated single photon counting technology allows one to record the arrival time of photons with respect to the beginning of the measurement (macrotime) and with respect to the excitation pulse time (microtime). From the microtime, we built histograms from which fluorescence lifetimes were determined. From the macrotime, recorded in first-in first-out (FIFO) mode, we can build autocorrelation functions from FCS to measure the diffusion coefficients. However, it is also possible to recover the microtime from FIFO data when using a pulsed laser. Consequently, one data file contained all the information necessary for extraction of diffusion, brightness, and lifetime.

Fluorescence lifetime, through the non-radiative decay factor, depends on local environmental factors such as hydration, oxygen concentration, and ionic strength (Lakowicz, 1999). Fluorescence intensity is usually represented by a sum of exponential decays Eq. 4.1:

$$I(t) = \sum_i \alpha_i \exp(-t/\tau_i) \qquad 4.1$$

where α_i is the the fraction of molecules with lifetime τ_i, normalized to unity.

Fluorescence correlation spectroscopy studies the transport properties of a fluorescently-tagged molecule in an observation volume defined by the diffraction limit of the excitation light beam and the confocal properties of the emission pathway. Fluorescent molecules moving in and out of the observation volume induce bursts in fluorescence which can be correlated in time. The resulting autocorrelation curve is fitted for particular expected transport phenomena. For 2-dimensional free-diffusing multiple species, the fitting function is of the form Eq. 4.2:

$$G(\tau) = \left(1 - T + T \cdot \exp\left(-\frac{\tau}{\tau_T}\right)\right) \cdot \left(\frac{0.5}{N(1 - T_r)}\right) \cdot \sum_{i=1}^{n} b_i \left[1 + \left(\tau / \tau_{Di}\right)\right]^{-1} \qquad 4.2$$

where b_i is the relative fraction of species i, τ_{Di} is the diffusion time of species i and N is the average number of fluorescent particle in the observation volume. The first factor accounts for triplet-state blinking: T_r is the average fraction from triplet-state and τ_T is its relaxation time.

Experiments were performed using < 100-μW excitation power at the objective back aperture in order to avoid photobleaching (Widengren and Rigler, 1996) and the system was calibrated using free diffusing rhodamine 6G dye (R6G) (Invitrogen, Eugene,

OR) with known diffusion coefficient and fluorescence lifetime (Widengren et al., 1995;Lakowicz and Berndt, 1991). The resulting observation volume characteristic radius was r ~ 443 nm with a structure factor (axial radius over lateral radius) maintained under 8.

Moment analysis is a model-independent and computationally-fast approach to count the number of fluorescence molecules in the observation volume (Qian and Elson, 1990). It is based on the computation of the moments of the photon count distribution from the PMT, where the average number of molecules, $\overline{N}$, is given by Eq. 4.3 :

$$\overline{N} = \frac{\gamma \langle k \rangle^2}{\langle \Delta k^2 \rangle - \langle k \rangle} \qquad 4.3$$

where γ is the geometric factor of the volume, $\langle k \rangle$ is the average photon count and $\langle \Delta k^2 \rangle$ its variance. Thus, the molecular brightness is (Eq. 4.4):

$$\varepsilon = \langle k \rangle / \overline{N} \qquad 4.4$$

Lifetime curves were fit in Fluofit software (PicoQuant, Berlin, Germany) by iterative reconvolution or tail fitting depending on the case studied (see Results). Good fit was assessed from minimization of the χ^2 values and absence of correlation in the residuals. Statistics and autocorrelation fits from FCS data were performed in Origin software (Originlab, Northampton, MA). Significant differences were evaluated by computing Two Sample Paired t-Tests with $p < 0.05$ (*) or $p < 0.01$ (**).

4.2.6 Experimental Procedures

Cellular and model membrane studies were performed over multiple days. Laser position with respect to the imaging system was checked and fluorescence correlation spectroscopy system was calibrated before each experiment. Once the cells were mounted onto the flow chamber, lateral positioning was accomplished using differential interference contrast (DIC). Axial positioning of the observation volume was set by rapid fluorescence count scan and correlation assessment. A custom-written Labview VI (National Instruments, Austin, TX) controlled stage position and recorded signal from the pressure transducer.

The effect of shear stress on endothelial cell membrane was studied by recording simultaneously changes in lifetime and diffusion coefficient of the membrane dye for 2 minutes before shear, 2 minutes during a 10-dyn/cm^2 shear, and 2 minutes after discontinuation of shear. Fluorescence data saved during the overall time of experiment were truncated in discrete steps. Autocorrelation functions from FCS data were computed and analyzed for 20-second time increments, and fluorescence fluctuation and lifetime data for both 20 and 5-sec time increments.

4.3 Results

4.3.1 Membrane phase-specific dye photophysics depends on the DiI chromophore and not on alkyl chain length

We wished to determine whether phase-specific differences in dye photophysics were due to the chromophore or alkyl chain interaction with surrounding lipids. Thus, fluorescence lifetime and diffusion coefficient values were measured in giant unilamellar vesicles to assess the behavior of DiI-C_{12} and DiI-C_{18} dyes in liquid-disordered (L_d) (DOPC) and liquid-ordered (L_o) phase (DOPC:cholesterol in a 1:1 mole fraction) (Table 4-1). Ten FIFO measurements, taken at room temperature, were recorded for each data set. Fluorescence lifetimes were obtain by fitting histograms of arrival times with a double exponential using iterative reconvolution, and diffusion coefficients were determined by fitting autocorrelation curves for 2-D diffusion. In a given membrane phase, lateral mobility is only marginally affected by the hydrocarbon chain length as evidence by the similarities in diffusion coefficient of DiI-C_{12} and DiI-C_{18} when dyes were incorporated into either liquid disordered ($D_{Ld} \sim 8 \times 10^{-8}$ cm^2/s) or liquid ordered phase lipids ($D_{Lo} \sim 5 \times 10^{-8}$ cm^2/s). Attempts to record diffusion coefficients in gel phase, using DPPC, resulted in photobleaching of dyes appearing immobile, as reported previously (Klausner and Wolf, 1980). Similarly, fluorescence lifetimes depended on membrane phase and not chain length as shown by the fact that the lifetimes for the two dyes were equivalent in all studied phases. Notably, lifetime values did not increase from the addition of cholesterol ($\tau_{fl} < 1.08$ns) but did when in gel phase ($\tau_{fl} > 1.28$ns). Packard and Wolf (Packard and Wolf, 1985) reported a lifetime increase from liquid to gel phase

but a consecutive increase and decrease in lifetime with increasing cholesterol content in DPPC. However, the results of the former study might be influenced by homo-FRET from high concentrations of dye.

Table 4-1: Diffusion coefficient and lifetime values with standard deviations of DiI-C_{12} and DiI-C_{18} in giant unilamellar vesicles exemplifying liquid-disordered (DOPC), liquid-ordered (DOPC:cholesterol in a 1:1 mole fraction) and gel (DPPC) phases. Courtesy Hari S. Muddana for GUV data.

D ($\times 10^{-8}$ cm^2/s) ; $\boldsymbol{\tau_1}$ (ns) , $\boldsymbol{\tau_2}$ (ns)		
	DiI-C_{12}	**DiI-C_{18}**
DOPC	8.2 ± 0.4 0.29 ± 0.01, 0.92 ± 0.01	7.8 ± 0.5 0.28 ± 0.02, 0.93 ± 0.02
DOPC:cholesterol (1:1)	5.0 ± 0.2 0.36 ± 0.02 , 1.07 ± 0.02	5.0 ± 0.2 0.36 ± 0.02, 1.08 ± 0.01
DPPC:cholesterol (1:1)	1.5 ± 0.2 0.30± 0.05, 1.36 ± 0.07	1.4 ± 0.1 0.29± 0.03, 1.37 ± 0.06
DPPC	immobile 0.34 ± 0.03, 1.28 ± 0.04	immobile 0.29 ± 0.05, 1.31 ± 0.02
Cells ($\mathbf{D_2}$ / $\boldsymbol{\tau_2}$)	8.23 ± 0.7 1.26 ± 0.02	5.38 ± 0.8 1.43 ± 0.05

4.3.2 Fluorescence lifetime of DiI depends on local viscosity surrounding the chromophore and is independent of dye chain length

Effect of local viscosity on dye lifetimes was estimated by varying the content of reagent-grade glycerol from 0 to 70% (v/v) in ethanol solutions (Figure 4-1). Viscosity of each sample was measured separately with a viscometer. The values of the fast component remain constant from 10 to 70 cp: $\tau_{1,C12}$ = 0.19 ± 0.01 ns and $\tau_{2,C18}$ = 0.17 ± 0.02 ns while the slow component increased approximately linearly (α_{C12} = 0.0073 ns/cp, α_{C18} = 0.0113 ns/cp) over the same range of viscosity.

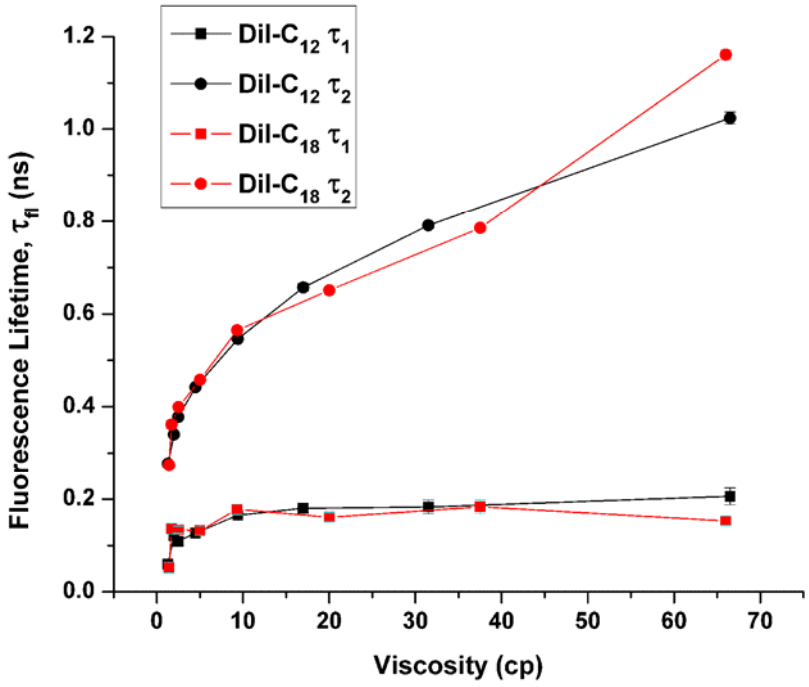

Figure 4-1: Increases in fluorescence lifetime (means and standard deviations) of DiI-C_{12} and DiI-C_{18} in solutions of increasing viscosity. Fast components do not vary for viscosities higher than 10 cp, while slow components seems to increase linearly (α_{C12} = 0.0073 ns/cp, α_{C18} = 0.0113 ns/cp). Courtesy Hari S. Muddana.

4.3.3 Cellular Plasma Membrane Fluorescence Spectroscopy

Confluent bovine aortic endothelial cells were subjected to a step shear of 10 dyn/cm^2 from fluid flow and the photophysics and dynamics of DiI-C_{12} and DiI-C_{18} were recorded continuously. The observation volume was a spot on the plasma membrane on the midpoint between the nucleus and cell border on the upstream of the cell (Butler et al., 2001). Fluorescence from DiI embedded in the membrane was collected in FIFO mode, allowing extraction of fluorescence fluctuations and lifetime data. The use of a

time-correlated single photon counting based system permitted the gathering of simultaneous information at the nanosecond (fluorescence lifetimes) and micro to milliseconds (lateral diffusion) timescales from single molecules. However, the in order to have single molecule sensitivity, one needs to acquire have less photons in each time step resulting in lower time resolution. Diffusion coefficients, in particular, necessitate more photons to build and fit the autocorrelation function. In addition, the standard error of FCS measurement reaches 20% for 2-species fits (Meseth et al., 1999), as seen in model membranes (Korlach et al., 1999). Considering all the above, the time step chosen to process lateral mobility data was 20 seconds, against 5 seconds for fluorescence lifetime. Measurements of DiI-C_{12} were averaged over 8 cells and DiI-C_{18} over 7 cells. Physical properties were normalized to the mean pre-shear values (60 s for 20-s time steps and 30 s for 5-s time steps) for each cell independently. Significance tests were performed by computing two-sample paired t-tests with respect to the last pre-shear value (at 100 s for 20-s time steps and 115 s for 5-s time steps).

4.3.4 Shear stress induces early and transient decrease in DiI-C_{12} lifetime and later and sustained decrease in DiI-C_{18} lifetime

Fluorescence lifetime data were reported for 20-s integration time steps and plotted with respect to the entire duration of the experiment. DiI-C_{12} and DiI-C_{18} dyes show double exponential lifetime but, from our solution results, model membrane results and literature (Packard and Wolf, 1985), the first component does not vary appreciably with viscosity. Thus, we focused on the shear-induced changes in variations of the longer exponent, for which values were recovered by tail fitting the histogram at 0.5ns from

maximum intensity (Benda et al., 2006;Ma et al., 2005). The mean lifetime values were $\tau_2 = 1.26 \pm 0.02$ ns for DiI-C_{12} and $\tau_2 = 1.43 \pm 0.05$ ns for DiI-C_{18} over the course of the experiment. Figure 4-2 shows a significant decrease in DiI-C_{12} normalized lifetime at 20 seconds after onset of shear. DiI-C_{18} exhibited a significant decrease in normalized lifetime for 20 s at 40, 80 and 120 seconds after onset of shear.

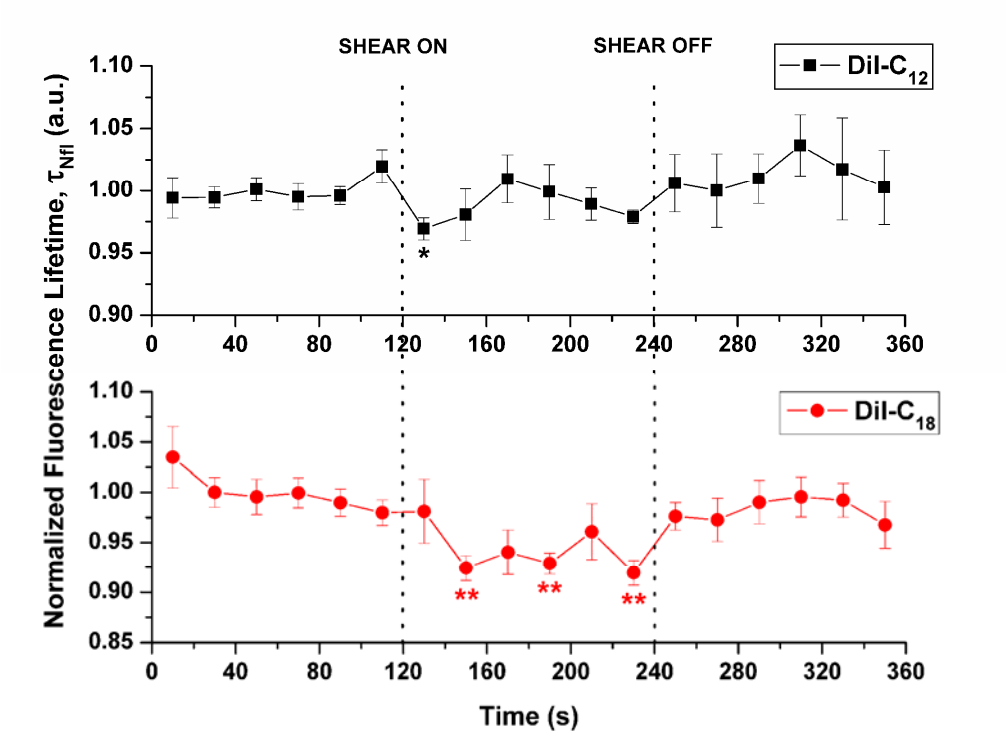

Figure 4-2: Effect of shear stress on normalized fluorescence lifetime of membrane dyes DiI-C_{12} and DiI-C_{18}: means and standard errors for 20-s integration times. The curves were tail fitted for the slow exponent only, showing a significant decrease in lifetime of DiI-C_{12} immediately at the onset of shear and for DiI-C_{18} at 40, 80 and 120 s after onset of shear.

Lifetime data were also processed for 5-second time increments from 30 s before to 60 s after onset of shear. The mean values and standard errors for each dye are displayed in Figure 4-3 for each time step. There was a significant decrease in the

fluorescence lifetime for DiI-C_{12} cells 5, 15 and 30 s after onset of shear. DiI-C_{18} exhibited a decrease in normalized lifetime 10, 20, 25, 35, 45 and 50 s after onset of shear. Thus shear stress induced a transient decrease in DiI-C_{12} lifetime with representative time on the order of 10 seconds, while the decrease with shear stress of DiI-C_{18} was delayed and sustained (Figure 4-3).

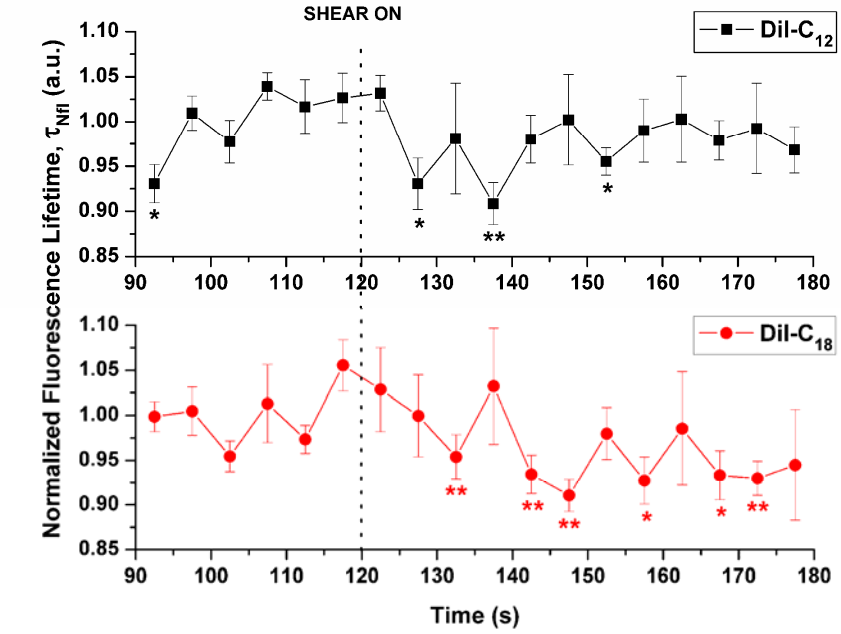

Figure 4-3: Effect of shear stress on normalized fluorescence lifetime of membrane dyes DiI-C_{12}: means and standard errors for 5-s integration time from 30 s pre-shear to 60 s of shear. Fluorescence lifetime curves were tail fitted for the slow exponent only, showing a significant decrease in lifetime after 5 s from onset of shear for DiI-C_{12} (5, 15 and 30 s) and after 10 s for DiI-C_{18}. The decrease is sustained for C_{18} until 55 s after onset of shear (10, 20, 25, 35, 45 and 50 s).

4.3.5 Shear stress induces a rapid increase in number of molecules for DiI-C_{12} domains and a decrease for DiI-C_{18} domains

Fluorescence fluctuations recorded from the FIFO data allow us to gather values for the number of molecules (*N*) in the observation volume other than from the FCS autocorrelation fit. Correction for the photomultiplier tube counting statistics through calculation of the molecular brightness gives more accurate values for *N* (Qian and Elson, 1990). For 5-s integration time, the normalized number of molecules in the observation volume of DiI-C_{12} increases significantly for 15 seconds (0, 5, 10s), as shown in Figure 4-4. DiI-C_{18} also shows a significant decrease for 5 seconds immediately after onset of shear (Figure 4-4).

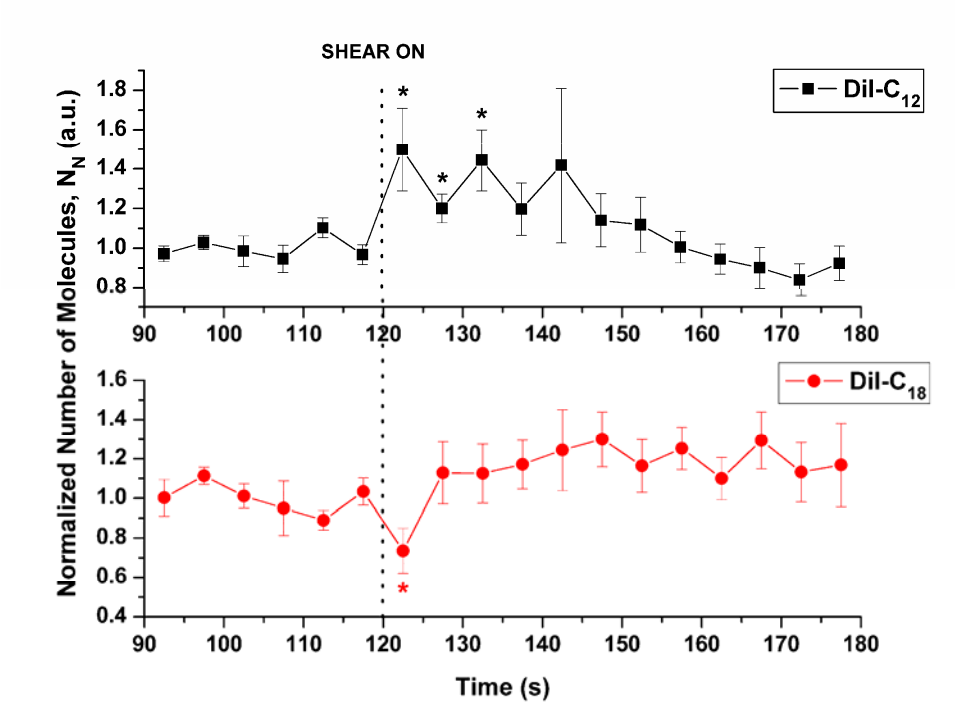

Figure 4-4: Increase for 15 seconds in the normalized number of molecules, *N*, in the observation volume for DiI-C_{12} (0, 5, 10 s) and decrease for 5 seconds for DiI-C_{18}. Means and standard errors for 5-s integration time from 30 s pre-shear to 60 s of shear.

4.3.6 Shear stress induced an increase in lateral diffusion of DiI-C_{18} but not DiI-C_{12}

Autocorrelation curves from fluorescence correlation spectroscopy measurements were integrating 20-second step data. They were fit for 2-component 2-D diffusion (Gielen et al., 2005;Schwille et al., 1999;Wawrezinieck et al., 2005), where the fast component diffusion coefficient was in the range of that of free dye. The mean values of the slow diffusion components are $D_2 = (8.23 \pm 0.66) \times 10^{-8}$ cm^2/s (ranging from 6.34×10^{-8} cm^2/s to 10.4×10^{-8} cm^2/s) for DiI-C_{12} and $D_2 = (5.38 \pm 0.81) \times 10^{-8}$ cm^2/s (ranging from 1.77×10^{-8} cm^2/s to 10.1×10^{-8} cm^2/s) for DiI-C_{18}. Mean values and standard errors for normalized diffusion coefficients of the slow component are plotted over the time course of the experiment in Figure 4-5. We see a significant increase in the diffusion coefficient of membranes carrying DiI-C_{18} dye between 20 and 40 s after onset of shear Figure 4-5.

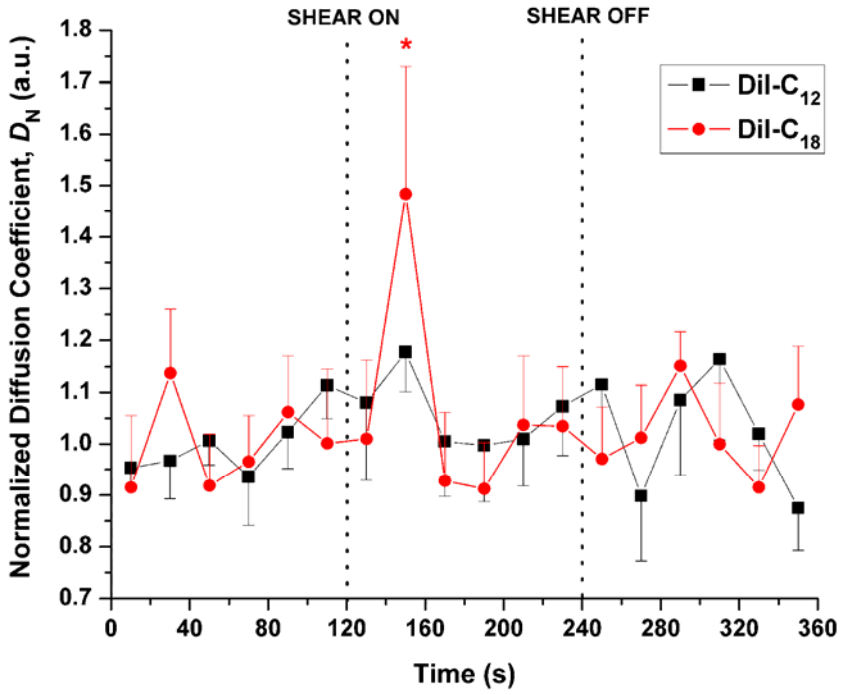

Figure 4-5: Fluorescence correlation spectroscopy data (means and standard errors) from 20-s integration time steps show an increase in diffusion of DiI-C_{18} from 20 to 40 s after onset of shear.

4.4 Discussion

To elucidate the role of endothelial cells plasma membrane to shear stress, we recorded the change in physical properties of fluorescent probes embedded in the lipid bilayer upon onset of shear. Principal results are as follows. First, the chain lengths of DiI determine the domain phase specificity and have no effect on the chromophore photophysics. Second, an increase in lifetime, based on control data from GUVs and increasing glycerol concentration solutions, indicate an increase in local molecular

viscosity. Third, shear stress induces an early and transient decrease in DiI-C_{12} lifetime and later a sustained decrease in DiI-C_{18} lifetime. Fourth, shear stress induces a rapid increase in number of molecules for DiI-C_{12} domains and a decrease for DiI-C_{18} domains, suggesting that the area of the membrane probed by the confocal volume increases and decreases, respectively. Fifth, shear stress induced a later and transient increase in lateral diffusion of DiI-C_{18} but not DiI-C_{12}, suggesting that DiI-C_{18}-labeled domains become smaller and more mobile during that period of time.

Our control studies on GUVs show that the shorter lifetime and faster diffusion of DiI-C_{12} relative to DiI-C_{18} in cells is due to the fact that its chromophore is responding to local differences in lipid phase, and is not a result of differences in chain length of the dyes. Diffusion coefficients of DiI-C_{12} and DiI-C_{18} collected in giant unilamellar vesicles were consistent with the literature (Almeida et al., 1992;Kahya et al., 2004;Sankaram and Thompson, 1990) and illustrate that both dyes behave very similarly in the same lipid phase (Table 4-1). Mean diffusion coefficients in cells show that the dyes in the plasma membrane probe two different domains: DiI-C_{12} is in a liquid-disordered environment, while DiI-C_{18} stays in more liquid-ordered domains. Nevertheless, the two dyes we used to probe the plasma membrane are dialkylindocarbocyanines dyes that only differ by the length of their alkyl chains. Chromophores are located within the lipid bilayer just below the lipid headgroups (Gullapalli et al., 2008) and we did not register large effects from increasing water accessibility on lifetime values (supplementary data). We assume uniformity of electrostatic charge fields around the bilayer and low dye concentration would prevent homo-FRET. Average lifetime values obtained from shear experiments are consistently higher than in our GUV and solution controls. A possible explanation is the

overall negatively charged electrostatic field surrounding the lipid bilayer. The glycocalyx and inner cell polarization could decrease the dielectric constant of the surrounding medium. The effective range of electrostatic interactions would potentially affect the radiative rate of the fluorophore (Toptygin, 2003). Thus, an increase in charge results in a decrease in refractive index and decrease in radiative rate of fluorophores. On the other hand, an increase in lifetime in increasing glycerol concentrations (Figure 4-1) seems to point toward local viscosity as the main cause of lifetime change. Thus decreases in fluorescence lifetime with shear stress indicate a reduction in local viscosity. Since DiI labels only the outer leaflet, we conclude that shear stress induces a decrease in viscosity of the outer leaflet of the membrane.

The two membrane domains under study behaved differently to the effect of shear. DiI-C_{12} showed an earlier change than DiI-C_{18}. The number of DiI-C_{12} molecules increased by about 30% for 15 seconds immediately after onset of shear (Figure 4-4). This phenomenon did not result from a change of focus or membrane axis angle since there was no decrease in molecular brightness (supplementary data) or decrease in diffusion coefficient (Milon et al., 2003;Sorscher and Klein, 1980). Thus, the increase in *N* is only possible when the surface area of the membrane probed by the confocal volume increases. A possible explanation are membrane ripples, that have been reported in cell previously (Gov and Safran, 2005;Gov and Gopinathan, 2006;Levin and Korenstein, 1991;Tuvia et al., 1997). The role of the glycocalyx has been brought forward for impairing fluid flow near the lipid bilayer (Damiano et al., 2004;Secomb et al., 2001) and for its role as mechanotransducer (Tarbell and Pahakis, 2006;Weinbaum et al., 2003). Although there is still controversy about its integrity (Potter and Damiano, 2008), it is

also present in cultured endothelial cells (supplementary data) (Florian et al., 2003;Vijayagopal et al., 1988). A documented pattern for the glycocalyx has displayed syndecans-actin cytoskeleton anchors 100 nanometers apart (Squire et al., 2001) and a mechanism for translation of the mechanical stress form fluid flow to the cell has been described by a moment about an axis normal to the direction of shear on anchored syndecans (Weinbaum et al., 2003). If undulations occurred between anchored points, the surface area between each would increase by 30%. Assuming a sinusoidal wave, the membrane undulation would have an 18-nm amplitude (Milon et al., 2003). Undulations that increase the surface area by 30% should decrease the apparent diffusion coefficient of the dye by approximately the same amount. Either FCS measurements could not detect that change, or the lateral mobility of the domain was also enhanced during that period of time. The decrease in lifetime at 5 and 15 seconds (Figure 4-3) is also not correlated with a decrease in molecular brightness (supplementary data), thus reflecting a decrease in viscosity. Since the dye resides in the upper leaflet during the experimental time, the recorded viscosity increase might come from the larger portion of the membrane going outward, resulting in lesser order of the lipids. GPI-anchored proteoglycans, glypicans, float on the upper leaflet and can also translate mechanical force through lateral motion. Finally, the decrease in lifetime for DiI-C_{12} with shear stress is consistent with a decrease in viscosity of the outer membrane leaflet resulting from outward curvature and the associated expansion of the leaflet (Discher et al., 1994).

The wider range of diffusion coefficient values of DiI-C_{18} shows the heterogeneous nature of the domains it sits in – some cells even show liquid-disordered-like diffusion. Similarly, DiI-C_{18} has been localized in higher-order domains (Davey et

al., 2007) as well as in less packed high-ordered domains (Loura et al., 2000) and GPI-anchored protein can display relatively fast lateral diffusion (Kenworthy et al., 2004;Subczynski and Kusumi, 2003). We recorded a delayed and transient increase in diffusion coefficient after shear (Figure 4-5). Lifetime values only started to decrease 10 seconds after onset of shear (Figure 4-3), but they remained low as long as shear was on (Figure 4-2). The absence of increase in the number of molecule (the meaning of the short decrease at 0 sec remains elusive) implies that there is no undulation. Fluorescence correlation spectroscopy records an increased lateral mobility that could be interpreted as a change in local viscosity, but the fluorescent probe has to travel in and out of the illuminated area which has a length scale of 1 μm. It is plausible that the higher-ordered domain increase in lateral mobility was a passive consequence to the increased mobility of the surrounding fluid phase. Fluorescence lifetimes, although more complex to interpret, could represent the local viscosity in a more confined region. For example, DiI-C_{18} has been shown to colocalize with IgE receptors, and its lifetime increased upon domains formation (Davey et al., 2007). Possible candidates in our case are, but not only, domains associated with the glycocalyx: decreased viscosity would come from a passive – or active – alteration of the packing and organization of lipids surrounding glypicans and syndecans (Chu et al., 2004;Fuki et al., 2000;Tkachenko and Simons, 2002). As described by recent descriptions of membrane domain dynamics (Anderson and Jacobson, 2002;Subczynski and Kusumi, 2003), and because of the potentially fast lateral diffusion of GPI-anchored protein (Kenworthy et al., 2004;Subczynski and Kusumi, 2003), the increase in diffusion of DiI-C_{18} could be from the domain associated with glypicans.

In summary, the increase in lateral mobility of DiI-C_{12} can be explained by undulations and local reduction in viscosity in the more fluidic phase domains. This could be due to the twisting of the lipid bilayer from the moment of force transmitted from the fluid flow to syndecans and glypicans. The increase in diffusion coefficient of DiI-C_{18} recorded by FCS would be caused by the increased mobility of the surrounding fluid phase that would be transferred to more ordered domains, in addition to a possible drag of glypicans. Also, the consistency of the decrease in lifetime of DiI-C_{18} during application of the fluid shear stress translates the constant mechanical strain felt locally. However, several signaling events are triggered within the course of this experiment. G proteins and ion channels, in particular, are activated within seconds (Cooke et al., 1991;Goligorsky, 1988;Gudi et al., 1996;Olesen et al., 1988) and could be the cause of the stress regulation that seems to take place. Lipid turnover, as well, can occur within seconds, as seen in neuronal cells (Dai et al., 1998). But from the perspective of a passive response, stress could be transferred from fluid phase to ordered domains within seconds. Liquid ordered domains, counter intuitively, might aggregate upon application of force, as seen in vesicle under tension (Ayuyan and Cohen, 2008). And, even though stress is still applied locally to those domains, as revealed by decreased lifetimes, the slow decay of their lateral motion could be due to a minimization of energy.

This study showed time-dependent changes in diffusion coefficients using fluorescence correlation spectroscopy and simultaneous fluorescence lifetime measurements of lipoid dyes embedded in endothelial cells membrane. This novel approach to single-molecule membrane dynamics outlined the temporal, spatial and domain-dependent alteration of the lipid bilayer in response to physiological shear stress.

4.5 References

1. Almeida, P. F., W. L. Vaz, and T. E. Thompson. 1992. Lateral diffusion in the liquid phases of dimyristoylphosphatidylcholine/cholesterol lipid bilayers: a free volume analysis. *Biochemistry* 31:6739-6747.

2. Anderson, R. G. and K. Jacobson. 2002. A role for lipid shells in targeting proteins to caveolae, rafts, and other lipid domains. *Science* 296:1821-1825.

3. Ayuyan, A. G. and F. S. Cohen. 2008. Raft composition at physiological temperature and pH in the absence of detergents. *Biophys. J.* 94:2654-2666.

4. Bacia, K., D. Scherfeld, N. Kahya, and P. Schwille. 2004. Fluorescence correlation spectroscopy relates rafts in model and native membranes. *Biophys. J.* 87:1034-1043.

5. Baird, B., E. D. Sheets, and D. Holowka. 1999. How does the plasma membrane participate in cellular signaling by receptors for immunoglobulin E? *Biophys. Chem.* 82:109-119.

6. Bao, X., C. B. Clark, and J. A. Frangos. 2000. Temporal gradient in shear-induced signaling pathway: involvement of MAP kinase, c-fos, and connexin43. *Am. J. Physiol Heart Circ. Physiol* 278:H1598-H1605.

7. Barbee, K. A. 2002. Role of subcellular shear-stress distributions in endothelial cell mechanotransduction. *Ann. Biomed. Eng* 30:472-482.

8. Becker, W., A. Bergmann, E. Haustein, Z. Petrasek, P. Schwille, C. Biskup, L. Kelbauskas, K. Benndorf, N. Klocker, T. Anhut, I. Riemann, and K. Konig. 2006. Fluorescence lifetime images and correlation spectra obtained by multidimensional time-correlated single photon counting. *Microscopy Research and Technique* 69:186-195.

9. Benda, A., V. Fagul'ova, A. Deyneka, J. Enderlein, and M. Hof. 2006. Fluorescence lifetime correlation spectroscopy combined with lifetime tuning: new perspectives in supported phospholipid bilayer research. *Langmuir* 22:9580-9585.

10. Brown, D. A. and E. London. 1997. Structure of detergent-resistant membrane domains: does phase separation occur in biological membranes? *Biochem. Biophys. Res. Commun.* 240:1-7.

11. Brown, D. A. and J. K. Rose. 1992. Sorting of GPI-anchored proteins to glycolipid-enriched membrane subdomains during transport to the apical cell surface. *Cell* 68:533-544.

12. Butler, P. J., G. Norwich, S. Weinbaum, and S. Chien. 2001. Shear stress induces a time- and position-dependent increase in endothelial cell membrane fluidity. *Am. J. Physiol Cell Physiol* 280:C962-C969.

13. Butler, P. J., T. C. Tsou, J. Y. Li, S. Usami, and S. Chien. 2002. Rate sensitivity of shear-induced changes in the lateral diffusion of endothelial cell membrane lipids: a role for membrane perturbation in shear-induced MAPK activation. *FASEB J.* 16:216-218.

14. Caiolfa, V. R., M. Zamai, G. Malengo, A. Andolfo, C. D. Madsen, J. Sutin, M. A. Digman, E. Gratton, F. Blasi, and N. Sidenius. 2007. Monomer-dimer dynamics and distribution of GPI-anchored uPAR are determined by cell surface protein assemblies. *Journal of Cell Biology* 179:1067-1082.

15. Caroni, P. 2001. New EMBO members' review: actin cytoskeleton regulation through modulation of PI(4,5)P(2) rafts. *EMBO J.* 20:4332-4336.

16. Chachisvilis, M., Y. L. Zhang, and J. A. Frangos. 2006. G protein-coupled receptors sense fluid shear stress in endothelial cells. *Proc. Natl. Acad. Sci. U. S. A* 103:15463-15468.

17. Chu, C. L., J. A. Buczek-Thomas, and M. A. Nugent. 2004. Heparan sulphate proteoglycans modulate fibroblast growth factor-2 binding through a lipid raft-mediated mechanism. *Biochem. J.* 379:331-341.

18. Cooke, J. P., Rossitch E Jr, N. A. Andon, J. Loscalzo, and V. J. Dzau. 1991. Flow activates an endothelial potassium channel to release an endogenous nitrovasodilator. *J. Clin. Invest* 88:1663-1671.

19. Dai, J., M. P. Sheetz, X. Wan, and C. E. Morris. 1998. Membrane tension in swelling and shrinking molluscan neurons. *J. Neurosci.* 18:6681-6692.

20. Damiano, E. R., D. S. Long, and M. L. Smith. 2004. Estimation of viscosity profiles using velocimetry data from parallel flows of linearly viscous fluids: application to microvascular haemodynamics. *Journal of Fluid Mechanics* 512:1-19.

21. Dangaria, J. H. and P. J. Butler. 2007. Macrorheology and adaptive microrheology of endothelial cells subjected to fluid shear stress. *Am. J. Physiol Cell Physiol* 293:C1568-C1575.

22. Davey, A. M., R. P. Walvick, Y. X. Liu, A. A. Heikal, and E. D. Sheets. 2007. Membrane order and molecular dynamics associated with IgE receptor cross-linking in mast cells. *Biophysical Journal* 92:343-355.

23. Davies, P. F. 1997. Overview: temporal and spatial relationships in shear stress-mediated endothelial signalling. *J. Vasc. Res.* 34:208-211.

24. Davies, P. F. 1995. Flow-mediated endothelial mechanotransduction. *Physiol Rev.* 75:519-560.

25. Davies, P. F., K. A. Barbee, M. V. Volin, A. Robotewskyj, J. Chen, L. Joseph, M. L. Griem, M. N. Wernick, E. Jacobs, D. C. Polacek, N. dePaola, and A. I. Barakat. 1997. Spatial relationships in early signaling events of flow-mediated endothelial mechanotransduction. *Annu. Rev. Physiol* 59:527-549.

26. De Clerck, L. S., C. H. Bridts, A. M. Mertens, M. M. Moens, and W. J. Stevens. 1994. Use of fluorescent dyes in the determination of adherence of human leucocytes to endothelial cells and the effect of fluorochromes on cellular function. *J. Immunol. Methods* 172:115-124.

27. dePaola, N., M. A. Gimbrone, Jr., P. F. Davies, and C. F. Dewey, Jr. 1992. Vascular endothelium responds to fluid shear stress gradients. *Arterioscler. Thromb.* 12:1254-1257.

28. Dimitrov, D. S. and M. I. Angelova. 1987. Electric-Field Mediated Lipid Swelling and Liposome Formation. *Studia Biophysica* 119:61-65.

29. Discher, D. E., N. Mohandas, and E. A. Evans. 1994. Molecular maps of red cell deformation: hidden elasticity and in situ connectivity. *Science* 266:1032-1035.

30. Drevot, P., C. Langlet, X. J. Guo, A. M. Bernard, O. Colard, J. P. Chauvin, R. Lasserre, and H. T. He. 2002. TCR signal initiation machinery is pre-assembled and activated in a subset of membrane rafts. *EMBO J.* 21:1899-1908.

31. Duncan, R. R., A. Bergmann, M. A. Cousin, D. K. Apps, and M. J. Shipston. 2004. Multi-dimensional time-correlated single photon counting (TCSPC) fluorescence lifetime imaging microscopy (FLIM) to detect FRET in cells. *Journal of Microscopy-Oxford* 215:1-12.

32. Elson, E. L. and D. Magde. 1974. Fluorescence Correlation Spectroscopy .1. Conceptual Basis and Theory. *Biopolymers* 13:1-27.

33. Ferko, M. C., Patterson B.P., and P. J. Butler. 2006. High-resolution solid modeling of biological samples imaged with 3-D fluorescence microscopy.

34. Florian, J. A., J. R. Kosky, K. Ainslie, Z. Pang, R. O. Dull, and J. M. Tarbell. 2003. Heparan sulfate proteoglycan is a mechanosensor on endothelial cells. *Circ. Res.* 93:e136-e142.

35. Frangos, J. A. and S. R. Gudi. 1997. Shear Stress Activates Reconstituted G-Proteins in the Absence of Protein Receptors By Modulating Lipid Bilayer Fluidity. A521.

36. Frangos, J. A., T. Y. Huang, and C. B. Clark. 1996. Steady shear and step changes in shear stimulate endothelium via independent mechanisms--superposition of transient and sustained nitric oxide production. *Biochem. Biophys. Res. Commun.* 224:660-665.

37. Fujiwara, K., M. Masuda, M. Osawa, Y. Kano, and K. Katoh. 2001. Is PECAM-1 a mechanoresponsive molecule? *Cell Struct. Funct.* 26:11-17.

38. Fuki, I. V., M. E. Meyer, and K. J. Williams. 2000. Transmembrane and cytoplasmic domains of syndecan mediate a multi-step endocytic pathway involving detergent-insoluble membrane rafts. *Biochem. J.* 351 Pt 3:607-612.

39. Galbraith, C. G., R. Skalak, and S. Chien. 1998. Shear stress induces spatial reorganization of the endothelial cell cytoskeleton. *Cell Motil. Cytoskeleton* 40:317-330.

40. Gielen, E., J. Vercammen, J. Sykora, J. Humpolickova, M. Vandeven, A. Benda, N. Hellings, M. Hof, Y. Engelborghs, P. Steels, and M. Ameloot. 2005. Diffusion of sphingomyelin and myelin oligodendrocyte glycoprotein in the membrane of OLN-93 oligodendroglial cells studied by fluorescence correlation spectroscopy. *C. R. Biol.* 328:1057-1064.

41. Girard, P. R. and R. M. Nerem. 1993. Endothelial cell signaling and cytoskeletal changes in response to shear stress. *Front Med. Biol. Eng* 5:31-36.

42. Girard, P. R. and R. M. Nerem. 1995. Shear stress modulates endothelial cell morphology and F-actin organization through the regulation of focal adhesion-associated proteins. *J. Cell Physiol* 163:179-193.

43. Goligorsky, M. S. 1988. Mechanical stimulation induces Ca2+i transients and membrane depolarization in cultured endothelial cells. Effects on Ca2+i in co-perfused smooth muscle cells. *FEBS Lett.* 240:59-64.

44. Gov, N. S. and A. Gopinathan. 2006. Dynamics of membranes driven by actin polymerization. *Biophys. J.* 90:454-469.

45. Gov, N. S. and S. A. Safran. 2005. Red blood cell membrane fluctuations and shape controlled by ATP-induced cytoskeletal defects. *Biophys. J.* 88:1859-1874.

46. Gudi, S. R., C. B. Clark, and J. A. Frangos. 1996. Fluid flow rapidly activates G proteins in human endothelial cells. Involvement of G proteins in mechanochemical signal transduction. *Circ. Res.* 79:834-839.

47. Gullapalli, R. R., M. C. Demirel, and P. J. Butler. 2008. Molecular dynamics simulations of DiI-C18(3) in a DPPC lipid bilayer. *Phys. Chem. Chem. Phys.* 10:3548-3560.

48. Gullapalli, R. R., T. Tabouillot, R. Mathura, J. H. Dangaria, and P. J. Butler. 2007. Integrated multimodal microscopy, time-resolved fluorescence, and optical-trap rheometry: toward single molecule mechanobiology. *J. Biomed. Opt.* 12:014012.

49. Haidekker, M. A., C. R. White, and J. A. Frangos. 2001. Analysis of temporal shear stress gradients during the onset phase of flow over a backward-facing step. *J. Biomech. Eng* 123:455-463.

50. Hao, M., S. Mukherjee, and F. R. Maxfield. 2001. Cholesterol depletion induces large scale domain segregation in living cell membranes. *Proc. Natl. Acad. Sci. U. S. A* 98:13072-13077.

51. Hess, S. T. and W. W. Webb. 2002. Focal volume optics and experimental artifacts in confocal fluorescence correlation spectroscopy. *Biophys. J.* 83:2300-2317.

52. Jacobs, E. R., C. Cheliakine, D. Gebremedhin, E. K. Birks, P. F. Davies, and D. R. Harder. 1995. Shear activated channels in cell-attached patches of cultured bovine aortic endothelial cells. *Pflugers Arch.* 431:129-131.

53. Kahya, N., D. Scherfeld, K. Bacia, and P. Schwille. 2004. Lipid domain formation and dynamics in giant unilamellar vesicles explored by fluorescence correlation spectroscopy. *J. Struct. Biol.* 147:77-89.

54. Kenworthy, A. K., B. J. Nichols, C. L. Remmert, G. M. Hendrix, M. Kumar, J. Zimmerberg, and J. Lippincott-Schwartz. 2004. Dynamics of putative raft-associated proteins at the cell surface. *J. Cell Biol.* 165:735-746.

55. Klausner, R. D. and D. E. Wolf. 1980. Selectivity of fluorescent lipid analogues for lipid domains. *Biochemistry* 19:6199-6203.

56. Korlach, J., P. Schwille, W. W. Webb, and G. W. Feigenson. 1999. Characterization of lipid bilayer phases by confocal microscopy and fluorescence correlation spectroscopy. *Proc. Natl. Acad. Sci. U. S. A* 96:8461-8466.

57. Kuchan, M. J., H. Jo, and J. A. Frangos. 1994. Role of G proteins in shear stress-mediated nitric oxide production by endothelial cells. *Am. J. Physiol* 267:C753-C758.

58. Kusumi, A. and K. Suzuki. 2005. Toward understanding the dynamics of membrane-raft-based molecular interactions. *Biochim. Biophys. Acta* 1746:234-251.

59. Lakowicz, J. R. 1999. Principles of Fluorescence Spectroscopy. Springer.

60. Lakowicz, J. R. and K. W. Berndt. 1991. Lifetime-Selective Fluorescence Imaging Using An Rf Phase-Sensitive Camera. *Review of Scientific Instruments* 62:1727-1734.

61. LaMack, J. A. and M. H. Friedman. 2007. Individual and combined effects of shear stress magnitude and spatial gradient on endothelial cell gene expression. *Am. J. Physiol Heart Circ. Physiol* 293:H2853-H2859.

62. Levin, S. and R. Korenstein. 1991. Membrane fluctuations in erythrocytes are linked to MgATP-dependent dynamic assembly of the membrane skeleton. *Biophys. J.* 60:733-737.

63. Li, S., M. Kim, Y. L. Hu, S. Jalali, D. D. Schlaepfer, T. Hunter, S. Chien, and J. Y. Shyy. 1997. Fluid shear stress activation of focal adhesion kinase. Linking to mitogen-activated protein kinases. *J. Biol. Chem.* 272:30455-30462.

64. Loura, L. M., A. Fedorov, and M. Prieto. 2000. Partition of membrane probes in a gel/fluid two-component lipid system: a fluorescence resonance energy transfer study. *Biochim. Biophys. Acta* 1467:101-112.

65. Ma, G., N. Mincu, F. Lesage, P. Gallant, and L. McIntosh. 2005. System IRF impact on fluorescence lifetime fitting in turbid medium.

66. Magde, D., E. L. Elson, and W. W. Webb. 1974. Fluorescence Correlation Spectroscopy .2. Experimental Realization. *Biopolymers* 13:29-61.

67. Meseth, U., T. Wohland, R. Rigler, and H. Vogel. 1999. Resolution of fluorescence correlation measurements. *Biophysical Journal* 76:1619-1631.

68. Milon, S., R. Hovius, H. Vogel, and T. Wohland. 2003. Factors influencing fluorescence correlation spectroscopy measurements on membranes: simulations and experiments. *Chemical Physics* 288:171-186.

69. Mochizuki, S., H. Vink, O. Hiramatsu, T. Kajita, F. Shigeto, J. A. Spaan, and F. Kajiya. 2003. Role of hyaluronic acid glycosaminoglycans in shear-induced

endothelium-derived nitric oxide release. *Am. J. Physiol Heart Circ. Physiol* 285:H722-H726.

70. Naruse, K. and M. Sokabe. 1993. Involvement of stretch-activated ion channels in Ca2+ mobilization to mechanical stretch in endothelial cells. *Am. J. Physiol* 264:C1037-C1044.

71. Ohno, M., G. H. Gibbons, V. J. Dzau, and J. P. Cooke. 1993. Shear stress elevates endothelial cGMP. Role of a potassium channel and G protein coupling. *Circulation* 88:193-197.

72. Olesen, S. P., D. E. Clapham, and P. F. Davies. 1988. Haemodynamic shear stress activates a K+ current in vascular endothelial cells. *Nature* 331:168-170.

73. Orr, A. W., B. P. Helmke, B. R. Blackman, and M. A. Schwartz. 2006. Mechanisms of mechanotransduction. *Dev. Cell* 10:11-20.

74. Packard, B. S. and D. E. Wolf. 1985. Fluorescence lifetimes of carbocyanine lipid analogues in phospholipid bilayers. *Biochemistry* 24:5176-5181.

75. Pahakis, M. Y., J. R. Kosky, R. O. Dull, and J. M. Tarbell. 2007. The role of endothelial glycocalyx components in mechanotransduction of fluid shear stress. *Biochem. Biophys. Res. Commun.* 355:228-233.

76. Park, H., Y. M. Go, R. Darji, J. W. Choi, M. P. Lisanti, M. C. Maland, and H. Jo. 2000. Caveolin-1 regulates shear stress-dependent activation of extracellular signal-regulated kinase. *Am. J. Physiol Heart Circ. Physiol* 278:H1285-H1293.

77. Potter, D. R. and E. R. Damiano. 2008. The hydrodynamically relevant endothelial cell glycocalyx observed in vivo is absent in vitro. *Circ. Res.* 102:770-776.

78. Qian, H. and E. L. Elson. 1990. On the analysis of high order moments of fluorescence fluctuations. *Biophys. J.* 57:375-380.

79. Rizzo, V., A. Sung, P. Oh, and J. E. Schnitzer. 1998. Rapid mechanotransduction in situ at the luminal cell surface of vascular endothelium and its caveolae. *J. Biol. Chem.* 273:26323-26329.

80. Roy, S., R. Luetterforst, A. Harding, A. Apolloni, M. Etheridge, E. Stang, B. Rolls, J. F. Hancock, and R. G. Parton. 1999. Dominant-negative caveolin inhibits H-Ras function by disrupting cholesterol-rich plasma membrane domains. *Nature Cell Biology* 1:98-105.

81. Sankaram, M. B. and T. E. Thompson. 1990. Modulation of phospholipid acyl chain order by cholesterol. A solid-state 2H nuclear magnetic resonance study. *Biochemistry* 29:10676-10684.

82. Schwille, P., J. Korlach, and W. W. Webb. 1999. Fluorescence correlation spectroscopy with single-molecule sensitivity on cell and model membranes. *Cytometry* 36:176-182.

83. Secomb, T. W., R. Hsu, and A. R. Pries. 2001. Effect of the endothelial surface layer on transmission of fluid shear stress to endothelial cells. *Biorheology* 38:143-150.

84. Seong, J., S. Lu, M. Ouyang, H. Huang, J. Zhang, M. C. Frame, and Y. Wang. 2009. Visualization of Src activity at different compartments of the plasma membrane by FRET imaging. *Chem. Biol.* 16:48-57.

85. Seveau, S., R. J. Eddy, F. R. Maxfield, and L. M. Pierini. 2001. Cytoskeleton-dependent membrane domain segregation during neutrophil polarization. *Mol. Biol. Cell* 12:3550-3562.

86. Sharma, M. R., E. C. Koc, P. P. Datta, T. M. Booth, L. L. Spremulli, and R. K. Agrawal. 2003. Structure of the mammalian mitochondrial ribosome reveals an expanded functional role for its component proteins. *Cell* 115:97-108.

87. Sheets, E. D., G. M. Lee, R. Simson, and K. Jacobson. 1997. Transient confinement of a glycosylphosphatidylinositol-anchored protein in the plasma membrane. *Biochemistry* 36:12449-12458.

88. Sigurdson, W. J., F. Sachs, and S. L. Diamond. 1993. Mechanical perturbation of cultured human endothelial cells causes rapid increases of intracellular calcium. *Am. J. Physiol* 264:H1745-H1752.

89. Sims, P. J., A. S. Waggoner, C. H. Wang, and J. F. Hoffman. 1974. Studies on the mechanism by which cyanine dyes measure membrane potential in red blood cells and phosphatidylcholine vesicles. *Biochemistry* 13:3315-3330.

90. Sorscher, S. M. and M. P. Klein. 1980. Profile of A Focused Collimated Laser-Beam Near the Focal Minimum Characterized by Fluorescence Correlation Spectroscopy. *Review of Scientific Instruments* 51:98-102.

91. Spink, C. H., M. D. Yeager, and G. W. Feigenson. 1990. Partitioning Behavior of Indocarbocyanine Probes Between Coexisting Gel and Fluid Phases in Model Membranes. *Biochimica et Biophysica Acta* 1023:25-33.

92. Squire, J. M., M. Chew, G. Nneji, C. Neal, J. Barry, and C. Michel. 2001. Quasi-periodic substructure in the microvessel endothelial glycocalyx: a possible explanation for molecular filtering? *J. Struct. Biol.* 136:239-255.

93. Subczynski, W. K. and A. Kusumi. 2003. Dynamics of raft molecules in the cell and artificial membranes: approaches by pulse EPR spin labeling and single molecule optical microscopy. *Biochim. Biophys. Acta* 1610:231-243.

94. Tabouillot, T., R. R. Gullapalli, and P. J. Butler. 2006. Monitoring cellular mechanosensing using time-correlated single photon counting. 63720D.

95. Takahashi, M., T. Ishida, O. Traub, M. A. Corson, and B. C. Berk. 1997. Mechanotransduction in endothelial cells: temporal signaling events in response to shear stress. *J. Vasc. Res.* 34:212-219.

96. Tarbell, J. M. and M. Y. Pahakis. 2006. Mechanotransduction and the glycocalyx. *J. Intern. Med.* 259:339-350.

97. Thi, M. M., J. M. Tarbell, S. Weinbaum, and D. C. Spray. 2004. The role of the glycocalyx in reorganization of the actin cytoskeleton under fluid shear stress: a "bumper-car" model. *Proc. Natl. Acad. Sci. U. S. A* 101:16483-16488.

98. Tkachenko, E. and M. Simons. 2002. Clustering induces redistribution of syndecan-4 core protein into raft membrane domains. *J. Biol. Chem.* 277:19946-19951.

99. Toptygin, D. 2003. Effects of the solvent refractive index and its dispersion on the radiative decay rate and extinction coefficient of a fluorescent solute. *Journal of Fluorescence* 13:201-219.

100. Tuvia, S., A. Almagor, A. Bitler, S. Levin, R. Korenstein, and S. Yedgar. 1997. Cell membrane fluctuations are regulated by medium macroviscosity: evidence for a metabolic driving force. *Proc. Natl. Acad. Sci. U. S. A* 94:5045-5049.

101. Tzima, E. 2006. Role of small GTPases in endothelial cytoskeletal dynamics and the shear stress response. *Circ. Res.* 98:176-185.

102. Vijayagopal, P., S. R. Srinivasan, E. R. Dalferes, Jr., B. Radhakrishnamurthy, and G. S. Berenson. 1988. Effect of low-density lipoproteins on the synthesis and secretion of proteoglycans by human endothelial cells in culture. *Biochem. J.* 255:639-646.

103. Wawrezinieck, L., H. Rigneault, D. Marguet, and P. F. Lenne. 2005. Fluorescence correlation spectroscopy diffusion laws to probe the submicron cell membrane organization. *Biophys. J.* 89:4029-4042.

104. Weinbaum, S., X. Zhang, Y. Han, H. Vink, and S. C. Cowin. 2003. Mechanotransduction and flow across the endothelial glycocalyx. *Proc. Natl. Acad. Sci. U. S. A* 100:7988-7995.

105. Widengren, J., U. Mets, and R. Rigler. 1995. Fluorescence Correlation Spectroscopy of Triplet States in Solution: A Theoretical and Experimental Study. *J. Phys. Chem.* 99:13368-13379.

106. Widengren, J. and R. Rigler. 1996. Photobleaching investigations of dyes using fluorescence correlation spectroscopy (FCS). *Progress in Biophysics & Molecular Biology* 65:H109.

107. Yoon, S. S., K. I. Jung, Y. L. Choi, E. Y. Choi, I. S. Lee, S. H. Park, and T. J. Kim. 2003. Engagement of CD99 triggers the exocytic transport of ganglioside GM1 and the reorganization of actin cytoskeleton. *FEBS Lett.* 540:217-222.

4.6 Supplementary data

Effect of water content on fluorescence lifetime of DiI dyes (Figure 4-6).

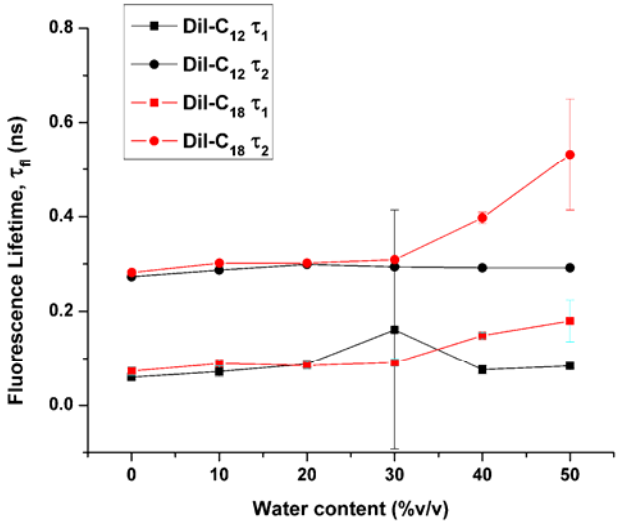

Figure 4-6: Increases in fluorescence lifetime (means and standard deviations) of DiI-C_{12} and DiI-C_{18} in ethanol solutions of increasing water content. Fast components do not vary, and slow component of DiI-C_{18} increases for 40% water and more. Courtesy Hari S. Muddana.

Molecular brightness of DiI dyes in plasma membranes for 5-s integration time (Figure 4-7).

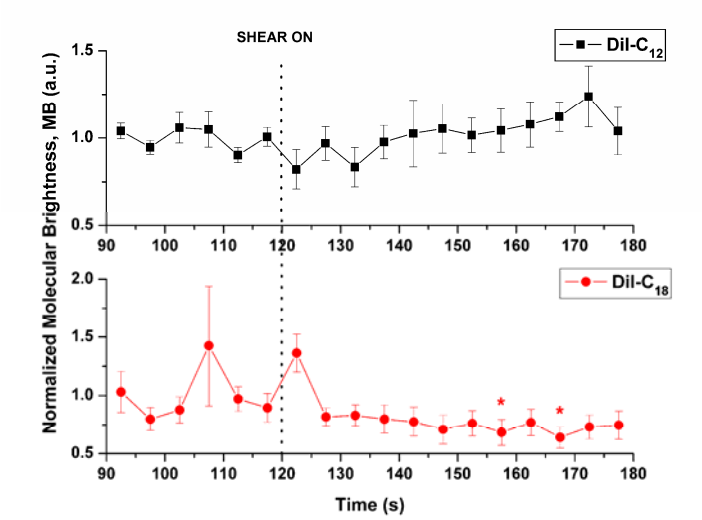

Figure 4-7: Molecular brightness of DiI-C_{12} remains constant for, while for DiI-C_{18}, there are significant decreases 35s and 45s from onset of shear. Means and standard errors for 5-s integration time from 30 s pre-shear to 60 s of shear.

Number of molecules of DiI in the observation volume in plasma membranes over 20-s integration time (Figure 4-8).

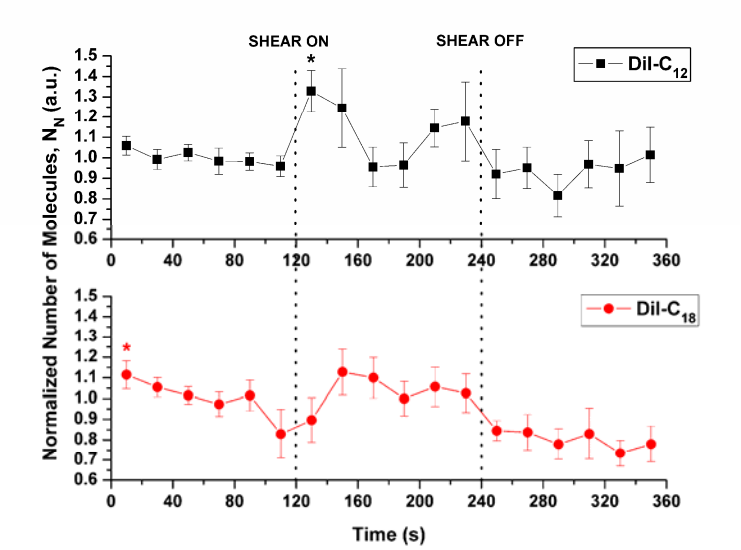

Figure 4-8: Normalized number of molecules (means and standard errors) from 20-s integration time steps show an increase in number of DiI-C_{18} dye molecules from immediately after onset of shear.

Glycocalyx staining picture with Alexa Fluor 647-tagged HepSS-1 on cultured endothelial cells (Figure 4-9).

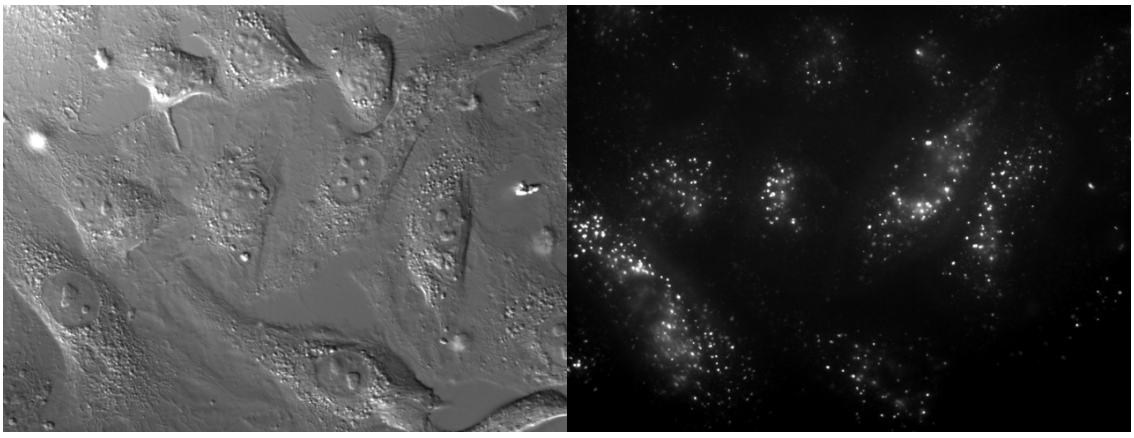

Figure 4-9: Cultured endothelial cells stained with Fluor 647-tagged HepSS-1 show similar patterns to literature (Thi et al., 2004).

Chapter 5

CONCLUSION

It is well recognized that forces applied to the cell are likely distributed to multiple locations (Davies et al., 1994;Ingber, 1997;Barbee, 2002). However, responses of cellular structures, such as focal adhesions, and many other responses, are generally measured at time points substantially later than the time of application of force. Thus, cell processes such as migration and the associated signaling pathways tend to be convoluted with mechanotransduction. It is therefore difficult to know when a mechanosensation event has occurred or whether the measured response represents a chronic or adaptive response to shear. Our approach in this study was to develop the instrumentation and methodology to definitely assess when and where mechanosensation was taking place. In addition, with the use of domain-selective dyes, we were able to delineate portions of the lipid bilayer that were more sensitive to shear than others.

Here, we have built a microscope-based optical setup to record molecular dynamics of lipoid dyes in cells, on timescales matching that of the earliest expected mechanotransduction events, and with single-molecule detection resolution. The sensitivity of the system was calibrated in solution studies and its efficiency was tested in model and native membranes. Finally, fluorescence spectroscopy measurements were performed in endothelial cell plasma membranes under application of fluid shear stress. Fluorescence correlation spectroscopy (FCS) allowed us to locate the dyes with their

respective phase or domain, and showed a large-scale increase in diffusion of DiI-C_{18} embedded in potential lipid rafts. Membrane undulations in the more fluidic parts of the lipid bilayer, probed by DiI-C_{12}, were also inferred from a combination of FCS, molecular brightness analysis and fluorescence lifetime (FL) measurements. Fluorescence lifetime seemed to be the most sensitive technique, with very high spatial and temporal resolution. Nonetheless, interpretation of changes in lifetime values is always very challenging in cells. FL results showed the biphasic nature of the membrane response to shear, temporally as well as domain-dependent: the more fluidic phase decreases in viscosity within the first 15 seconds, followed by the more ordered phase that decreases in viscosity in a more sustained manner.

While this study showed that the endothelial plasma membrane is a mechanosensor, it also opens the door to many other questions. Different lipid phases responded differently to a step in shear, suggesting that these domains have different roles in translation of the mechanical stimulus into biochemical signals. Lipid rafts probably play a major role in translating the information, either in propagation of the stress to embedded proteins – actin cytoskeleton for example (Caroni, 2001), or more directly by alteration of its lipid content – as cholesterol content affects the calcium response (Munro, 2003). Further cell studies, however, will be hard without disrupting key components of the regular cell machinery. For example, interpretation of experiments in which glycocalyx disruption attenuates the shear response, are difficult to determine since it is likely that the glycocalyx plays a role in ordering the membrane. Experimental verification of this interaction awaits further testing. Forster resonance energy transfer (FRET) might be able to help by combining local physical perturbations and

colocalization with a protein of interest. Potential candidates are glycocalyx anchors, upstream in the signaling/translation of force, and G proteins or ion channels on the downstream side. On the other side, a more robust characterization of the photophysics of dialkylindocarbocyanine dyes would be necessary to interprate fluorescence lifetime changes. Going back to more controlled environment like model membrane studies could be very useful: describing the physical and photophysical properties of DiI dyes in liquid-ordered domains before attempting to understand results from colocalization and FRET measurements.

This study demonstrated time-dependent changes in diffusion coefficients using fluorescence correlation spectroscopy and simultaneous fluorescence lifetime measurements of lipoid dyes embedded in endothelial cells membrane. This novel approach to single-molecule membrane dynamics outlined the temporal, spatial and domain-dependent alteration of the lipid bilayer in response to physiological shear stress.

References

1. Barbee, K. A. 2002. Role of subcellular shear-stress distributions in endothelial cell mechanotransduction. *Ann. Biomed. Eng* 30:472-482.

2. Caroni, P. 2001. New EMBO members' review: actin cytoskeleton regulation through modulation of PI(4,5)P(2) rafts. *EMBO J.* 20:4332-4336.

3. Davies, P. F., A. Robotewskyj, and M. L. Griem. 1994. Quantitative studies of endothelial cell adhesion. Directional remodeling of focal adhesion sites in response to flow forces. *J. Clin. Invest* 93:2031-2038.

4. Ingber, D. E. 1997. Tensegrity: the architectural basis of cellular mechanotransduction. *Annu. Rev. Physiol* 59:575-599.

5. Munro, S. 2003. Lipid rafts: elusive or illusive? *Cell* 115:377-388.

VITA

Tristan Tabouillot

EDUCATION

Masters, Doctorate of Philosophy, Bioengineering (GPA 3.38) May 2009
Pennsylvania State University, University Park PA

Bachelor of Science, Electrical Engineering (GPA 3.53) December 2000
Florida Institute of Technology, Melbourne FL

PUBLICATIONS

Peer Reviewed Publications

- "Shear stress elicits a transient domain-dependent alteration of membrane fluidity in endothelial cells" **Tabouillot T**, Muddana HS, Butler PJ. *Biophysical Journal* (in preparation)
- "Single cell poration using acoustic streaming of PDMS grooves inside microfluidic channel" Ahmed D, **Tabouillot T**, Mao X, Alam S, Huang TJ. *Lab on a Chip* (in preparation)
- "Endocytosis-mediated uptake and dissolution of dye-encapsulated calcium phosphate nanoparticles in vitro" Muddana HS, Morgan TT, **Tabouillot T**, Adair JH, Butler PJ. *Molecular Pharmaceutics* (in preparation)
- "Encapsulation of organic molecules in calcium phosphate nanocomposite particles for intracellular imaging and drug delivery" Morgan TT, Muddana HS, Altınoğlu Eİ, Rouse SM, Tabaković A, **Tabouillot T**, Russin TJ, Butler PJ, Eklund PC, Yun JK, Kester M, Adair JH. *Nano Letters Dec;8(12):4108* (2008) [*(Research Highlight)* "Nontoxic nanoparticle enables drug delivery and tracking", Chemical Engineering Progress (CEP) magazine, Vol. 105, No. 1, January, 2009. *(In the NEWS)* "Nontoxic nanoparticle can deliver and track drugs", ScienceDaily, Nov 26, 2008.]
- "Integrated multimodal microscopy, time resolved fluorescence, and optical-trap rheometry: toward single molecule mechanobiology" Gullapalli RR**, Tabouillot T** (first authorship shared), Dangaria J, Mathura R, Butler PJ. *Journal of Biomedical Optics Jan-Feb;12(1):014012* (2007) [Selected for special edition of *Virtual Journal of Ultrafast Science*]
- "Multimodal microscopy and single molecule spectroscopy for mechanotransduction research" **Tabouillot T**, Gullapalli RR, Butler PJ. *Transactions of Optics East (SPIE)* (2006)

Book Chapter

- "Fluorescence methods in cellular and molecular mechanobiology" Butler PJ, Gullapalli RR, **Tabouillot T**, Ferko M. In *The Annual Reviews in Fluorescence*. Editor: Chris Geddes and Joseph Lakowicz. Springer press. (53 pages) (Target publication date Summer 2009) [at amazon.com]